REPORT 1077

TWO- AND THREE-DIMENSIONAL UNSTEADY LIFT PROBLEMS IN HIGH-SPEED FLIGHT [1]

By HARVARD LOMAX, MAX. A. HEASLET, FRANKLYN B. FULLER, and LOMA SLUDER

SUMMARY

The problem of transient lift on two- and three-dimensional wings flying at high speeds is discussed as a boundary-value problem for the classical wave equation. Kirchhoff's formula is applied so that the analysis is reduced, just as in the steady state, to an investigation of sources and doublets. The applications include the evaluation of indicial lift and pitching-moment curves for two-dimensional sinking and pitching wings flying at Mach numbers equal to 0, 0.8, 1.0, 1.2, and 2.0. Results for the sinking case are also given for a Mach number of 0.5. In addition, the indicial functions for supersonic-edged triangular wings in both forward and reversed flow are presented and compared with the two-dimensional values.

INTRODUCTION

The usual idealizations introduced in the development of linearized aerodynamic theory describe a frictionless, perfectly elastic, model fluid. As is well known, the effect of small disturbances in such a fluid can be analyzed by means of the familiar wave equation.

The solution to the wave equation known as Kirchhoff's formula (see reference 1) is found to be of considerable use in unsteady-motion problems involving thin wings with supersonic edges. The problem is reduced to one of summing elementary solutions, analogous to sources and doublets in steady flow, over a region determined by the position of the wing as well as its traversed path. The theoretical development leads naturally to the concepts (defined later) of, first, inverse sound waves, which have a counterpart in the Mach forecones used in steady-state wing theory; second, acoustic plan forms; and, third, homogeneous flow, which reduces in part to the familiar conical flow as the wing approaches a steady supersonic velocity.

There are several simple types of unsteady motion on which the analysis can be based. The so-called indicial motion, in which the velocity undergoes an initial discontinuous change will be considered here. It is possible to conceive the perturbation field due to the unsteady motion in two slightly different ways. For one, it can be supposed that the wing has been traveling at the constant velocity V_0 for an infinitely long time and then, at time equals zero, starts suddenly to sink without pitching (or pitch at a constant angle of attack) while maintaining the forward velocity V_0. On the other hand, the wing may be considered to be at rest in still air until at time zero it starts suddenly either to sink or to pitch and, at the same instant, attains the forward velocity V_0. The latter physical picture will be used in this report. Problems of unsteady motion can also be approached with the initial assumption that the velocity potential depends harmonically on the time. These two approaches are quite compatible in that they can be related through the use of superposition methods (Duhamel's integral, Fourier's integral) of the operational calculus.

Detailed results for two classes of indicial responses (time response to a step input) will be given in this report. The first of these is the complete set of responses (c_{l_α}, c_{m_α}, c_{l_q}, c_{m_q}) for two-dimensional wings flying at Mach numbers equal to 0, 0.8, 1.0, 1.2, and 2.0. In addition, results for c_{l_α} and c_{m_α} are given for a Mach number equal to 0.5. The part of the analysis pertaining to the response of wings traveling at subsonic speeds is lengthy and somewhat tedious regardless of the method of approach. With the use of indicial functions, however, the calculations are reasonably straightforward, especially for Mach numbers around 0.8 to 1.0. Further, the use of indicial functions sheds considerable light on the manner in which Mach number variations affect the section aerodynamic characteristics. The results for the two-dimensional wings traveling at supersonic speeds are compared with the indicial responses developed by rectangular wings of aspect ratios 2, 4, and 6, the latter curves having been presented by J. W. Miles in reference 2.

The second class of indicial responses considered is that concerned with the forces and moments induced on sinking and pitching triangular wings. First, the loading on a flat triangular wing with supersonic edges undergoing an indicial sinking motion is determined. (See also reference 3.) Then a simplified method is developed whereby total lift and pitching-moment coefficients for the wing with supersonic edges may be obtained. (See also reference 4.) Again a complete set of indicial responses is presented for supersonic-edged wings in both forward and reversed flow. Lastly, the triangular wing with subsonic edges is partially analyzed, and the indicial responses for a slender triangular wing are given.

[1] Supersedes NACA TN 2403, "The Indicial Lift and Pitching Moment for a Sinking or Pitching Two-Dimensional Wing Flying at Subsonic or Supersonic Speeds" by Harvard Lomax, Max. A. Heaslet, and Loma Sluder, 1951; NACA TN 2387, "Three-Dimensional Unsteady Lift Problems in High-Speed Flight—The Triangular Wing" by Harvard Lomax, Max. A. Heaslet, and Franklyn B. Fuller, 1951; and also contains material from NACA TN 2256, "Three-Dimensional, Unsteady-Lift Problems in High-Speed Flight—Basic Concepts" by Harvard Lomax, Max. A. Heaslet, and Franklyn B. Fuller, 1951.

SYMBOLS

a_0 speed of sound in the undisturbed fluid

c chord of wing

C_L lift coefficient $\left(\frac{\text{lift}}{\frac{1}{2}\rho_0 V_0^2 S}\right)$

C_{L_α} indicial lift coefficient due to angle-of-attack change, without pitching $\left(C_{L_\alpha}=\frac{\partial C_L}{\partial \alpha}\bigg|_{\alpha=0}\right)$

C_{L_q}' indicial lift coefficient due to pitching for a wing rotating about its leading edge or apex $\left(C_{L_q}=\frac{\partial C_L}{\partial \frac{c\dot{\theta}}{V_0}}\bigg|_{\dot{\theta}=0}\right)$

C_m pitching-moment coefficient, positive when trailing edge tends to sink relative to leading edge $\left(\frac{\text{moment}}{\frac{1}{2}\rho_0 V_0^2 cS}\right)$

C_{m_α}' indicial pitching-moment coefficient due to angle-of-attack change (without pitching) measured about the leading edge or apex; positive when trailing edge is forced downward with respect to the leading edge or apex $\left(C_{m_\alpha}=\frac{\partial C_m}{\partial \alpha}\bigg|_{\alpha=0}\right)$

C_{m_q}' indicial pitching-moment coefficient due to pitching measured about the leading edge or apex, for a wing rotating about its leading edge or apex; positive when trailing edge is forced downward with respect to the leading edge or apex $\left[C_{m_q}=\frac{\partial C_m}{\partial\left(\frac{c\dot{\theta}}{V_0}\right)}\bigg|_{\dot{\theta}=0}\right]$

c_l two-dimensional lift coefficient $\left(\frac{\text{lift}}{\frac{1}{2}\rho_0 V_0^2 c}\right)$

c_m two-dimensional pitching-moment coefficient $\left(\frac{\text{moment}}{\frac{1}{2}\rho_0 V_0^2 c^2}\right)$

m cotangent of sweep angle ($\cot \Lambda$)

M_0 Mach number in the undisturbed fluid

P_0 $\frac{M_0}{2\alpha s}\int_{-s}^{s}\frac{\Delta p}{q_0}\,dy$

P_1 $\frac{mM_0V_0}{2\dot{\theta}s^2}\int_{-s}^{s}\frac{\Delta p}{q_0}\,dy$

$\frac{\Delta p}{q_0}$ loading coefficient (pressure on the lower surface minus pressure on the upper surface divided by free-stream dynamic pressure)

q_0 free-stream dynamic pressure $\left(\frac{1}{2}\rho_0 V_0^2\right)$

q dimensionless rate of pitching $\left(\frac{c\dot{\theta}}{V_0}\right)$

s local semispan of wing

S wing area

t' time

t, t_0 a_0t', a_0t'/c

u, v, w perturbation velocities in x, y, z directions, respectively

V_0 free-stream velocity

x, y, z Cartesian coordinates, fixed relative to the fluid at infinity

$(x/c)_{c.p.}$ distance of center of pressure from leading edge or apex, in percent chord

α angle of attack (angle between flight path and plane of wing), radians

$\dot{\alpha}$ $\frac{d\alpha}{dt'}$

β $\sqrt{|1-M_0^2|}$

Γ circulation

$\delta(t')$ Dirac δ function, normalized with respect to t', thus $\delta(t')=0$ for $t'\neq 0$, $\delta(0)=\infty$, and $\int_{-\infty}^{\infty}\delta(t')\,dt'=1$

Δ discontinuity in the quantity in question across the plane of a wing

θ wing angle of pitch relative to horizontal, positive when trailing edge lies below leading edge, radians

$\dot{\theta}$ wing rate of pitch $\left(\frac{d\theta}{dt'}\right)$

Λ angle of sweep of leading edge, positive for sweepback

ρ_0 free-stream density

τ_0 chord lengths traveled $\left(\frac{V_0t'}{c}\right)$

φ perturbation velocity potential

SUBSCRIPTS

u upper surface of a wing

l lower surface of a wing

x, y, z, t indicate differentiation with respect to the variable in question

PART I—THE USE OF INDICIAL FUNCTIONS IN UNSTEADY LIFT PROBLEMS

In the first part of this report, a discussion of three unsteady lift problems will be given. The three problems are:

(i) Determination of the indicial response in lift and moment on a sinking or rotating wing;

(ii) Determination of frequency response in lift and moment on a fluttering wing; and

(iii) Determination of frequency response in lift and moment on a slowly oscillating wing.

The method by which the latter two problems may be solved with the aid of the solution to the first is also described, as well as the application of these results to the determination of lift and moment on wings undergoing arbitrary maneuvers.

THE INDICIAL FUNCTIONS

By definition, an indicial function is the response to a disturbance which is applied abruptly at time zero and is held constant thereafter; that is, a disturbance given by a step function. For example, if the angle of attack of a wing varies with time as shown in figure 1, the corresponding response, also shown in figure 1, is designated as the indicial lift coefficient due to angle of attack. Four such indicial functions will be evaluated, namely, C_{L_α}, C_{m_α}', C_{L_q}', C_{m_q}'. The primes on the coefficients indicate that the axes about which pitching motion occurs and pitching moments are measured either coincide with the leading edge of the wing or with a line through the apex normal to the root chord of the wing.

The equations which transform these functions to those for a wing pitching about an axis a distance ac back from the leading edge and having its moment center a distance bc back from the leading edge are simply

$$\left.\begin{aligned} C_{L_\alpha}&=C_{L_\alpha} \\ C_{m_\alpha}&=C_{m_\alpha}'+b\ C_{L_\alpha} \\ C_{L_q}&=C_{L_q}'-a\ C_{L_\alpha} \\ C_{m_q}&=C_{m_q}'+b\ C_{L_q}'-a\ C_{m_\alpha}'-ab\ C_{L_\alpha} \end{aligned}\right\} \tag{1}$$

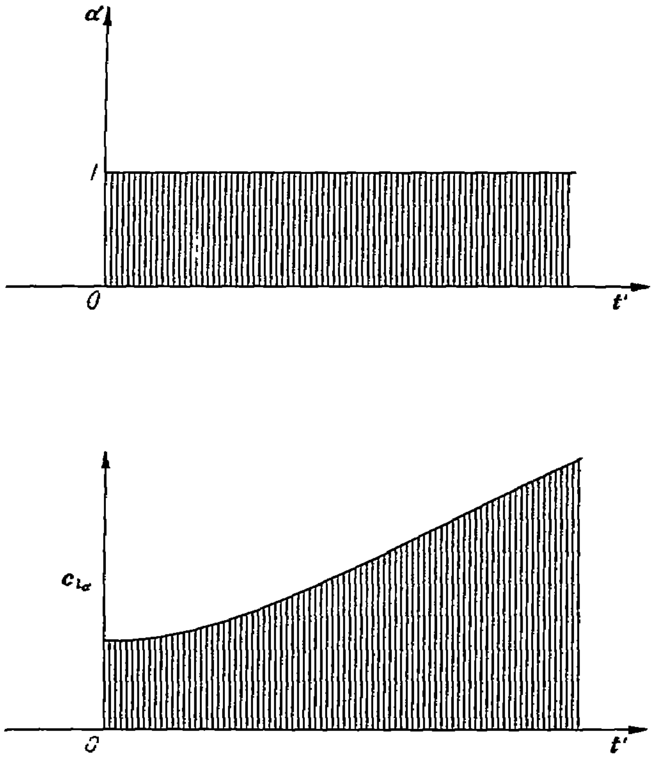

FIGURE 1.—Indicial excitation and response.

In linearized, thin-airfoil theory the boundary condition that applies to the indicial functions due to angle of attack is simply

$$w_u=w_l=-V_0\alpha \tag{2}$$

over a certain planar area in the xyz space at the time t'. If we consider a coordinate system fixed relative to the fluid at infinity and a wing with span measured along the y axis, moving away from the origin along the negative x axis with a velocity V_0, then equation (2) applies to the area in the $z=0$ plane occupied by the wing at any given time. It is further required that the φ be continuous everywhere except across the wing plan form and wake. In the case of the indicial functions due to pitch for a wing rotating about its leading edge or apex, the boundary conditions for a wing the leading edge or apex of which is at the origin at $t'=0$ are that the upwash be given by the expression

$$w_u=w_l=-(x+V_0t')\ \dot{\theta} \tag{3}$$

over the same region in the $z=0$ plane as for the angle-of-attack case and, again, that φ be continuous except across the wing and its wake. The angle of pitch, θ, is taken as positive when the trailing edge is lower than the leading edge, and $\dot{\theta}$ is the time derivative, $d\theta/dt'$, positive when the trailing edge is falling with reference to the leading edge.

The difference between θ and α is illustrated in figure 2 (a). The angle of attack α is the angle between the flat wing surface and the tangent to the flight path of some point fixed at a distance ac back from the wing leading edge. For example, in applications involving the dynamic behavior of an entire airplane the distance ac would usually be taken as the distance back to the center of gravity of the airplane. The angle θ is the angle between the flat wing surface and the horizontal. Figure 2 (b) shows a wing undergoing a sinusoidal angle-of-attack variation with a zero angle of

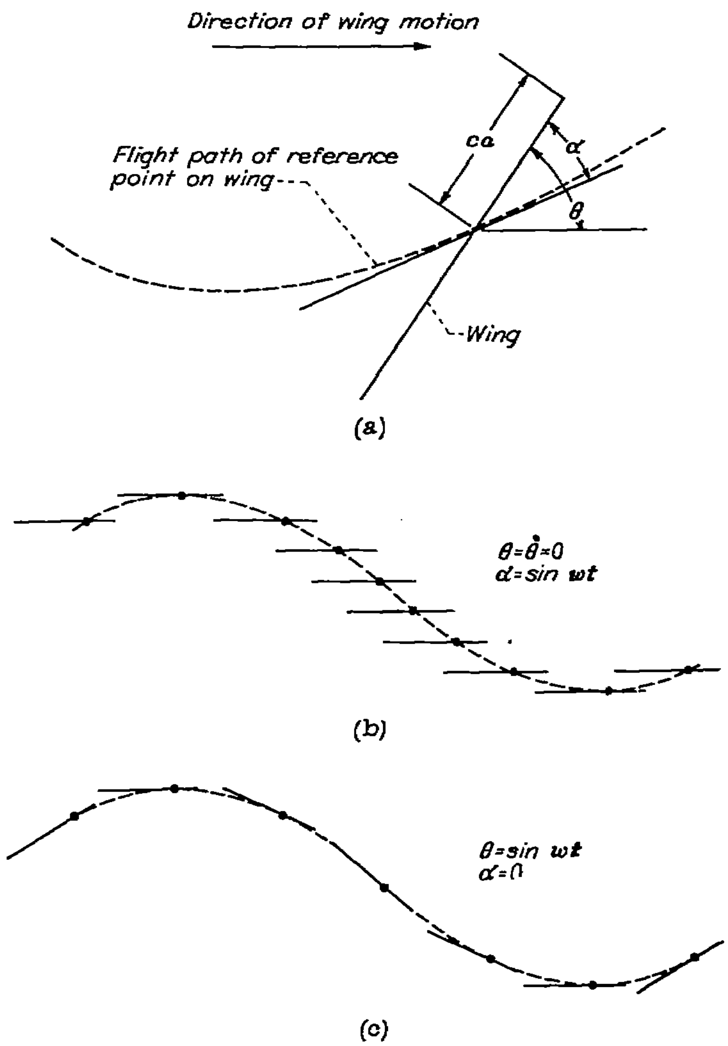

(a) Angle convention.
(b) Sinking wing.
(c) Pitching wing.

FIGURE 2.—Definition of angles of attack and pitch.

pitch throughout. For convenience and in order to distinguish from the pitching wing, such a wing will be referred to as a sinking wing. Figure 2 (c) shows a wing undergoing a sinusoidal angle-of-pitch variation taken about the axis ac back from the leading edge. In the case shown the wing has a constant (zero) angle of attack.

The variable q to which the lift and pitching-moment coefficients of the pitching wing are referred is equal to $\dot{\theta}c/V_0$, a dimensionless form of expression for rate of pitch.

ADAPTATION OF THE INDICIAL FUNCTIONS TO MANEUVERS

Since the theory is linear, the lift and moment on a wing undergoing an arbitrary maneuver (in which both α and $\dot{\theta}$ remain small) can be calculated from the indicial functions by the principle of superposition. For example, consider a wing performing some arbitrary maneuver involving small variations of both α and θ. Let α and θ be defined [2] with respect to the flight path of a point ac back from the leading edge. The appropriate indicial functions can then be calculated from those referred to the flight path of the leading edge by means of equations (1). (The moment center is still arbitrary at a point a distance bc back from the leading edge. However, for convenience, b is usually taken to be equal to a.) Finally, by Duhamel's integral, the lift and moment induced on the wing by the arbitrary maneuver are given by the equations

$$\left.\begin{aligned} C_L&=\frac{d}{dt'}\int_0^{t'}[C_{L_\alpha}(t'-t_1')\,\alpha(t_1')+C_{L_q}(t'-t_1')\,q(t_1')]\,dt_1' \\ C_m&=\frac{d}{dt'}\int_0^{t'}[C_{m_\alpha}(t'-t_1')\,\alpha(t_1')+C_{m_q}(t'-t_1')\,q(t_1')]\,dt_1' \end{aligned}\right\}\quad(4a)$$

or alternatively

$$\left.\begin{aligned} C_L&=\frac{d}{dt'}\int_0^{t'}[C_{L_\alpha}(t_1')\alpha(t'-t_1')+C_{L_q}(t_1')q(t'-t_1')]dt_1' \\ C_m&=\frac{d}{dt'}\int_0^{t'}[C_{m_\alpha}(t_1')\alpha(t'-t_1')+C_{m_q}(t_1')q(t'-t_1')]dt_1' \end{aligned}\right\}\quad(4b)$$

where, for example, $C_{L_\alpha}(t'-t_1')$ means that the indicial function C_{L_α} is to be evaluated at the time $t'-t_1'$.

THE FLUTTER DERIVATIVES

By definition, a flutter derivative is the response to a harmonic oscillation in vertical displacement (angle of attack) or pitch, such oscillation having continued so long that all transient effects of its origin are damped out and the induced forces and moments are periodic. In the notation used in reference 5 the induced responses are given in terms of the flutter derivatives L_1, L_2, L_3', L_4' and M_1', M_2', M_3', M_4'. The relation between the indicial responses and the flutter derivatives follows from equations (4) and can be written

$$\left.\begin{aligned} L_1+iL_2&=\lim_{t'\to\infty}\frac{ie^{-i\omega t'}}{4k}\frac{d}{dt'}\int_0^{t'}c_{l_\alpha}(t'-t_1')e^{i\omega t_1'}dt_1' \\ M_1'+iM_2'&=\lim_{t'\to\infty}\frac{-ie^{-i\omega t'}}{2k}\frac{d}{dt'}\int_0^{t'}c_{m_\alpha}'(t'-t_1')e^{i\omega t_1'}dt_1' \\ L_3'+iL_4'&=\lim_{t'\to\infty}\frac{e^{-i\omega t'}}{4k^2}\frac{d}{dt'}\int_0^{t'}[c_{l_\alpha}(t'-t_1')+ \\ &\qquad 2ikc_{l_q}'(t'-t_1')]e^{i\omega t_1'}dt_1' \\ M_3'+iM_4'&=\lim_{t'\to\infty}\frac{-e^{-i\omega t'}}{2k^2}\frac{d}{dt'}\int_0^{t'}[c_{m_\alpha}'(t'-t_1')+ \\ &\qquad 2ikc_{m_q}'(t'-t_1')]e^{i\omega t_1'}dt_1' \end{aligned}\right\}\quad(5)$$

where ω is the frequency and k is the reduced frequency, $\omega c/2V$. The primes on the quantities again indicate that the wing is pitching about and the moments are measured about the leading edge of the wing.

The responses in lift and moment for harmonically oscillating wings can be expressed in terms of their absolute values and phase shifts with reference to the period of the forcing disturbance. Thus, if an angle of attack variation given by the equation $\alpha=e^{i\omega t'}$ is impressed on the wing, the response in lift would be $|c_{l_\alpha}|e^{i(\omega t'+\psi)}$. In terms of the indicial functions this can be written

$$|c_{l_\alpha}|e^{i\psi}=\lim_{t'\to\infty}e^{-i\omega t'}\frac{d}{dt'}\int_0^{t'}c_{l_\alpha}(t'-t_1')e^{i\omega t_1'}dt_1'$$

which, by comparison with equations (5), can be re-expressed in terms of the flutter derivatives as

$$|c_{l_\alpha}|e^{i\psi}=4k(L_2-iL_1)=4k\sqrt{L_2^2+L_1^2}\,e^{-i\tan^{-1}(L_1/L_2)}$$

Similarly, each of the stability derivatives can be expressed in terms of the indicial functions and the flutter derivatives, hence:

Term	Maximum value	Phase angle
c_{l_α}	$4k\sqrt{L_1^2+L_2^2}$	$-\tan^{-1}\dfrac{L_1}{L_2}$
c_{m_α}'	$2k\sqrt{M_1'^2+M_2'^2}$	$-\tan^{-1}\dfrac{M_1'}{M_2'}$
$ik(c_{l_{\dot\alpha}}+c_{l_q}')$	$2k\sqrt{L_3'^2+L_4'^2}$	$\tan^{-1}\dfrac{L_4'}{L_3'}$
$ik(c_{m_{\dot\alpha}}'+c_{m_q}')$	$k^2\sqrt{M_3'^2+M_4'^2}$	$\tan^{-1}\dfrac{M_4'}{M_3'}$

(6)

where it is assumed that unit absolute values of angle of attack and pitch are impressed and the term $\dot{\alpha}=c\dfrac{d\alpha/dt'}{V_0}$.

[2] Notice that if α' and θ' are the angle of attack and pitch measured with respect to the flight path of the leading edge, and α and θ the same angles measured with respect to the flight path of a point ac back from the leading edge, the relation between the two sets of angles is given, for small deflections, by

$$\alpha'=\alpha-\frac{ac\dot{\theta}}{V_0}$$
$$\theta'=\theta$$

A WING UNDERGOING SLOW HARMONIC OSCILLATIONS

The boundary conditions for these problems are exactly the same as those used for evaluating the flutter derivatives, being in fact a special case of the latter when the frequency of oscillation is very low. This added simplification is important, however, because the frequency of angle of attack and pitch oscillations for the entire airplane is, relative to the flutter frequencies, very low. Further, special methods based on the assumption that the wing is oscillating slowly have been devised. Thus, if the lift and moment are expanded in powers of the frequency, solutions for the coefficients of the lowest-order terms have been found for both triangular and rectangular wings flying at supersonic speeds. (See, e. g., references 6, 7, 8, and 9.)

For a given set of indicial functions these expansions can be carried out with relative ease. Consider the case of L_1 and L_2 as given by equations (5). If the indicial curve for $c_{l_\alpha}(t')$ contains no pulse function,[3] the expression for L_1+iL_2 can be written

$$L_1+iL_2=\lim_{t'\to\infty}\frac{ie^{-i\omega t'}}{4k}\frac{d}{dt'}\int_0^{t'}[c_{l_\alpha}(\infty)-\Delta c_{l_\alpha}(t')]e^{i\omega(t'-t_1')}dt_1'$$

where $\Delta c_{l_\alpha}(t')$ is the difference between the indicial lift and its asymptotic value, thus

$$\Delta c_{l_\alpha}(t')=c_{l_\alpha}(\infty)-c_{l_\alpha}(t')$$

Since $\Delta c_{l_\alpha}(\infty)$ is zero, it follows

$$L_1+iL_2=\frac{i}{4k}\left[c_{l_\alpha}(\infty)-i\omega\int_0^\infty \Delta c_{l_\alpha}(t_1')e^{-i\omega t_1'}dt_1'\right]$$

or, in terms of the reduced frequency parameter $k=\omega c/2V_0$ and the number of chord lengths traveled $\tau_0=V_0t'/c$,

$$L_1+iL_2=\frac{i}{4k}\left[c_{l_\alpha}(\infty)-2ik\int_0^\infty \Delta c_{l_\alpha}(\tau_0)e^{-2ik\tau_0}d\tau_0\right]$$

In case the flow is supersonic, these expressions can be expanded in powers of k, thus

$$4L_1=2\int_0^\infty \Delta c_{l_\alpha}(\tau_0)d\tau_0-4k^2\int_0^\infty \tau_0^2\Delta c_{l_\alpha}(\tau_0)d\tau_0+\ldots \quad (7a)$$

$$4kL_2=c_{l_\alpha}(\infty)-4k^2\int_0^\infty \tau_0\Delta c_{l_\alpha}(\tau_0)d\tau_0+\ldots \quad (7b)$$

Similarly, the expressions for the other coefficients become

$$-2M_1'=2\int_0^\infty \Delta c_{m_\alpha}'(\tau_0)d\tau_0-4k^2\int_0^\infty \tau_0^2\Delta c_{m_\alpha}'(\tau_0)d\tau_0+\ldots \quad (7c)$$

$$-2kM_2'=c_{m_\alpha}'(\infty)-4k^2\int_0^\infty \tau_0\Delta c_{m_\alpha}'(\tau_0)d\tau_0+\ldots \quad (7d)$$

$$2k^2L_3'=\frac{1}{2}c_{l_\alpha}(\infty)+2k^2\int_0^\infty[\Delta c_{l_q}'(\tau_0)-\tau_0\Delta c_{l_\alpha}(\tau_0)]d\tau_0+\ldots \quad (7e)$$

$$2kL_4'=c_{l_q}'(\infty)-\int_0^\infty \Delta c_{l_\alpha}(\tau_0)d\tau_0-2k^2\int_0^\infty[2\tau_0\Delta c_{l_q}'(\tau_0)-\tau_0^2\Delta c_{l_\alpha}(\tau_0)]d\tau_0+\ldots \quad (7f)$$

$$-k^2M_3'=\frac{1}{2}c_{m_\alpha}'(\infty)+2k^2\int_0^\infty[\Delta c_{m_q}'(\tau_0)-\tau_0\Delta c_{m_\alpha}'(\tau_0)]d\tau_0+\ldots \quad (7g)$$

$$-kM_4'=c_{m_q}'(\infty)-\int_0^\infty \Delta c_{m_\alpha}'(\tau_0)d\tau_0-2k^2\int_0^\infty[2\tau_0\Delta c_{m_q}'(\tau_0)-\tau_0^2\Delta c_{m_\alpha}'(\tau_0)]d\tau_0+\ldots \quad (7h)$$

It is interesting to examine these equations briefly with regard to the problem of one-degree-of-freedom oscillatory instability. As was shown in reference 5, an oscillatory stability boundary is given by the equation $M_4=0$. Hence, a wing pivoted about its leading edge can be neutrally stable if $M_4'=0$. Such a condition arises only if the frequency is very low[4] for which case the above expansion for kM_4' applies. Hence, to a first order the stability boundary is given by the condition

$$c_{m_q}'(\infty)=\int_0^\infty \Delta c_{m_\alpha}'(\tau_0)d\tau_0$$

This leads to the interpretation of the indicial curves shown in figure 3; namely, an airfoil pivoted at its leading edge can

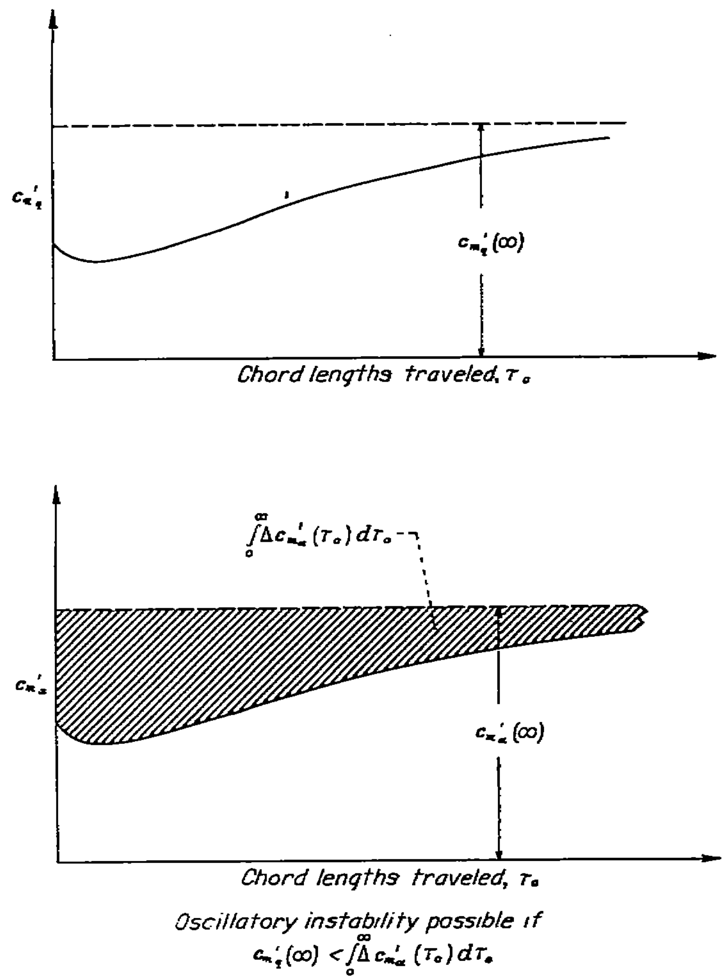

FIGURE 3.—Interpretation of single-degree-of-freedom stability boundary in terms of indicial response curves.

[3] A pulse function occurs only for the case $M_0=0$. Its treatment in expressions such as equations (5) is discussed in a subsequent section.
[4] That is, the moment of inertia is large. Experimental verification of the existence of this type of instability can be found in reference 10.

have an oscillatory instability if the steady-state value of c_{m_q}' is less than the area between the steady-state value of c_{m_α}' and its indicial value when expressed in chord lengths traveled.

PART II—METHODS FOR SOLVING UNSTEADY LIFT PROBLEMS

BASIC EQUATIONS AND SOLUTIONS

In terms of the perturbation velocity potential φ, the wave equation can be written

$$\varphi_{xx}+\varphi_{yy}+\varphi_{zz}=\frac{1}{a_0^2}\varphi_{t't'} \tag{8}$$

where a_0 is the speed of pressure propagation, t' is the time, and x,y,z are spatial coordinates. This equation applies to a flow field which is stationary at large distances from the disturbance region; furthermore, the coordinate system is stationary relative to the fluid infinitely distant so that, if a moving wing is being analyzed, the wing moves with respect to the x,y,z axes. The last equation can be put in a more convenient form by introducing the notation

$$t=a_0t'$$

so that the dimension of t is length just as are the dimensions of the geometric variables $x,y,$ and z. Equation (8), together with this transformation, yields the canonical form of the wave equation

$$\varphi_{xx}+\varphi_{yy}+\varphi_{zz}=\varphi_{tt} \tag{9}$$

and it is this form which will be considered.

The first task is to study the relation between the motion of the wing and the coordinate system. As has already been mentioned, equation (9) is valid for a flow field produced by a wing moving relative to a coordinate system fixed with respect to the fluid at infinity. It is pertinent to consider the possibility of finding a transformation which will fix the origin of the coordinate system on the wing and, at the same time, retain the wave equation as the governing equation of the flow. Certainly the first of these requirements is simple to fulfill if the second is neglected.

The following transformation (known in relativity theory as a Lorentz transformation)

$$\left.\begin{aligned}\xi&=\frac{x-M_0t}{\sqrt{1-M_0^2}}\\ \eta&=y\\ \zeta&=z\\ \tau&=\frac{t-M_0x}{\sqrt{1-M_0^2}}\end{aligned}\right\} \tag{10}$$

where $M_0=\frac{V_0}{a_0}<1$, will satisfy both the above conditions. For example, suppose that the wing is moving along the x axis with velocity V_0. Application of equations (10) to equation (9) makes the origin of the new system of axes also travel along the x axis with a velocity V_0. This is seen to be so since ξ is always zero when $x=V_0t'=M_0t$. Hence, the ξ axis is "fixed" on the wing. As to the second condition, a straightforward exercise in partial differentiation yields

$$\varphi_{\xi\xi}+\varphi_{\eta\eta}+\varphi_{\zeta\zeta}=\varphi_{\tau\tau} \tag{11}$$

so that, in going from x,y,z to ξ,η,ζ space, the wave equation remains invariant; consequently, both the requirements mentioned have been fulfilled.

It is instructive to consider briefly the consequences of applying the Lorentz transformation. Although the wave equation remains invariant, such physical quantities as length and pressure do not. For example, a wing with a chord c in the x,y,z space has, according to equations (10), a chord $c/\sqrt{1-M_0^2}$ in the ξ,η,ζ space. Furthermore, the loading coefficient which, on the basis of linearized theory, is given in the x,y,z,t space by

$$\frac{\Delta p}{q_0}=\frac{4}{V_0M_0}\frac{\partial\varphi}{\partial t} \tag{12}$$

becomes for the ξ,η,ζ,τ space

$$\frac{\Delta p}{q_0}=\frac{4}{V_0\sqrt{1-M_0^2}}\left(\frac{1}{M_0}\frac{\partial\varphi}{\partial\tau}-\frac{\partial\varphi}{\partial\xi}\right) \tag{13}$$

If the wing motion is steady and there are no transient effects, equations (11) and (13) are independent of time and, together with the resulting length transformations, become

$$\left.\begin{aligned}&\varphi_{\xi\xi}+\varphi_{\eta\eta}+\varphi_{\zeta\zeta}=0\\ &\frac{\Delta p}{q_0}=-\frac{4\varphi_\xi}{V_0\sqrt{1-M_0^2}}\\ &\xi=\frac{x}{\sqrt{1-M_0^2}},\ \eta=y,\ \zeta=z\end{aligned}\right\} \tag{14}$$

These are immediately recognized to be Laplace's equation for incompressible flow and the familiar Prandtl-Glauert compressibility corrections.[5]

The preceding discussion has an important qualification, however, in the fact that the velocity of the moving coordinate system cannot exceed the speed of sound. A glance at equations (10) serves to verify this statement since those equations show M_0 must be less than 1 in order that ξ and τ be real for real x and t. In fact, it has been shown that there is no transformation which will fix the moving system of axes in a wing traveling at a uniform supersonic speed away from the original fixed axes and still keep the wave equation invariant. Therefore, for analyzing a wing in supersonic

[5] The equation $\xi=x/\sqrt{1-M_0^2}$ would first read $\xi=(x-M_0t_0)/\sqrt{1-M_0^2}$ where t_0 is a constant representing the time required for the motion to reach its steady state. However, the x coordinate can always be translated to any fixed position without affecting any of the equations for potential, loading, etc. Such a translation is assumed to have been made in equations (14).

flight, it is necessary to abandon one of the two proposed requirements: Either the coordinate system cannot be fixed in the wing, or the field equation must be modified. The latter of these two alternatives has been studied by several authors (see references 2, 3, 4, 5) but it is the former which will be considered in the present analysis. Further, since the axes cannot be made to travel as fast as the wing, they will not be made to move at all and equation (9) will be adopted throughout as the basic equation.

Having decided upon the form of the partial differential equation, we must next establish the boundary conditions. For any given time these conditions are similar to those studied in steady-state thin-airfoil problems; namely, either that the given slope of the wing surface is proportional to the vertical induced velocity φ_z over the region occupied by the wing in the $z=0$ plane,[6] or that the prescribed surface pressure is proportional to the timewise gradient φ_t in velocity potential over the same region. The addition of time simply means that this region moves about in the $z=0$ plane in conformity with the direction and velocity of the wing.

The solution to equation (9), subject to the boundary conditions just mentioned, can be expressed by a formula which may be regarded as requiring either the evaluation of a double integral or the solution of a double-integral equation, depending upon whether a boundary-value problem of first or second kind is considered. This solution is known as Kirchhoff's formula. (See reference 1.) It may be written in a form convenient for aerodynamic applications as follows:

$$\varphi=-\frac{1}{4\pi}\int_{S_a}\int\left(\frac{1}{r_0}\Delta\frac{\partial}{\partial z_1}\varphi(x_1,y_1z_1,t-r_0)-\Delta\frac{\partial}{\partial z_1}\frac{\varphi(x_1,y_1,0,t-r)}{r}\right)dS \quad (15)$$

where the Δ indicates the jump $\left(\text{value on the upper surface minus value on the lower surface when applied to } \varphi \text{ or } \frac{\partial\varphi}{\partial z}\right)$ of the function in passing through the $z_1=0$ plane, $r=\sqrt{(x-x_1)^2+(y-y_1)^2+(z-z_1)^2}$, $r_0=\sqrt{(x-x_1)^2+(y-y_1)^2+z^2}$, and where the area of integration S_a will be discussed in more detail later.

The terms in the integrand of equation (15) can be shortened by introducing the following notation:

$$\frac{1}{r_0}\Delta\frac{\partial}{\partial z_1}\varphi(x_1,y_1,z_1,t-r_0)=\frac{1}{r_0}\Delta\left[\frac{\partial\varphi}{\partial z_1}\right]_r \quad (16a)$$

$$\Delta\frac{\partial}{\partial z_1}\frac{\varphi(x_1,y_1,0,t-r)}{r}=\Delta\left(\frac{\partial r}{\partial z_1}\frac{\partial}{\partial r}\frac{\varphi(x_1,y_1,0,t-r)}{r}\right)=-\frac{\partial r_0}{\partial z}\Delta\frac{\partial}{\partial r}\left[\frac{\varphi}{r}\right] \quad (16b)$$

In this notation, the subscript r in equation (16a) means that r is to be held constant in the differentiation, and the prefix Δ obviates the necessity of indicating that the functions considered are to be evaluated for $z_1=0$, since it indicates that the difference of the values of the function across the $z_1=0$ plane is to be taken. The right-hand side of equation (16a) can be recognized as a term representing a source located in the $z_1=0$ plane, and the right-hand side of equation (16b) is seen to represent a doublet located in and with axis normal to the $z_1=0$ plane. The brackets [ ] about the functions in equations (16a) and (16b) have a special meaning which is defined in the following way: If f is a function the value of which at a fixed point P depends upon the coordinates x_1, y_1, z_1, t of a moving point Q, so that

$$f=f(x_1,y_1,z_1,t)$$

then

$$[f]=f(x_1,y_1,z_1,t-r) \quad (17)$$

where r is the distance from P to Q. As an example, consider the potential φ at a point P due to a moving source, the location of which at any time is Q. Then φ satisfies the condition just mentioned that it depends on the coordinates x_1, y_1, z_1, t of Q. The brackets [ ] indicate that the potential $[\varphi]$ depends not upon the source strength now at "time" t, but rather upon the source strength that existed "time" r ago.[7] For convenience, $[\varphi]$ is referred to as the retarded value of φ.

The expression for a doublet (equation (16b)) is usually expanded as follows:

$$\left.\begin{aligned}-\frac{\partial r_0}{\partial z}\Delta\frac{\partial}{\partial r}\left[\frac{\varphi}{r}\right]&=-[\Delta\varphi]\frac{\partial r_0}{\partial z}\frac{\partial}{\partial r_0}\left(\frac{1}{r_0}\right)-\frac{\partial r_0}{\partial z}\frac{1}{r_0}\left[\Delta\frac{\partial\varphi}{\partial r}\right]\\&=-[\Delta\varphi]\frac{\partial}{\partial z}\left(\frac{1}{r_0}\right)+\frac{1}{r_0}\frac{\partial r_0}{\partial z}\left[\Delta\frac{\partial\varphi}{\partial t}\right]\end{aligned}\right\} \quad (18)$$

Finally, equation (15) becomes

$$\varphi=-\frac{1}{4\pi}\int_{S_a}\int\left\{\frac{1}{r_0}\Delta\left[\frac{\partial\varphi}{\partial z_1}\right]_r+[\Delta\varphi]\frac{\partial}{\partial z}\left(\frac{1}{r_0}\right)-\frac{1}{r_0}\frac{\partial r_0}{\partial z}\left[\frac{\partial\Delta\varphi}{\partial t}\right]\right\}dS \quad (19)$$

The application of equation (19) awaits only a discussion of the area S_a over which the integration is to be made. This discussion is important enough, however, to merit consideration in some detail and will be given in the following section.

THE ACOUSTIC PLAN FORM

Suppose that a line of sources is placed along the y_1 axis and that the strength of these sources is zero for $t<0$. At $t=0$ they are "turned on" and, at the same time, start moving along the negative x_1 axis with the velocity V_0. After time t' has passed, the source line has traveled a distance M_0t as shown in figure 4 (which is drawn for the case $M_0>1$). Suppose next that there are two sensing elements, or detectors, placed at the point $P(x,y)$ located somewhere ahead of the y_1 axis; one of these detectors is responsive to light and the other to sound. Now, the light

[6] The $z=0$ plane is assumed to be the "plane of the wing"; that is, if the angle of attack were zero and the wing had no thickness it would lie entirely in the $z=0$ plane.

[7] Quotes are used around the word time since the dimension of t is actually length, not time. It is convenient, however, to refer to t as "time," and, since the actual value of time is simply t divided by the constant a_0, this should cause no confusion.

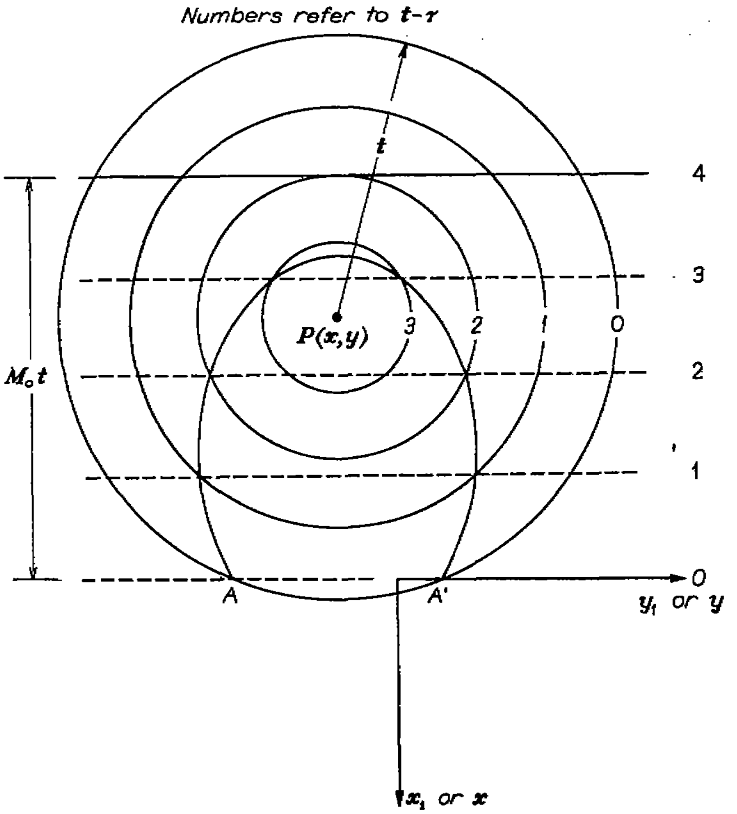

FIGURE 4.—Acoustic wave pattern for a moving line of sources.

detector at any given time will show the sources lying in a straight line just as they would appear visually at each particular instant. The situation is entirely different, however, for the sound detector. First it is necessary to understand the nature of a spherical sound wave. Such a wave travels outward from its origin at a velocity a_0, so that in the time t' it has traveled a distance t. Before the wave reaches a point, the point is completely unaware (unaware is used in the sense that an instrument will record no change in any of the physical properties of the air at the point in question) of its existence and, further, after the wave has passed, the point remains subsequently unaware of its existence. Hence the only points disturbed by the wave are those momentarily on the spherical surface itself. (In this connection see reference 1, pp. 1–3.)

The sound detector, therefore, can only "hear" sources which are so located that their spherical sound waves are just, at the given instant of time, reaching the detector. The locus of all the points which, at a time t ago, emitted sound waves that are just now reaching the point $P(x,y)$ is itself a sphere and for convenience this sphere will be referred to as an "inverse sound wave."[8] The traces of these inverse sound waves in the $z=0$ plane are drawn in figure 4 as concentric circles about the point $P(x,y)$. The intersection of an inverse sound wave of radius $t-\tau$ with the line representing the position of the sources at a time $t'-\tau'$ ago gives the position of the sources which are just now signaling their presence to the sound detector at P. For example, when the source line started, it was lying along the y_1 axis. With reference to the present time t this was a_0t' removed. Hence the intersection of the circle about P of radius t with the y_1 axis fixes the two points A and A', the spherical sound waves of which are now reaching P. A continuation of this process yields, for the locus of all points from which waves emanated that are just now touching the point P, the part of the ellipse shown in figure 4.

In the sense that the light detector, because of the very large velocity of light, is "seeing" a straight line of sources, the sound detector, because of the relatively slow velocity of sound, is "hearing" an elliptic line of sources. Extending this concept to include a sheet of sources distributed over the surface of the wing, one can refer to the outline of that part of the wing which generates disturbances which can be measured by the light detector as the plan form (i. e., the visual plan form), and to the outline of that part of the wing which affects the sound detector as the acoustic plan form. In a mathematical sense, the acoustic plan form is the area S_a over which the integration of equation (19) is to be made.

The equation for the acoustic plan form can be formulated by means of the two equations

$$(x-x_1)^2+(y-y_1)^2+z^2=(t-\tau)^2 \tag{20}$$

$$f(y_1, x_1, \tau)=0 \tag{21}$$

where x, y, z are the coordinates of the point at which the induced effects are to be measured; x_1, y_1, the variable points of the sources; t, "time" now; and $t-\tau$, "time" ago. Equation (20) is that of the inverse sound waves and equation (21) represents the position of the visual plan form at a "time" τ. It is necessary to include the region behind the wing covered by the vortex wake as part of the visual plan form. In case the vorticity in the wake vanishes, as in the thickness problem, the wake may still be considered as part of the visual plan form, but the strength of the source-doublet distribution over that part of the acoustic plan form corresponding to the wake will vanish. If $t^2-z^2<0$, the acoustic plan form does not exist since, for such a case, no source on the x_1, y_1 plane has had time to transmit its effect to the point x, y, z. On the other hand, if the circle (in the x_1, y_1 plane) given by the equation

$$(x-x_1)^2+(y-y_1)^2=t^2-z^2$$

lies entirely within the area occupied by the visual plan form of the wing at the beginning of the motion, the acoustic plan form is just this circle itself. For any other situation the acoustic plan form is formed in part, or in whole, by the curve found by eliminating τ from equations (20) and (21) and in part, or not at all, by an arc of the circle $(x-x_1)^2+(y-y_1)^2=t^2-z^2$. One of the principal advantages of the acoustic-plan-form concept arises in the study of problems involving source or doublet distributions having constant strength. In such cases, the retarded values of the potential

[8] The inverse sound wave has for its analogue in steady lifting-surface theory the Mach forecone. In that theory a disturbance outside the Mach forecone cannot affect the values of the induced velocities at the point where they are being measured. Similarly, in the present study, a source located outside the inverse sound wave of radius t cannot affect the values of any measurement made at the point P.

and its gradient appearing in equation (19) are constant and can be taken outside the integral signs. The problem is thereby reduced to the integration of a simple geometric variable over S_a.

A few examples will serve to fix the idea of the acoustic plan form. Consider first a two-dimensional, unswept wing moving at a constant supersonic speed in the negative x_1 direction. At time zero the leading edge of the wing was along the y_1 axis and now, at time equal to t', the wing has moved so that the leading edge coincides with the line $x_1=-M_0t$. Choose three points that are now lying on the wing. Let one point have its x coordinate in the range $c-\sqrt{t^2-z^2}\geq x\geq\sqrt{t^2-z^2}$ (where c is the chord of the wing), the second in the interval $\sqrt{t^2-z^2}>x>-\sqrt{t^2-z^2}$, and the third in the range $-\sqrt{t^2-z^2}\geq x\geq -M_0t$. Designating these points by P_1, P_2, and P_3 (see fig. 5), it can be shown that their acoustic plan forms are, respectively, a complete circle, a part circle and part ellipse, and a complete ellipse. The points P are at the centers of the circles and at focal points of the ellipses. Since, moreover, the circular plan form about P_1 receives no signals from sources on the leading or trailing edge, conditions at P_1 are consequently completely independent of the actual (visual) plan form of the wing. The elliptical plan form about P_3, on the other hand, depends entirely on the shape of the leading edge; and finally the mixed plan form about P_2 is in certain regions (the circular portion) independent of the leading edge, and in other regions (the elliptic portion) entirely dependent upon it. Since the wing is traveling at supersonic speeds, the trailing edge and vortex wake can have no effect on the measurements taken on the wing and, in the same way, a point ahead of the wing leading edge, P_4 in figure 5, is undisturbed.

Next consider a wing moving at a constant subsonic speed in the negative x_1 direction. As before, the leading edge was on the y_1 axis at $t'=0$ and has traveled a distance $-M_0t$. Choose now three points P_1, P_2, and P_3 on the wing and unaffected by the wing tips. The acoustic plan forms for these points are combinations of circles and hyperbolas as contrasted with the circle-ellipse combination in the supersonic case. Just as in the supersonic case, however, there is a certain region represented by P_1 in which the acoustic plan form is a complete circle and is independent of the visual shape of the wing (see fig. 6). Point P_2 is surrounded by a plan form which is part hyperbolic and part circular, the point itself being the center of the circle and the focus of the hyperbola. Point P_3 is a limiting value of P_2; it lies on the leading edge of the wing and the hyperbolic sides of its plan form have degenerated into straight lines. Finally, P_4 lies ahead of the wing; its plan form is still a combination of a hyperbola and a circle, but P_4 is now the focal point lying ahead of the hyperbolic branch used.

Figure 6 was constructed so that the portion of the visual plan form behind the trailing edge had no effect on the potential at the various points P_1, etc. If these points had been chosen at positions where the wake could signal its effect, one of two acoustic configurations would result. First, if the wing is symmetric about the $z=0$ plane, no lift is developed and the vorticity in the wake is zero so that the visual plan form need not include the wake, but effectively ends at the trailing edge. In this case, the leading edge of the acoustic plan form is then determined as before, while its modified trailing edge may be made up, in part, of circular arcs formed by the primary wave and, in part, by an arc of the hyperbola formed by the (acoustic) intersection of the straight visual trailing edge with the primary wave (such an arc being identical with the leading edge of the acoustic plan form but displaced backwards). On the other hand, if the wing has no thickness but is inclined to the free stream, it develops lift and the vorticity in the wake does not vanish; the acoustic plan form has a trailing edge made up entirely of an arc of the primary inverse sound wave. The space between this arc and the acoustic trace of the visual trailing edge is covered by a sheet of doublets, the strength of which is determined by the vorticity distribution of the vortex wake.

It is interesting to notice the conversion of terminology which arises in the analysis of unsteady lift problems. In the study of steady-state wings, it is customary (because of the nature of the governing partial differential equation) to speak of the subsonic problems as elliptic and the supersonic

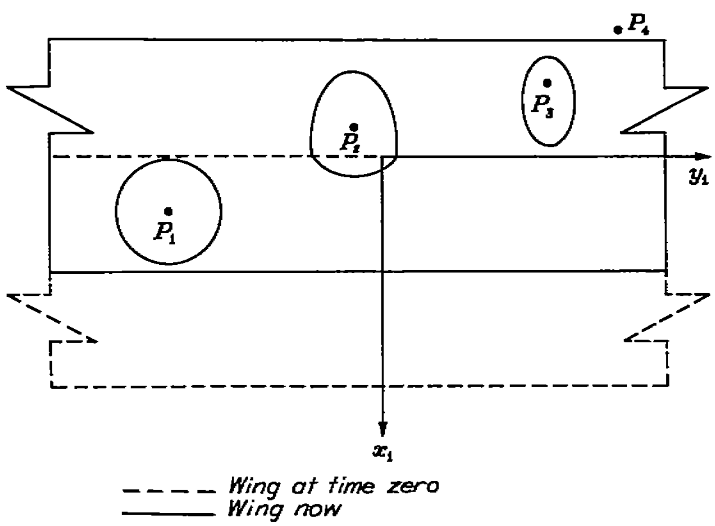

FIGURE 5.—Acoustic plan forms for points on wing traveling at supersonic speed.

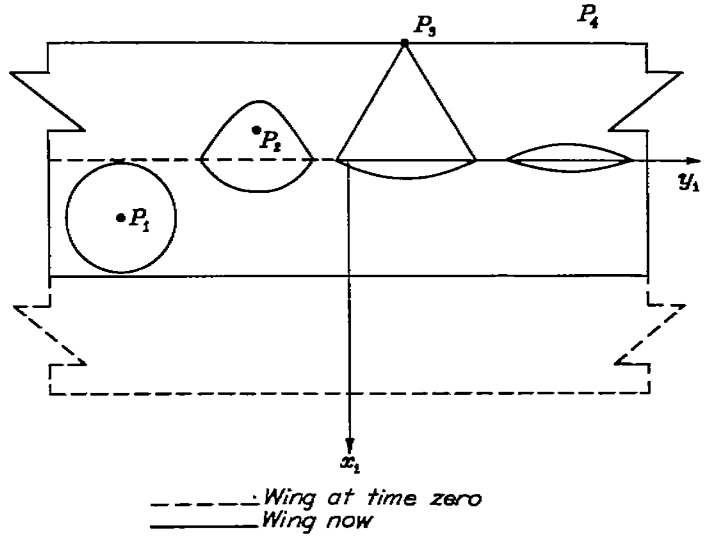

FIGURE 6.—Acoustic plan forms for points on wing traveling at subsonic speed.

problems as hyperbolic. Yet the acoustic plan forms just presented involved ellipses for the supersonic wing and hyperbolas for the subsonic case.

To complete the remark, it can be observed that when the velocity of the wing is sonic the steady-state partial differential equation becomes parabolic and, in this case, the acoustic plan form of a straight-edged wing also involves parabolas. When the leading edge is linear and normal to the stream direction, the eccentricity of the conic sections bounding the acoustic plan form for a point on the wing is equal to $1/M_0$. From this relation it is apparent that for M_0 less than, equal to, and greater than 1 the sections are, respectively, hyperbolas, parabolas, and ellipses. As might be presumed, the value of the eccentricity satisfies simple sweep theory so that, for an infinitely long straight leading edge, the eccentricity of the acoustic plan form is $1/M_0 \cos \Lambda$ where Λ is the angle of sweepback. The principal axes of the conic sections are always normal and parallel to straight leading edges.

HOMOGENEOUS BOUNDARY-VALUE PROBLEMS

Kirchhoff's solution to the wave equation can be applied to arbitrary wing plan forms undergoing arbitrary maneuvers. The boundary values for such general problems, however, usually lead to the development of double integral equations which are difficult to solve. As is usual in such cases, there are many special types of plan forms and maneuvers which lead to boundary-value problems that are simpler to analyze. An important class of these simplified problems is that arising from homogeneous boundary conditions.

Let $\varphi(x,y,z,t)$ be a solution to equation (9). In certain special cases this can be written $\varphi=(t)^n\varphi_0\left(\frac{x}{t},\frac{y}{t},\frac{z}{t}\right)$, in which case φ is called a homogeneous function of degree n. The number of variables affecting φ_0 is only three as compared to the four which are necessary to determine φ. If, therefore, a partial differential equation can be set up for φ_0, it will contain one less mathematical "dimension" than the equation for φ. Following this observation it is necessary to proceed in two directions; one to find the partial differential equation for φ_0, and the other to find the physical problem and consequent boundary values leading to a homogeneous flow field. The latter path will be first explored.

First, consider an example of a homogeneous boundary-value problem. Suppose that a rectangular flat plate starts suddenly from rest and moves forward at an angle of attack at a supersonic Mach number M_0. At "time" t_1 the initial spherical wave generated by the forward right-hand corner has traveled outward to a radius t_1 and, at "time" $2t_1$, to a radius $2t_1$. Figure 7 indicates the traces of these spheres in the $z=0$ plane together with the original and present position of the wing leading edge. Let the points P_1 and P_2 be located on the same rays through the origin of the circles and the wing corners. The problem is to find the pressures at P_1 and P_2.

It is apparent that, if every dimension in the figure involving P_2 is divided by $2t_1$ and every dimension in the figure involving P_1 is divided by t_1, the two figures will be similar in every respect and point P_1 will coincide with point P_2.

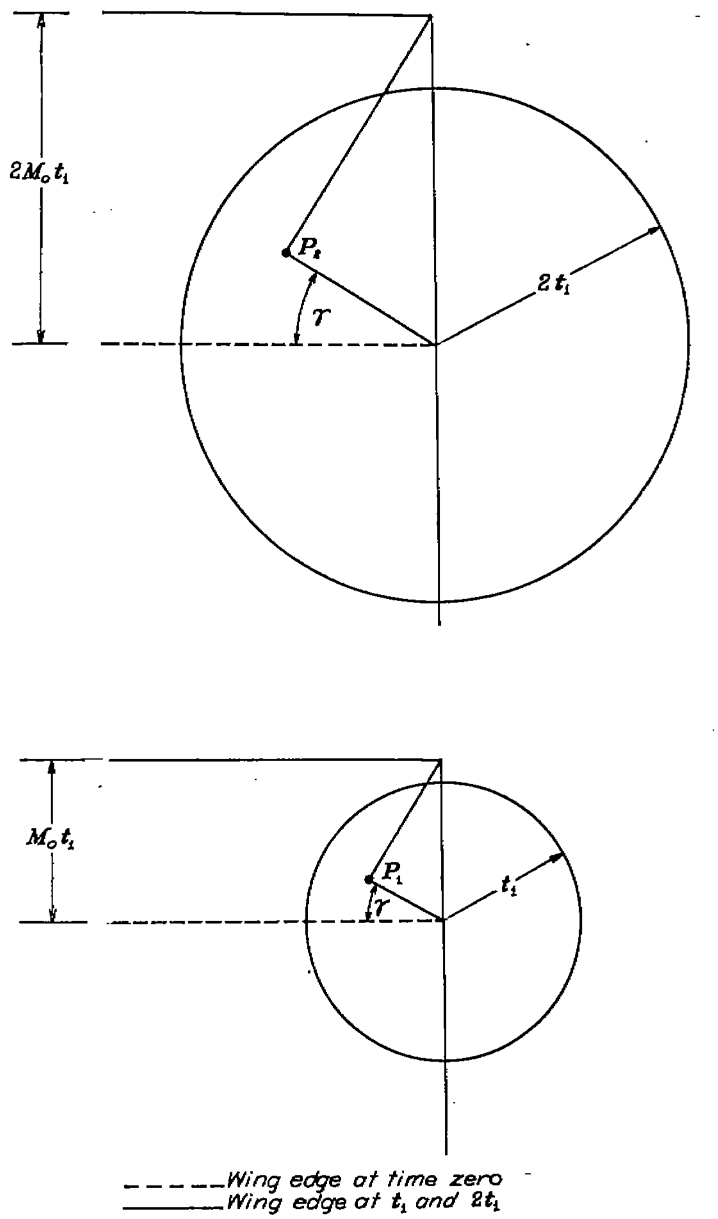

FIGURE 7.—Geometric relationship for homogeneous flow.

Since the vertical velocity w_0 is constant over the plan form, a simple change in scale has made the boundary conditions for both problems identical. But this means that the solutions at P_1 and P_2 are identical since the wave equation is invariant to change in scale. Hence, in regions of a rectangular wing unaffected by the waves from the trailing edge, the pressure can be written

$$\frac{\Delta p}{q_0}(x,y,z,t)=\frac{\Delta p}{q_0}\left(\frac{x}{t},\frac{y}{t},\frac{z}{t}\right) \tag{22}$$

and the pressure is a homogeneous function of degree zero. A generalization of this example is contained in the following statement:

(1) The pressure in any region affected by only two intersecting edges of a straight-sided flat plate traveling at a uniform subsonic or supersonic speed is homogeneous and of degree zero (i. e., satisfies equation (22)).

Consider as another example the case of a flat rectangular wing traveling forward at a subsonic or supersonic speed and rolling about one edge, taken to be coincident with the x axis. The argument follows the same lines as before, and again a change in scale, proportional to the time, makes the geometry of the wing-wave combinations identical (in regions affected by only two intersecting edges) for different times. The boundary values over the wings will not be the same, however, unless the slope of the w_0 distribution is adjusted in each case. But w_0 can be adjusted by reducing it an amount proportional to the distance from the axis of rotation. The boundary-value problems are then similar for different values of time. Finally, therefore, the pressure can be written

$$\frac{\Delta p}{q_0}(x,y,z,t)=y\,\frac{\Delta p}{q_0}\left(\frac{x}{t},\frac{y}{t},\frac{z}{t}\right) \tag{23}$$

which is a homogeneous function of degree one. A generalization of this example is expressed as follows:

> (2) The pressure in any region affected by only two intersecting edges of a straight-sided flat plate traveling at a uniform subsonic or supersonic speed and rotating at a constant rate of pitch or roll is homogeneous and of degree one (i. e., satisfies equation (23)).

It should be noted that both (1) and (2) are equally true for the steady-state case when all transient effects have disappeared. In supersonic wing theory they lead to conical and quasi-conical flows, respectively while in the subsonic case they lead to flows about wings having infinite chordwise extent. In general, homogeneous flow occurs when the boundary conditions after a change in scale are proportional to their original values.

Consider next the modification of the basic partial differential equation (equation (9)) under the assumption that the flow is homogeneous. If the pressure is given by a function that is homogeneous and of degree zero, then, by equation (12), the velocity-potential function will be homogeneous and of degree one. If the notation

$$\left.\begin{aligned}&\frac{x}{t}=x_0,\ \frac{y}{t}=y_0,\ \frac{z}{t}=z_0\\&\varphi(x,y,z,t)=t\Phi(x_0,y_0,z_0)\end{aligned}\right\} \tag{24}$$

is used, then equation (9) becomes

$$(1-x_0^2)\Phi_{x_0x_0}+(1-y_0^2)\Phi_{y_0y_0}+(1-z_0^2)\Phi_{z_0z_0}-2x_0y_0\Phi_{x_0y_0}-2x_0z_0\Phi_{x_0z_0}-2y_0z_0\Phi_{y_0z_0}=0 \tag{25}$$

and a linear partial differential equation with three independent variables is therefore obtained.

In the general theory of partial differential equations of second order, the character of an equation is determined from the geometric nature of a related quadric surface. The character of equation (25) can be shown from such considerations to depend on the sign of the expression $1-x_0^2-y_0^2-z_0^2$. It is immediately apparent, however, that within the unit sphere in the x_0,y_0,z_0 space the sign of $1-x_0^2-y_0^2-z_0^2$ is everywhere positive and outside the sign is everywhere negative. It follows that outside the unit sphere equation (25) is hyperbolic and inside the unit sphere it is elliptic.

The character of equation (25) is of particular interest since the difficulties inherent in the determination of the solutions can be estimated without actually obtaining the solutions. For example, consider the two configurations shown in figure 8. These wings started moving at $t=0$ with the foremost portion of their leading edges on the y_0 axis and have by now traveled forward at a supersonic speed to attain the positions represented by the figure, the unit circle being in each case the trace of the primary wave from the vertex on the $z=0$ plane. Outside the unit sphere, the governing equation is hyperbolic and the behavior of the flow is similar to that in steady-state supersonic-wing problems. Inside the unit sphere, on the other hand, the character of equation (25) is elliptic.

It is instructive to notice that this entire development has a direct analogue in the study of three-dimensional, steady-state, supersonic wings. In that case the original equation is the three-dimensional wave equation

$$\varphi_{xx}-\varphi_{yy}-\varphi_{zz}=0 \tag{26}$$

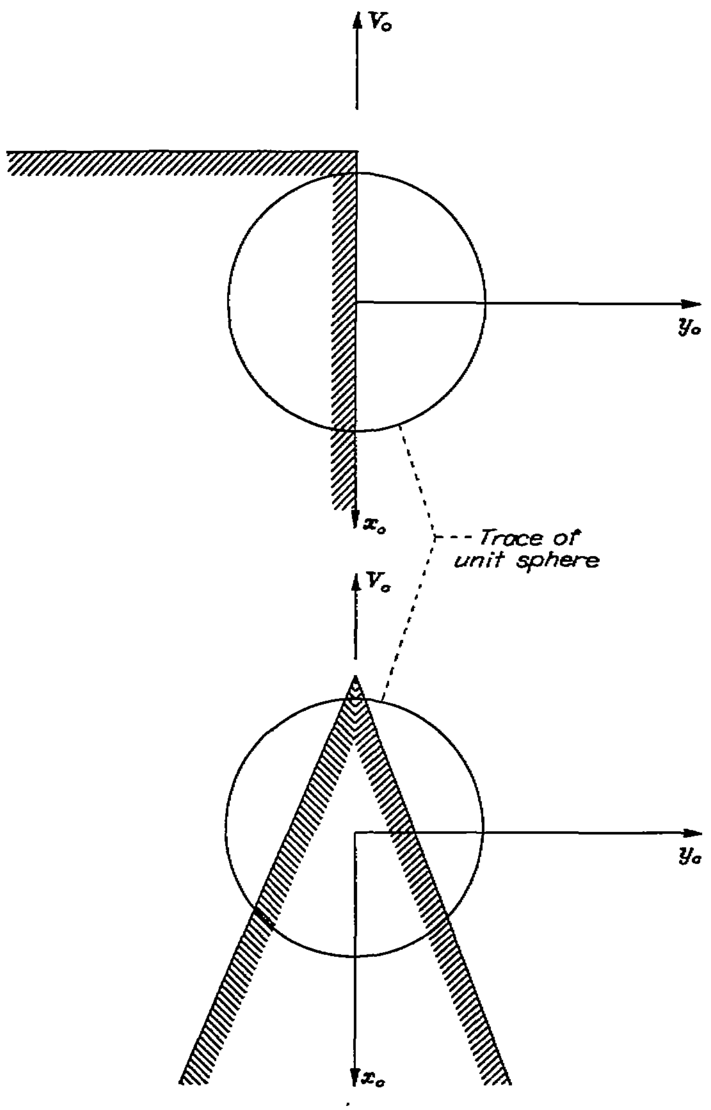

FIGURE 8.—Homogeneous flow fields.

By considering the velocity potential to be homogeneous and of degree one, Busemann in reference 11 was able to introduce the transformations

$$y_0=\frac{y}{x} \qquad z_0=\frac{z}{x}$$

$$\varphi(x,y,z)=x\Phi\,(y_0,z_0)$$

and transform equation (26) to the form

$$(1-y_0^2)\,\Phi_{y_0y_0}+(1-z_0^2)\,\Phi_{z_0z_0}-2y_0z_0\Phi_{y_0z_0}=0 \tag{27}$$

which is the two-dimensional form of equation (25). Flows governed by equation (27) have become known as conical flows. A study of equation (27) shows it to be elliptic inside and hyperbolic outside the unit circle. In this case, however, the equation has only two independent variables so that once the equation has been transformed (by means of the Tschapligin transformation) to the two-dimensional form of Laplace's equation solutions are not difficult to find.

The simplification of the four-dimensional theory brought out by the introduction of homogeneous flow was more apparent than real since the resulting partial differential equation, although containing one less dimension, was unwieldy.

BOUNDARY-VALUE PROBLEMS INVOLVING NONINTERACTING SURFACES

Another class of wing problems which is simplified both in theory and in practice by reasoning from physical knowledge of the flow behavior is that in which the wing has a supersonic edge (i. e., an edge which is traveling with a supersonic normal component of velocity).

When the acoustic plan form is affected only by a supersonic edge, it is apparent that the flow on the upper surface of the wing is independent of that on the lower surface. Hence the solution to such problems can always be written in terms only of sources as follows:

$$\varphi=-\frac{1}{2\pi}\int_{S_a}\int\frac{1}{r_0}\left[\frac{\partial\varphi}{\partial z_1}\right]_r dS \tag{28}$$

where $\partial\varphi/\partial z_1=w_u(x_1,y_1)=V_0\lambda_u(x_1,y_1)$, λ_u being the local slope of the surface in the direction of V_0. Since the equation (28) is equally valid for symmetrical nonlifting surfaces and lifting plates, its value and simplicity are evident.

If the wing plan form is further specialized by having not only supersonic leading edges, but also having a straight trailing edge perpendicular to the direction of motion, additional simplifications can be used.[9] Consider, for example, the two-dimensional wing (a) in figure 9. Let this wing have an angle of attack $\alpha(t)$ which varies with time in an arbitrary manner. There results from such an angle-of-attack variation a certain lift which also varies with time. Hence, if L^* represents the total lift on an airfoil of very high aspect ratio and $c_{l_\alpha}{}^*$ represents the section lift-curve slope, then [10]

$$\frac{L^*}{q_0\alpha}=c\,c_{l_\alpha}{}^*(c,t)\,(\text{span})$$

Next it is clear by reason of symmetry that the total lift on wings (b) and (c) in the figure are equal. Then, since the

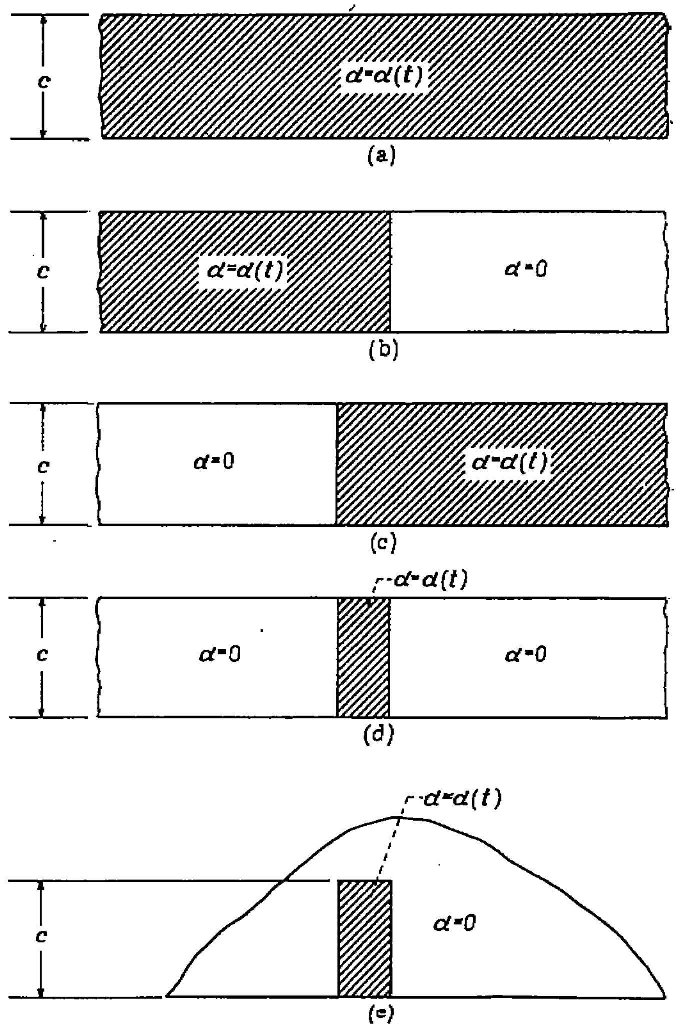

FIGURE 9.—Development of elemental lifting strip.

analysis is based on a linear partial differential equation, by superposition principles the total lift on wing (b) or (c) is just half of that on wing (a). In another sense, the lift coefficient for the whole wing based on the deflected area is the same for all three cases. A suitable superposition of wings (a), (b), and (c) will give wing (d), which then has the same lift coefficient based on deflected area. Finally, because of the supersonic stream, wing (e) can be obtained from (d), hence it also has the lift coefficient common to the other wings. It is, of course, necessary that the variation of α with the time be the same in each case.

The preceding process can be extended one step farther to the development of the lift due to a single deflected element. By considering figure 10, it can be seen that

$$\frac{L^*}{q_0\alpha}=\frac{c\,c_{l_\alpha}{}^*(c,t)-(c-\Delta c)c_{l_\alpha}{}^*(c-\Delta c,t)}{\Delta c}\Delta S$$

where ΔS is the area of the deflected element and c is the distance from the centroid of ΔS to the trailing edge. By the usual limiting process the latter equation becomes

$$\frac{L^*}{q_0\alpha}=\frac{\partial}{\partial c}\,[c\,c_{l_\alpha}{}^*(c,t)]\,dS$$

[9] The following method simply extends, to include the effects of unsteady motion, a theorem given by Lagerstrom and Van Dyke. (See reference 12.)

[10] The asterisks on quantities indicate that two-dimensional values are taken, or that a high-aspect-ratio wing is considered and tip effects are neglected.

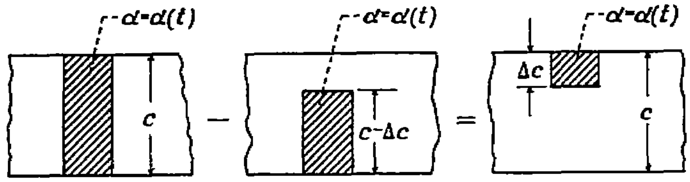

FIGURE 10.—Development of lifting element.

Finally, if a wing is composed of a distribution of these elements, then, for a coordinate system centered at the apex of the wing leading edge, there results

$$C_L=-\frac{1}{S}\int_S\int\alpha(x,y)\frac{\partial}{\partial x}\,[(c_0-x)c_{l_\alpha}{}^*(c_0-x,t)]dydx \qquad (29)$$

where c_0 is the maximum chord (see fig. 11). In the development of equation (29) each element is assumed to have the same variation of motion with time.

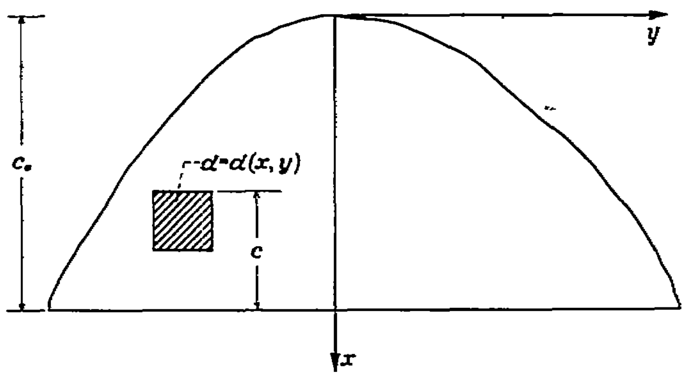

FIGURE 11.—Example of use of lifting element.

Notice that when the wing is a flat plate flying at a steady speed so that all transient effects have disappeared, $c_{l_\alpha}{}^*$ is independent of t and of the chord length, being, in fact, equal to $4/\beta$. Then equation (29) becomes

$$C_L=\frac{4}{\beta S}\int_S\int\alpha(x,y)dxdy=\frac{4\bar{\alpha}}{\beta}$$

where $\bar{\alpha}$ is the average angle of attack of the wing. This result has already been obtained in reference 12. When $\alpha(x, y)$ is independent of x (as for a flat wing sinking or rolling), equation (29) becomes

$$C_L=\frac{1}{S}\int_{-\frac{b}{2}}^{\frac{b}{2}}\alpha(y)\;c\;c_{l_\alpha}{}^*(c,t)dy \qquad (30)$$

where c is the local chord which is, in general, a function of y. Equation (30) simply indicates that longitudinal strip theory is exact for calculating the total lift on such wings.

Finally, notice that the calculation of the unsteady lift on three-dimensional wings with supersonic leading edges and straight trailing edges perpendicular to the free-stream direction has been reduced to an integration involving the relatively simple results for a two-dimensional wing undergoing the same unsteady motion. For example, the lift on a flat unyawed triangular wing with supersonic leading edges rising and sinking with a harmonic motion can be computed from a single integration of the results presented in reference 5.

There is another simplified method for obtaining the total lift and moment on a wing with all supersonic edges and a straight trailing edge. In this presentation it will be assumed that the trailing edge is normal to the free stream. However, since the wave equation is invariant to a rotation, it will be apparent that the solution can be generalized to include a straight, supersonic trailing edge yawed with respect to the free stream.

Consider equation (9) and integrate each term with respect to y between the limits minus and plus infinity.[11] There results the equation

$$\int_{-\infty}^{\infty}\frac{\partial^2\varphi}{\partial x^2}dy+\int_{-\infty}^{\infty}\frac{\partial^2\varphi}{\partial y^2}dy+\int_{-\infty}^{\infty}\frac{\partial^2\varphi}{\partial z^2}dy-\int_{-\infty}^{\infty}\frac{\partial^2\varphi}{\partial t^2}dy=0$$

If $y=y_l(x, z, t)$ and $y=y_r(x,z,t)$ are the equations of the Mach waves streaming back from the leading edges on the left and right sides of the wing, respectively (see fig. 12), then, since φ is continuous across these waves but φ_x, φ_y, φ_z, and φ_t are not,

$$\frac{\partial^2}{\partial x^2}\int_{y_l}^{y_r}\varphi dy=\frac{\partial y_r}{\partial x}u_r-\frac{\partial y_l}{\partial x}u_l+\int_{y_l}^{y_r}\frac{\partial^2\varphi}{\partial x^2}dy$$

where u_r and u_l are the values of u on the interior faces of the right and left Mach waves, respectively, and

$$\int_{y_l}^{y_r}\frac{\partial^2\varphi}{\partial y^2}dy=v_r-v_l$$

Values of the terms involving φ_z and φ_t are similar to those involving φ_x so that finally, if

$$\Phi=\int_{y_l}^{y_r}\varphi\,dy \qquad (31)$$

then

$$\frac{\partial^2\Phi}{\partial x^2}+\frac{\partial^2\Phi}{\partial z^2}-\frac{\partial^2\Phi}{\partial t^2}=\left(\frac{\partial y_r}{\partial x}u_r+\frac{\partial y_r}{\partial z}w_r-\frac{\partial y_r}{\partial t}\varphi_t-v_r\right)-\left(\frac{\partial y_l}{\partial x}u_l+\frac{\partial y_l}{\partial z}w_l-\frac{\partial y_l}{\partial t}\varphi_t-v_l\right) \qquad (32)$$

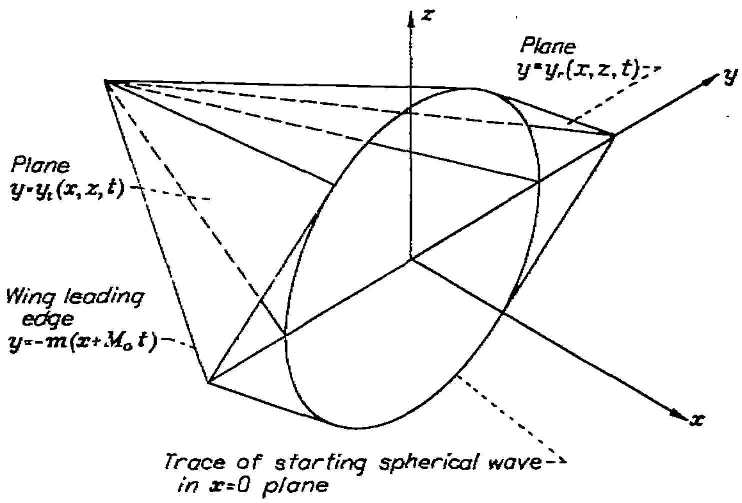

FIGURE 12.—Forward portion of Mach wave system for a supersonic-edged, triangular wing.

[11] The basic idea for this solution was given by P. A. Lagerstrom in his lectures at the California Institute of Technology.

The terms enclosed within the parentheses in the last equation combine internally so that each is zero. For the case of interest here, this is not difficult to show. Consider, for example, the Mach wave streaming from the right edge. Then, since the equation of this wave is

$$y_r = -z\sqrt{\beta^2 m^2 - 1} + mx + mM_0 t$$

and the value of the potential is the steady-state two-dimensional value given by the expression

$$\varphi_r = -w_u \frac{m(x+M_0 t) - y - z\sqrt{\beta^2 m^2 - 1}}{\sqrt{\beta^2 m^2 - 1}}$$

the term

$$\left(\frac{\partial y_r}{\partial x} u_r + \frac{\partial y_r}{\partial z} w_r - \frac{\partial y_r}{\partial t} \varphi_t - v_r\right)$$

becomes

$$-w_u\left(m\frac{m}{\sqrt{\beta^2 m^2 - 1}} + \sqrt{\beta^2 m^2 - 1} - \frac{m^2 M_0^2}{\sqrt{\beta^2 m^2 - 1}} + \frac{1}{\sqrt{\beta^2 m^2 - 1}}\right)$$

and this is identically zero.[12] Finally, therefore, equation (9) has been reduced in terms of equation (31) to

$$\Phi_{tt} - \Phi_{xx} - \Phi_{zz} = 0 \tag{33}$$

The boundary condition in terms of Φ for a triangular wing with supersonic edges is given by

$$\left.\frac{\partial \Phi}{\partial z}\right|_{z=0} = \frac{\partial}{\partial z}\int_{y_l}^{y_r} \varphi\, dy = \int_{y_l}^{y_r} \left.\frac{\partial \varphi}{\partial z}\right|_{z=0} dy = \int_{y_l}^{y_r} w_u\, dy \tag{34}$$

where w_u is the vertical induced velocity in the plane of the triangular wing. The derivative with respect to z can be carried through the integral sign because the extra terms involving the value of φ at y_l and y_r vanish. In fact, since equation (34) applies to the $z=0$ plane, the limits y_l and y_r can be replaced with the expressions for the left and right leading edges of the triangular wing, respectively. The boundary condition expressed by equation (34), used in conjunction with equation (33), suggests a problem exactly like those posed by lifting surfaces in steady-state wing theory; in fact, the problem of a wing tip of specified camber in a free stream at Mach number $\sqrt{2}$. Figure 13 shows a lifting surface in the x,t plane. The solution for the potential Φ in the steady-state problem can be written

$$\Phi|_{z=0} = -\frac{1}{\pi}\int_\sigma\int \frac{\left.\frac{\partial \Phi}{\partial z}\right|_{z=0}}{\sqrt{(t-t_1)^2 - (x-x_1)^2}}\, dt_1 dx_1$$

where σ is the area on the wing plan form in figure 13 that is included in the forecone $(t-t_1)^2 = (x-x_1)^2$.

Now from equation (12) we have

$$\int_{-s}^{s} \frac{\Delta p}{q_0}\, dy = \frac{4}{V_0 M_0} \left.\frac{\partial \Phi}{\partial t}\right|_{z=0}$$

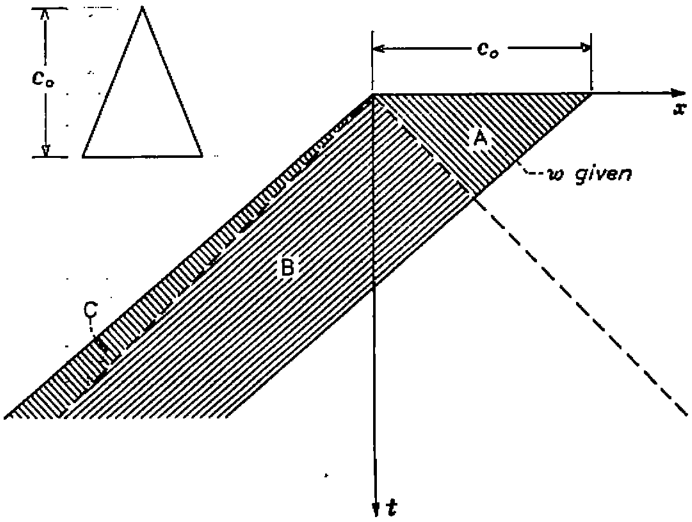

FIGURE 13.—Region of xt plane in which boundary conditions for Φ are known.

where s is the local semispan of the triangular wing. This equation shows how the solution to the lifting surface problem in Φ will aid in the solution of the unsteady problem, for the unsteady lift on the triangular wing is given by

$$C_L = \frac{1}{S}\int_0^{c_0} dx \int_{-s}^{s} \frac{\Delta p}{q_0}\, dy = \frac{4}{SM_0 V_0}\int_0^{c_0} \left.\frac{\partial \Phi}{\partial t}\right|_{z=0} dx$$

where S is the area of the triangular wing. It is therefore seen to be convenient to evaluate the quantity $\left.\frac{\partial \Phi}{\partial t}\right|_{z=0}$, given by

$$\left.\frac{\partial \Phi}{\partial t}\right|_{z=0} = -\frac{1}{\pi}\frac{\partial}{\partial t}\int_\sigma\int \frac{\left.\left(\frac{\partial \Phi}{\partial x}\right)\right|_{z=0}}{\sqrt{(t-t_1)^2 - (x-x_1)^2}}\, dt_1 dx_1 \tag{35}$$

The pitching-moment coefficient for the triangular wing in unsteady motion can be evaluated similarly. Specific applications of this method will be found in a subsequent section.

TWO-DIMENSIONAL BOUNDARY-VALUE PROBLEMS

The simplification brought about when the flow is independent of one dimension is obvious. In such cases, the three-dimensional wave equation (9) reduces immediately to the two-dimensional wave equation. Typical examples of this type of problem can be constructed by considering flat plates which start suddenly at $t=0$ and travel thereafter at constant supersonic velocities. Two examples, one a corner of a rectangular wing and the other a triangular wing, are shown in figure 14. After time $t=0$, the edges of the wings send out cylindrical waves and the outer boundaries of these waves at time t are shown as dashed lines parallel to the edges in question. Since points in regions 1 and 2 are affected only by a single edge, the wave phenomena in these regions are cylindrical, and the physical quantities are in both cases independent of distance parallel to the edge which acts as their generator. Hence, the flow field in these regions is two-dimensional. (Region 3, incidentally, is independent of distance in both x and y directions and is, therefore, one-dimensional.)

[12] It is not necessary to perform a direct calculation in order to prove the above result for arbitrary plan forms. The terms in parentheses in equation (32) represent the directional derivative of the velocity potential taken along the so-called "conormal" of the foremost disturbance surface. Since φ is constant on the surface, and since the conormal lies along the surface, the terms in parentheses are zero.

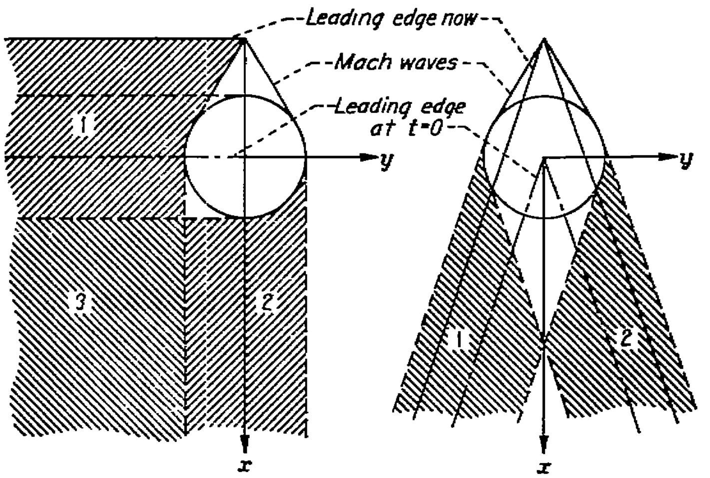

FIGURE 14.—Cases of two-dimensional flow fields.

Solutions to the two-dimensional unsteady problems are sometimes especially easy to find because of the analogy they have with three-dimensional, steady-state, lifting-surface problems. For example, consider an infinitely long unyawed wing which starts from rest and travels forward at a velocity V_0 which may or may not be a function of time. The trace of this wing in the x, t plane is like that shown in figure 15. (In the figure shown, the wing velocity is varying and is always less than the speed of sound.) The boundary conditions are that φ_z is specified over the shaded area and the loading $\Delta\varphi_t$ is zero everywhere except within the shaded area. But if x is replaced by y and t by x, these boundary conditions are exactly the same as those for a plate of known camber and angle of attack, with a plan form as indicated by the shaded area, placed in a free stream directed along the positive x axis at a Mach number equal to $\sqrt{2}$. The solution for the one problem may be used, therefore, as a solution to the other with only a change in notation.

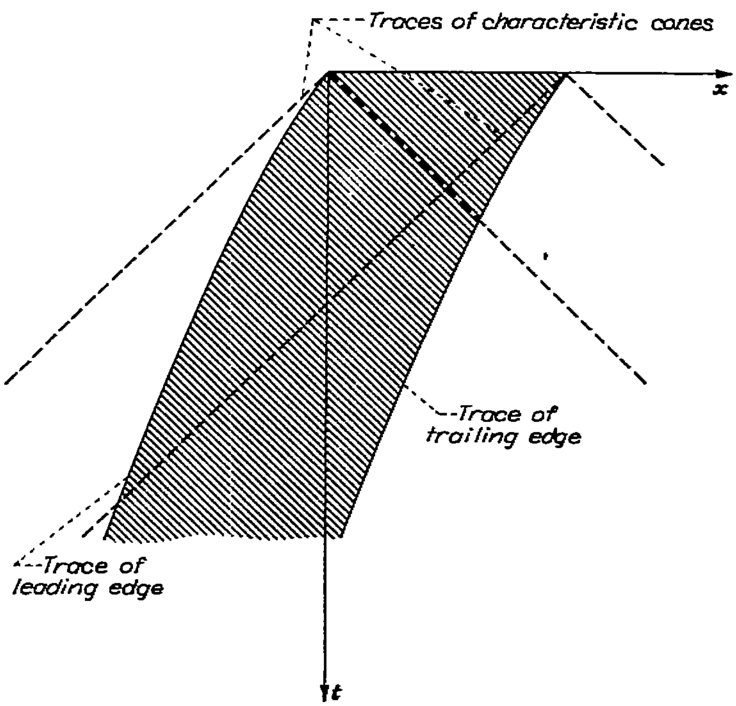

FIGURE 15.—Decelerating wing in xt plane.

BOUNDARY CONDITIONS FOR VERY SLENDER WINGS

When the wing plan form is slender in the sense that its length in the streamwise direction is large compared to its span, an estimation of the loading on it can be obtained by neglecting in the partial differential equation the gradient of the induced velocity component in the stream direction. Thus, if the wing is moving in the negative x direction, equation (9) reduces to

$$\varphi_{yy}+\varphi_{zz}=\varphi_{tt} \tag{36}$$

which is again the wave equation but in two space dimensions. Since equation (36) is independent of x, study can be made independently in each plane x=constant. This is an extension of steady-state slender wing theory, see, e. g., reference 13. Figure 16 (a) shows a typical section in the yt plane. If the wing is a flat plate at a constant angle of attack,

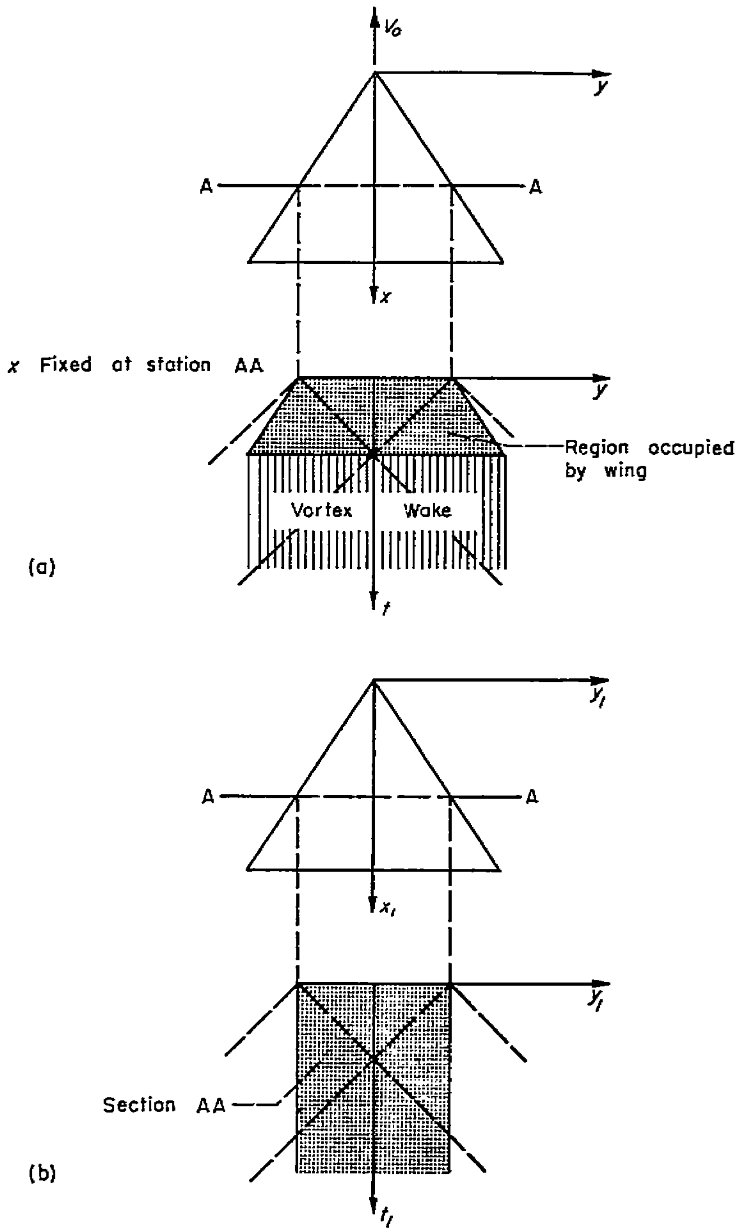

(a) Axes fixed relative to still air at infinity.
(b) Axes fixed on wing.

FIGURE 16.—Slender wing in unsteady flow.

the value of φ_z over the part of the yt plane occupied by the wing is a constant and the jump in φ across the vortex wake must be consistent with its value at the wing trailing edge. The analogy with three-dimensional, steady-state, supersonic, lifting surface theory is apparent.

There is another way by means of which the effects of unsteady motion on slender wing pressures can be estimated. If instead of using the stationary $xyzt$ coordinate system, the reference axes are fixed on the wing by the simple set of transformations

$$x_1=x+M_0t$$
$$t_1=t$$
$$y_1=y$$
$$z_1=z$$

equation (9) becomes

$$(1-M_0^2)\varphi_{x_1x_1}-2M_0\varphi_{x_1t_1}+\varphi_{y_1y_1}+\varphi_{z_1z_1}=\varphi_{t_1t_1}$$

Again, if the induced velocity components in the stream direction are neglected, the simplified equation

$$\varphi_{y_1y_1}+\varphi_{z_1z_1}=\varphi_{t_1t_1}$$

results. The latter equation is identical in form to equation (36). However, now the axes are fixed on the wing and a typical section in the y_1t_1 plane is similar to that shown in figure 16 (b). In this case, a flat plate wing is represented by a constant value of φ_{z_1} over the entire shaded area in the figure and elsewhere φ must be continuous.[13]

TWO-DIMENSIONAL UNSTEADY INCOMPRESSIBLE FLOW

The analogy between two-dimensional unsteady and three-dimensional steady flow includes the case of a two-dimensional, unsteady, incompressible flow field the analog of which is a three-dimensional, steady flow field having a free-stream Mach number equal to 1. This can be demonstrated by inspecting equation (8). Since the flow is two-dimensional and since for an incompressible medium the speed of sound a_0 is infinite, the basic equation governing the flow can be written

$$\varphi_{xx}+\varphi_{zz}=0$$

It must be remembered, however, that time still appears in the boundary conditions and in the equation for the loading coefficient which, according to equation (12), can be written

$$\frac{\Delta p}{q_0}=\frac{4}{V_0^2}\frac{\partial\varphi}{\partial t'}$$

Hence, the basic partial differential equation and the expression for the loading coefficient are the same, except for a change in notation, as those governing three-dimensional, steady-state problems when $M_0=1$.

If a two-dimensional wing in an incompressible fluid starts from rest and travels forward at a speed V_0, the trace of the wing is as shown in figure 17. The essential difference

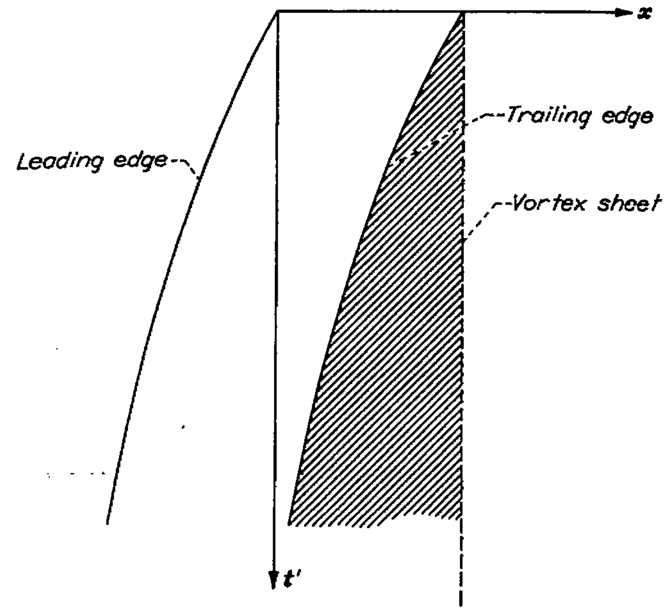

FIGURE 17.—Two-dimensional wing in xt' plane; $M_0=0$.

between this problem and the more general case of two-dimensional compressible flow lies in the fact that in this case the traces of the characteristic cones are normal to the t' axis. The boundary conditions are therefore satisfied along lateral strips and, in lifting-surface terminology, the analysis corresponds to slender-wing theory. These latter methods are well established and in reference 13, for example, the manner in which the Kutta condition is imposed is discussed in some detail. The trailing vortex sheet for the lifting wing has the same distribution of vorticity that exists behind the unsteady two-dimensional airfoil and the rolling up of the vortex sheet can be studied from either standpoint.

PART III—SOME APPLICATIONS OF THE METHOD

STARTING LIFT OF A WING

One of the simplest and yet most general results which can be derived on the basis of the present theory is the initial value of pressure on a wing surface starting suddenly from rest with a velocity V_0. The discussion will be made for a wing without thickness although the method will be seen to apply to the thickness case as well.

Consider a surface with a plan form as indicated in figure 18. The acoustic plan form of a point $P(x,y)$ on the surface is a small circle of radius t. Since no point on the wing outside this circle can influence the pressure at P, the upper surface is independent of the lower surface, except for a band of width t around the edge of the wing. It is, therefore, evident that the boundary-value problem to be solved has been treated in the section Boundary-Value Problems Involving Noninteracting Surfaces. The solution follows directly from equation (28) and can be written

$$\varphi=-\frac{1}{2\pi}\int_{S_a}\int\frac{1}{r_0}\left[\frac{\partial\varphi}{\partial z_1}\right]_r dS$$

[13] The analogous problem in steady-state wing theory is that of a low-aspect-ratio, rectangular, flat plate in a free stream having a Mach number equal to $\sqrt{2}$.

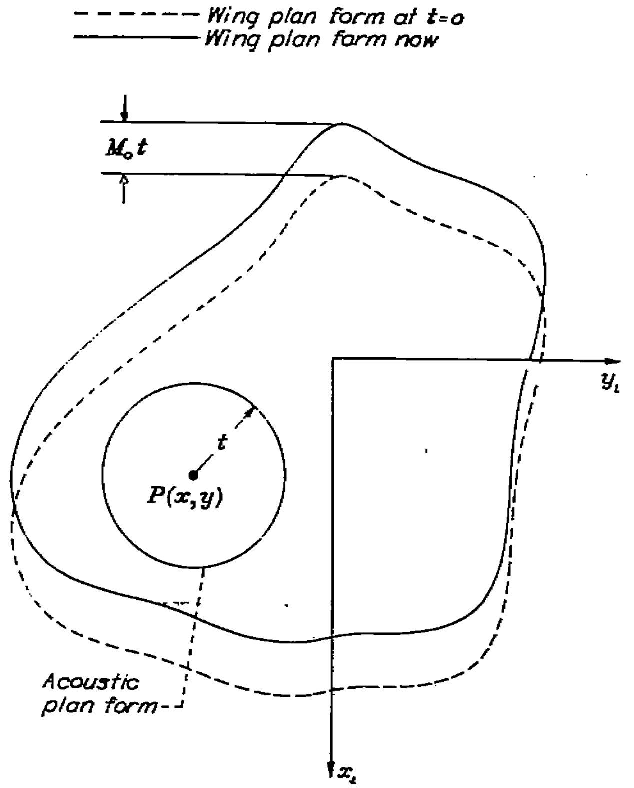

FIGURE 18.—Acoustic plan form at start of motion.

Using a polar coordinate system defined by

$$x-x_1=r\cos\theta$$
$$y-y_1=r\sin\theta$$
$$dx_1\,dy_1=r dr d\theta$$

there results [14]

$$\varphi\approx-\frac{w_u(x,y)}{2\pi}\int_0^{2\pi}d\theta\int_0^t dr=-tw_u(x,y)$$

so that

$$\left(\frac{\Delta p}{q_0}\right)_{t=0}=+\frac{4}{V_0M_0}\left(\frac{\partial\varphi}{\partial t}\right)_{t=0}=-\frac{4w_u(x,y)}{V_0M_0}$$

If $\alpha=-w_u(x,y)/V_0$ is the local slope of the wing, the expression for load coefficient becomes

$$\left(\frac{\Delta p}{q_0}\right)_{t=0}=\frac{4\alpha(x,y)}{M_0}$$

The starting value of lift coefficient can, therefore, be written

$$C_L=\frac{4\bar{\alpha}}{M_0}$$

where $\bar{\alpha}$ is the average angle of attack of the surface defined by

$$\bar{\alpha}=\frac{1}{S}\int_{S_u}\int\alpha\,dx\,dy$$

S being the area of the wing plan form.

INDICIAL FUNCTIONS FOR A TWO-DIMENSIONAL FLAT PLATE, $M_0=0$

The basic partial differential equation governing an unsteady flow field in the two-dimensional incompressible case is Laplace's equation in two dimensions

$$\varphi_{xx}+\varphi_{zz}=0 \qquad (37)$$

where x is distance along the chord and z is height above the plane of the wing. It was also pointed out in Part I that the boundary-value problems arising in the study of the unsteady, two-dimensional plate flying in an incompressible medium were directly analogous to those which are studied in three-dimensional, steady-state, lifting-surface theory under the classification "slender-wing theory." This analogy is useful since well-established concepts in one field can be immediately carried over into the other. It should be mentioned, however, that the subsequent treatment of the incompressible case is not intended to be an improvement on Wagner's original derivation (see reference 14) but rather it is a rederivation along lines that will be used later in the analysis of the compressible case.

The initial pulse.—The first analogy with slender-wing theory which will be used concerns the initial pulses that occur in the values of lift and pitching moment. It is a well-known result (reference 15) that the total lift, as given by slender-wing theory, on the wing shown in figure 19 (a) is a function only of the maximum span and the value of w_u along the section of maximum span (section AA). It is, therefore, independent of the wing twist and leading-edge shape ahead of section AA. This concept has been extended in slender-wing theory to the extreme case shown in figure 19 (b) of a rectangular wing. The lift on such a wing is concentrated entirely along the leading edge and is a function only of the span of that edge and the value of w_u there. By the analogy existing between the two theories, therefore, it is evident that the solution to the indicial problems in two-dimensional, incompressible, unsteady flow (fig. 19 (c)) will contain a pulse at $t'=0$.

The evaluation of this pulse will be treated briefly. A solution to equation (37) for the vertical induced velocity in the $z=0$ plane can be written in terms of the jump in u across the $z=0$ plane (see reference 13); thus, for the shaded area in figure 20 this is

$$w_u(x)=-\frac{1}{2\pi}\int_{-a}^{b}\frac{\Delta u(x_1)}{x-x_1}\,dx_1 \qquad (38)$$

The general inversion of equation (38) can be written

$$\Delta u(x)=\frac{A}{\pi\sqrt{(x+a)(b-x)}}+\frac{2}{\pi\sqrt{(x+a)(b-x)}}\int_{-a}^{b}\frac{w_u(x_1)}{x-x_1}\sqrt{(x_1+a)(b-x_1)}\,dx_1 \qquad (39)$$

where

$$A=\int_{-a}^{b}\Delta u\,dx$$

[14] The mean value theorem gives $\varphi=-\frac{w_u(\xi,\eta)}{2\pi}\int\int_{S_u}\frac{dS}{r_1}$ where ξ and η lie somewhere in S_u. Hence, as t approaches 0, ξ and η approach x and y, respectively.

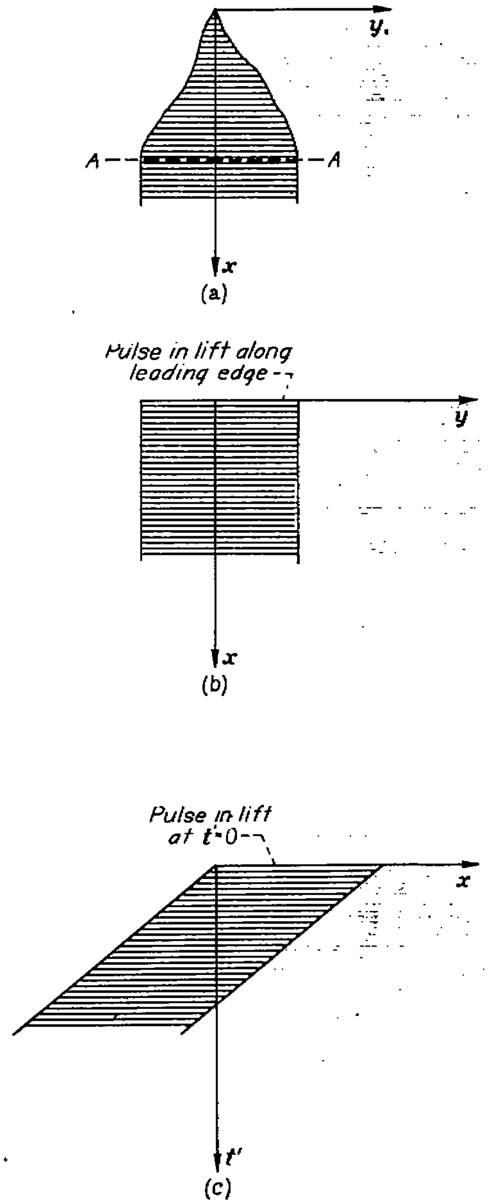

FIGURE 19.—Lift pulses in slender-wing theory.

In the present case A is zero, since $\Delta\varphi$ is zero at $x=-a$ and $x=b$, and an integration of both sides of equation (39) with respect to x between the limits b and x gives

$$\Delta\varphi(t',x)=-\frac{4}{\pi}\int_{-a}^{b} w(t',x_1)\, ln\frac{\sqrt{(b-x_1)(a+x)}+\sqrt{(a+x_1)(b-x)}}{\sqrt{(x-x_1)(a+b)}}\, dx_1$$

Adoption of the notation

$$\nu(t',x_1)+\text{constant}=\int w(t',x_1)dx_1$$

and integration by parts leads to the equation (since

$\int_{-a}^{b}\frac{dx_1}{(x-x_1)\sqrt{(b-x_1)(a+x_1)}}$ vanishes if $b>x>-a$)

$$\Delta\varphi=-\frac{2\sqrt{(b-x)(a+x)}}{\pi}\int_{-a}^{b}\frac{\nu(t',x_1)dx_1}{(x-x_1)\sqrt{(b-x_1)(a+x_1)}} \tag{40}$$

The loading can now be determined by using equation (12) (and differentiating with respect to t' rather than t)

$$\frac{\Delta p}{q_0}=\frac{4}{V_0^2}\frac{\partial\varphi}{\partial t'}$$

If the shaded area in figure 20 is allowed to vanish, all the loading accumulates along the x axis in the region $0\leq x\leq c$. Therefore, the integral of the loading with respect to t' over the shaded portion must be considered. The final result for the pulse loading $(\Delta p/q_0)_\delta$ at $t'=0$ can be expressed in terms of the δ function (see list of symbols) as

$$\left(\frac{\Delta p}{q_0}\right)_\delta=-\frac{4\delta(t')}{\pi V_0^2}\sqrt{(c-x)x}\int_0^c\frac{\nu(0,x_1)dx_1}{(x-x_1)\sqrt{(c-x_1)x_1}} \tag{41}$$

The boundary conditions for the sinking and pitching wing given by equations (2) and (3), when inserted into equation (41), yield

$$\left.\begin{aligned}\left(\frac{\Delta p}{q_0\alpha}\right)_\delta&=\frac{4\delta(t')}{V_0}\sqrt{(c-x)x}\\ \left(\frac{\Delta p}{q_0\theta}\right)_\delta&=\frac{(c+2x)\delta(t')}{V_0^2}\sqrt{(c-x)x}\end{aligned}\right\} \tag{42}$$

After integration, the pulse values for lift and pitching moment may also be obtained. Hence,

$$\left.\begin{aligned}(c_{l_\alpha})_\delta&=\frac{\pi c}{2V_0}\,\delta(t')\\ (c_{m_\alpha}{}')_\delta&=-\frac{\pi c}{4V_0}\,\delta(t')\\ (c_{l_q}{}')_\delta&=\frac{\pi c}{4V_0}\,\delta(t')\\ (c_{m_q}{}')_\delta&=-\frac{9}{64}\frac{\pi c}{V_0}\,\delta(t')\end{aligned}\right\} \tag{43}$$

where the primes indicate that the wings are pitching about and the moments are measured about the leading edge. These expressions may be inserted in equations (4) and, since the integrand becomes zero everywhere except at the point $t_1'=t'$, the contributions of the initial pulse to the expressions for the lift and pitching-moment coefficient developed by an arbitrary variation of α and θ with time are

$$c_{l_\delta}=\frac{\pi c}{2V_0}\dot{\alpha}+\frac{\pi c^2}{4V_0^2}\ddot{\theta}$$

$$c_{m_\delta}{}'=-\frac{\pi c}{4V_0}\dot{\alpha}-\frac{9}{64}\frac{\pi c^2}{V_0^2}\ddot{\theta}$$

where $\dot{\alpha}$ and $\ddot{\theta}$ are evaluated at t'.

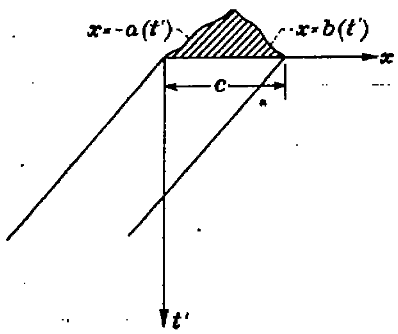

FIGURE 20.—Undegenerate form of initial pulse in lift.

The variation for $t'>0$.—The integral equation (38) is still perfectly valid when applied to the flow field for $t'>0$. It is convenient to rewrite the equation in this case, however, so that the effects of the vorticity on the wing and in the wake are separated. Thus,

$$w_u=-\frac{1}{2\pi}\int_{-V_0t'}^{c-V_0t'}\frac{\Delta u(t',x_1)}{x-x_1}\,dx_1-\frac{1}{2\pi}\int_{c-V_0t'}^{c}\frac{\Delta u^*(x_1)}{x-x_1}\,dx_1 \tag{44}$$

where $\Delta u^*(x_1)$ is the value of Δu in the starting vortex wake. It is independent of t' since its value at all points along the line ab in figure 21 is the same as at the point a.

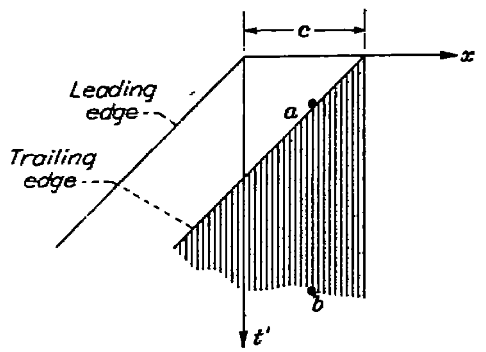

FIGURE 21.—Wing and trailing vortex sheet in xt' plane.

A reduction of equation (44) can be obtained for the case of the sinking wing, where $w_u=-V_0\alpha$, by using the inversion given by equation (39). Thus,

$$\pi\Delta u(t',x)\sqrt{(x+V_0t')(c-V_0t'-x)}=A-\pi(2x+2V_0t'-c)V_0\alpha+\int_{c-V_0t'}^{c}\Delta u^*(x_1)\left[1+\frac{\sqrt{(x_1+V_0t')(x_1-c+V_0t')}}{(x-x_1)}\right]dx_1$$

Since A is given by the relation

$$A=\int_{-V_0t'}^{c-V_0t'}\Delta u(t',x_1)dx_1=-\int_{c-V_0t'}^{c}\Delta u^*(x_1)dx_1$$

it follows that

$$\Delta u(t',x)=-\frac{V_0\alpha(2x+2V_0t'-c)}{\sqrt{(x+V_0t')(c-V_0t'-x)}}+\frac{1}{\pi\sqrt{(x+V_0t')(c-V_0t'-x)}}\int_{c-V_0t'}^{c}\frac{\Delta u^*(x_1)}{x-x_1}\sqrt{(x_1+V_0t')(x_1-c+V_0t')}\,dx_1 \tag{45}$$

According to the Kutta condition $\Delta u(t',x)$ remains finite as x approaches $c-V_0t'$; the integral equation for $\Delta u^*(x_1)$ thus becomes

$$V_0\alpha=-\frac{1}{\pi c}\int_{c-V_0t'}^{c}\Delta u^*(x_1)\sqrt{\frac{x_1+V_0t'}{x_1-c+V_0t'}}\,dx_1 \tag{46}$$

which was derived and studied originally by Wagner (reference 14).

The section lift and pitching moment can be derived in terms of $\Delta u^*(x_1)$ in the following manner. By definition, the section lift l is

$$l=\frac{1}{2}\rho_0V_0^2\int_{-V_0t'}^{c-V_0t'}\frac{\Delta p}{q_0}\,dx=\rho_0\int_{-V_0t'}^{c-V_0t'}\frac{\partial\Delta\varphi}{\partial t'}\,dx \tag{47}$$

Since the value of $\Delta\varphi$ is zero at the leading edge and at the trailing edge is equal to the total circulation Γ, two alternative forms for the lift can be written

$$l=\rho_0V_0\Gamma+\rho_0\frac{d}{dt'}\int_{-V_0t'}^{c-V_0t'}\Delta\varphi(t',x)\,dx \tag{48}$$

and

$$l=\rho_0(c-V_0t')\frac{d\Gamma}{dt'}-\rho_0\frac{d}{dt'}\int_{-V_0t'}^{c-V_0t'}x\,\Delta u(t',x)\,dx \tag{49}$$

By substituting equation (45) into (49) and integrating, it can be shown that

$$l=\pi\rho_0cV_0^2\alpha+\frac{\rho_0cV_0}{2}\int_{c-V_0t'}^{c}\frac{\Delta u^*(x_1)}{\sqrt{(x_1+V_0t')(x_1-c+V_0t')}}\,dx_1 \tag{50}$$

Since the value of $\Delta u^*(x_1)$ has been determined by Wagner, equation (50) can be evaluated to obtain a solution for the section lift. A plot of the section lift coefficient is shown in figure 22. Initially there is the pulse having an intensity defined by equations (43). After the pulse at $t'=0$, the value of the section lift coefficient starts at one-half its asymptotic value. It then increases, slowly approaching its asymptote of $2\pi\alpha$.

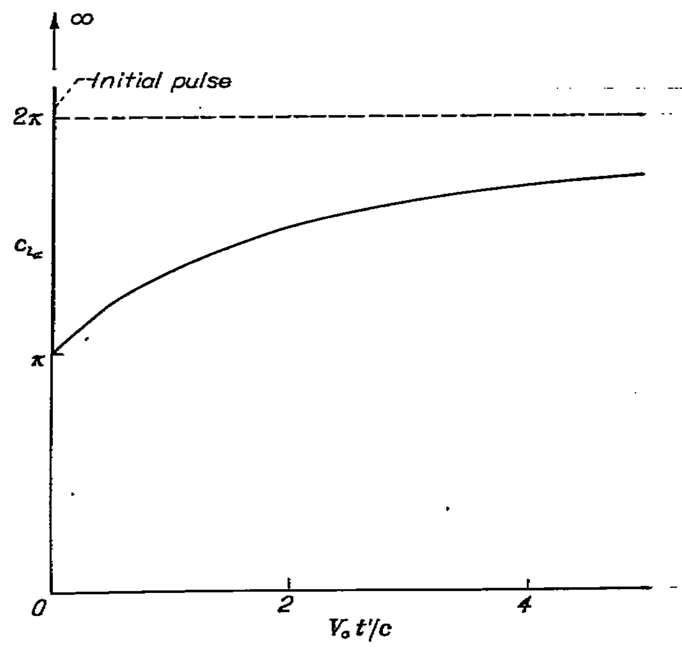

FIGURE 22.—Indicial lift curve for incompressible flow.

By definition, the pitching moment can be written

$$m=-\frac{1}{2}\rho_0V_0^2\int_{-V_0t'}^{c-V_0t'}(V_0t'+x)\frac{\Delta p}{q_0}\,dx$$
$$=-\rho_0\int_{-V_0t'}^{c-V_0t'}(V_0t'+x)\frac{\partial\Delta\varphi}{\partial t'}\,dx \tag{51}$$

where the moment is taken about the leading edge and is positive when the trailing edge is forced down. A development, similar to the one given for the lift, gives

$$m=-\frac{c}{4}l \tag{52}$$

This result, that for $t>0$ the indicial center of pressure remains constant at the quarter chord throughout the motion, is classical.

If the boundary condition for a pitching wing, $w_u=-(x+V_0t')\dot{\theta}$, is substituted into equation (44) and the inversion given by equation (39) is again used, it can be shown in the same manner used in the derivation of equation (46) that for $x=c-V_0t'$ the relation

$$\frac{3}{4}c^2\dot{\theta}=-\frac{1}{\pi}\int_{c-V_0t'}^{c}\Delta u^*(x_1)\sqrt{\frac{x_1+V_0t'}{x_1-c+V_0t'}}\,dx_1$$

applies. This integral equation applies to a wing pitching about its leading edge. If, instead, the wing is pitching about the three-quarter-chord position, an essential simplification is achieved. In this latter case, downwash is given by the expression

$$w_u=-\dot{\theta}\left(x+V_0t'-\frac{3}{4}c\right) \tag{53}$$

and the resulting integral equation becomes

$$0=\int_{c-V_0t'}^{c}\Delta u_3^*(x_1)\sqrt{\frac{x_1+V_0t'}{x_1-c+V_0t'}}\,dx_1 \tag{54}$$

where $\Delta u_3^*(x_1)$ represents the vorticity in the wake following such a motion. The solution to equation (54) is simply

$$\Delta u_3^*(x_1)=0 \tag{55}$$

From equation (55) it follows that the total indicial lift for $t'>0$ on a wing pitching about the three-quarter chord point is zero, and that the wing wake is free of vorticity. Further, it can be shown that the total indicial pitching moment (still measured about the leading edge) is

$$m=-\frac{\rho\pi c^3}{16}V_0\dot{\theta} \tag{56}$$

The transfer of equations (55) and (56) back to the case in which the wing is pitching about its leading edge can be readily accomplished by means of the boundary condition shown in figure 23. Hence, if $(c_{l_q})_{3/4}$ refers to the lift coefficient on a wing pitching about the three-quarter-chord point and $(c_{m_q}{}')_{3/4}$ refers to the pitching-moment coefficient measured about the leading edge of a wing pitching about the three-quarter-chord point, then

$$\left.\begin{aligned}(c_{l_q})_{3/4}&=c_{l_q}{}'-\frac{3}{4}c_{l_\alpha}\\(c_{m_q}{}')_{3/4}&=c_{m_q}{}'-\frac{3}{4}c_{m_\alpha}{}'\end{aligned}\right\} \tag{57}$$

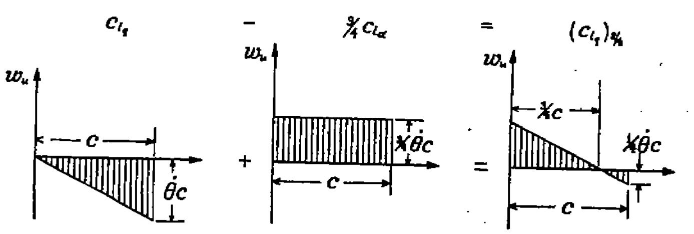

FIGURE 23.—Change in boundary conditions corresponding to change in pitching axis.

By means of equations (52) and (57) the expressions of the three indicial functions, $c_{m_\alpha}{}'$, $c_{l_q}{}'$, and $c_{m_q}{}'$, can all be written in terms of the indicial lift function for $t>0$. Hence,

$$\left.\begin{aligned}c_{m_\alpha}{}'&=-\frac{1}{4}c_{l_\alpha}\\c_{l_q}{}'&=\frac{3}{4}c_{l_\alpha}\\c_{m_q}{}'&=-\frac{3}{16}c_{l_\alpha}-\frac{\pi}{8}\end{aligned}\right\} \tag{58}$$

The variations of the four indicial functions will be shown later in Part IV. For values of $\tau_0(=V_0t'/c)$ larger than those shown in figure 22 the approximate equation suggested in reference 16 can be used, namely,

$$c_{l_\alpha}=2\pi\left[1-\frac{1}{2+\tau_0}\right] \tag{59}$$

This alternative result has, according to reference 16, an error of 2 percent or less for the entire range of time from 0+ to infinity.

INDICIAL FUNCTIONS FOR A TWO-DIMENSIONAL FLAT PLATE, M_0=0.5, 0.8

When the Mach number is no longer small, the analysis in the preceding section must be modified. As an example of this modification, we shall evaluate the indicial response on a sinking wing flying at a Mach number equal to 0.5 and the indicial response on a sinking or pitching wing flying at a Mach number equal to 0.8.

Since the wing is two-dimensional, the partial differential equation governing the flow field (equation (9)) reduces to

$$\varphi_{xx}+\varphi_{zz}=\varphi_{tt} \tag{60}$$

where it must be remembered that the axes are fixed with reference to the still air at infinity and the wing is moving in the $z=0$ plane. The equation for the loading coefficient remains as in equation (12). The analogy which existed in the incompressible case between the theory for the unsteady, two-dimensional wing and slender-wing theory exists in this case between the theory for the unsteady two-dimensional wing and the theory for a steady-state, three-dimensional wing traveling at a supersonic speed. Thus, in the three-dimensional, steady-state case the partial differential equation governing the flow is

$$\varphi_{yy}+\varphi_{zz}=\beta^2\varphi_{xx} \tag{61}$$

and the equation for the loading coefficient is

$$\frac{\Delta p}{q_0}=\frac{4}{V_0}\frac{\partial\varphi}{\partial x} \tag{62}$$

The boundary conditions are in both cases that φ_z is given over a portion of the $z=0$ plane. It is evident by a comparison of equations (60) and (61) and equations (12) and (62) that results from the three-dimensional, supersonic, steady-state case (hereinafter referred to as the steady-state case) can be transferred to the two-dimensional, unsteady case (hereinafter referred to as the unsteady case) simply by replacing x, y, and β in the former case by t, x, and 1, respectively, and by dividing the result for the loading coefficient by M_0.

The analog to the boundary condition for the problem of finding the indicial loading on a two-dimensional wing flying at a subsonic Mach number (fig. 24(a)) is the boundary condition for the problem of finding the loading on a constant-chord, swept-forward wing tip with a subsonic trailing edge such as that shown in figure 24(b). The Mach cones in the steady-state case, traces of which are shown as dotted lines in figure 24(b), become, in the unsteady-state analog, the locus of the sound waves which started at $t=0$ from the leading and trailing edges of the two-dimensional wing (fig. 24(a)). Finally, the analog in the steady-state field of the unsteady wing would be a flat plate for the unsteady sinking wing and a plate with a linear variation of twist for the unsteady pitching wing.

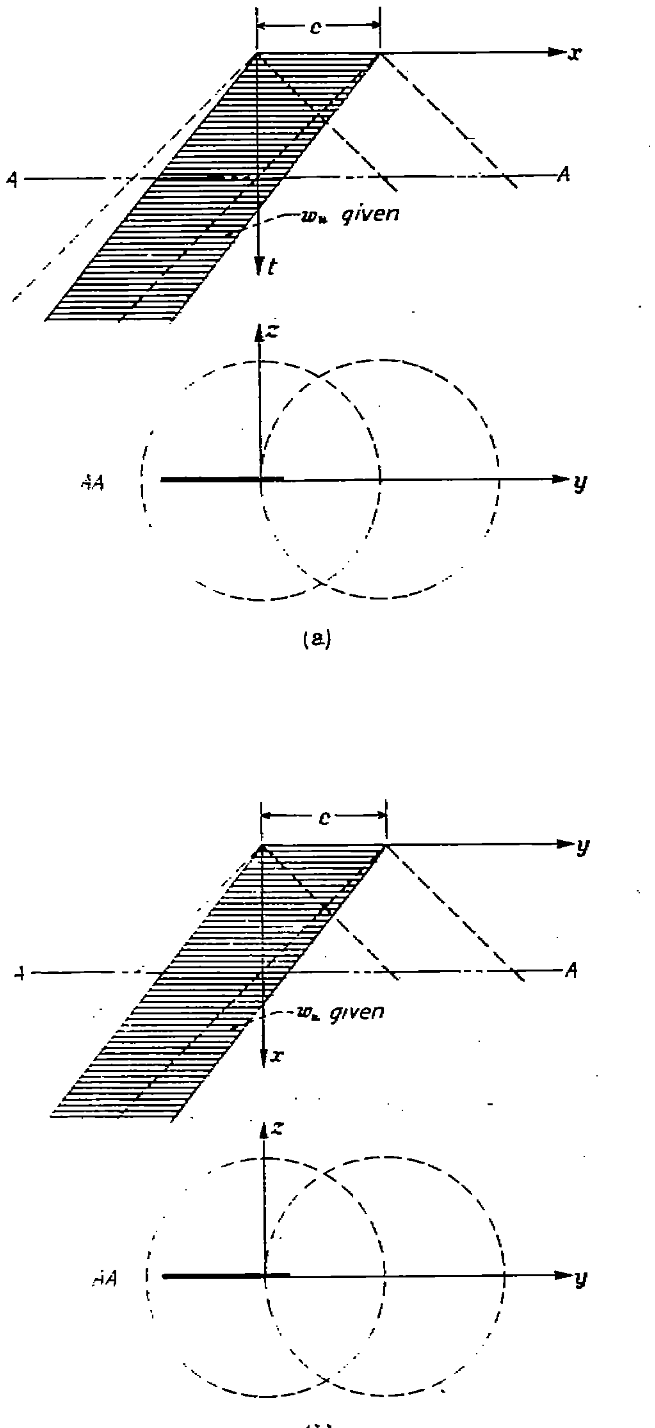

(a) Unsteady case.
(b) Steady-state case.

FIGURE 24.—Boundary conditions for a two-dimensional unsteady wing moving at subsonic speed and the analogous three-dimensional, steady-state wing.

Just as in the section on incompressible flow, the analysis will be divided into two parts. In cases for which $M_0\neq 0$, however, the indicial functions contain no pulse at $t=0$. Hence, the first part of the study will be concerned with the behavior of the indicial functions in an interval for which t is small but finite and the second part, with their asymptotic behavior.

The early stage.—The analog which exists between the steady-state and unsteady cases may be utilized to great advantage since the special methods and techniques developed for the solution of problems in the former case may be applied to the solution of the analogous problems in the latter field. In this manner an exact solution for the loading over the first five regions shown in figure 25 was obtained for a Mach number equal to 0.8, and for all the regions indicated for a Mach number equal to 0.5. Solutions for larger values of the time could also be calculated, but the labor involved in computing such cases becomes prohibitive and, as will be shown later, approximate methods can be developed which extend the solutions for the indicial lift and pitching-moment curves to their asymptotic values.

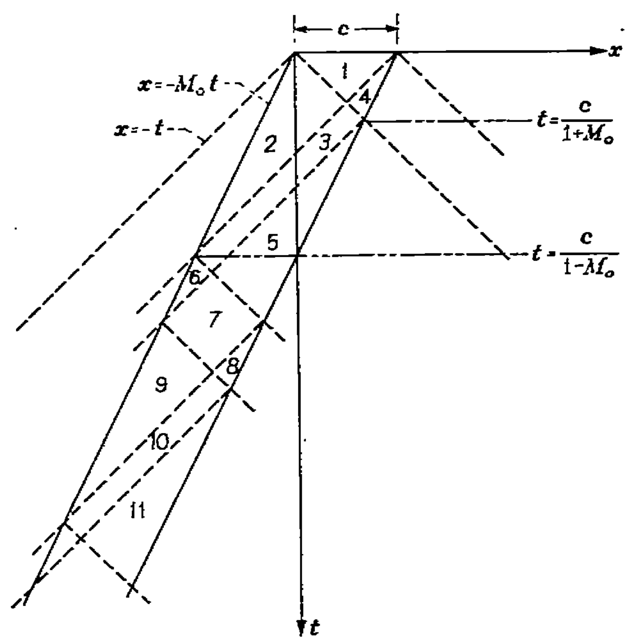

FIGURE 25.—Regions used in analysis of subsonic unsteady wing.

The analysis used to calculate the loading over the regions shown in figure 25 is outlined in appendix A. Plots of the indicial loading on a sinking and a pitching plate flying at a Mach number equal to 0.8 are shown in figure 26. At time equal to zero the loading is constant for the sinking wing, and as time increases the loading-coefficient curve

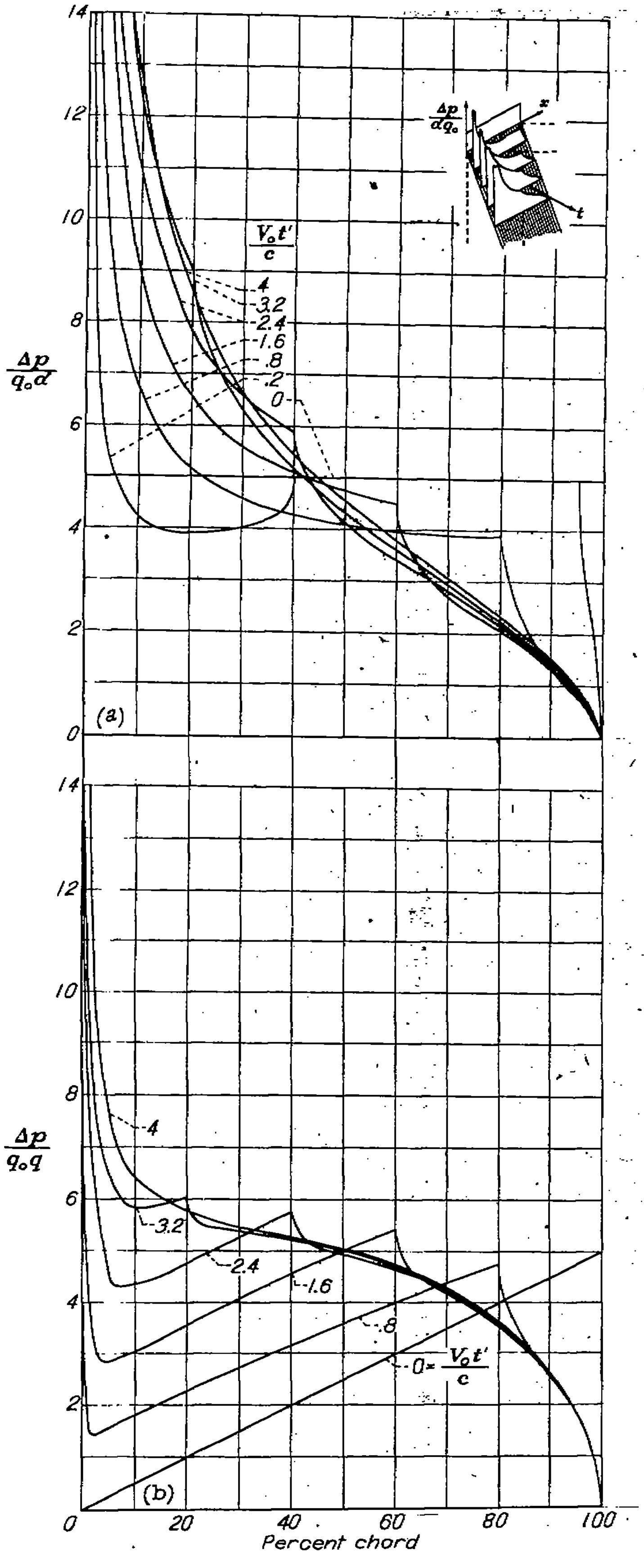

(a) Sinking wing.
(b) Wing pitching about its leading edge.

FIGURE 26.—Variation of two-dimensional indicial load distribution with percent chord for a Mach number equal to 0.8.

approaches the familiar two-dimensional, steady-state shape given by the equation

$$\frac{\Delta p}{q_0}=\frac{4\alpha}{\beta}\sqrt{\frac{c-x}{x}} \tag{63}$$

where x is distance from the leading edge which is at $x=0$.

Figure 27 shows the load distributions for $M_0=0.5$ and 0.8 at the last value of time for which the exact loading curve was calculated. Notice that in each case the distribution is essentially the same as that obtained at time equal to infinity (i. e., the agreement is good with the curve produced by multiplying the right side of equation (63) by a constant factor).[15] The use of this fact simplifies the subsequent analysis concerning the asymptotic behavior of the indicial curve.

The indicial lift and pitching-moment functions were also calculated (see appendix A) up to the time $\tau_0=2.333$ for the wing flying at $M_0=0.5$ and $\tau_0=4$ for the wing flying at $M_0=0.8$. Their variation in this interval will be shown in a subsequent figure (fig. 59). It is evident from a glance at

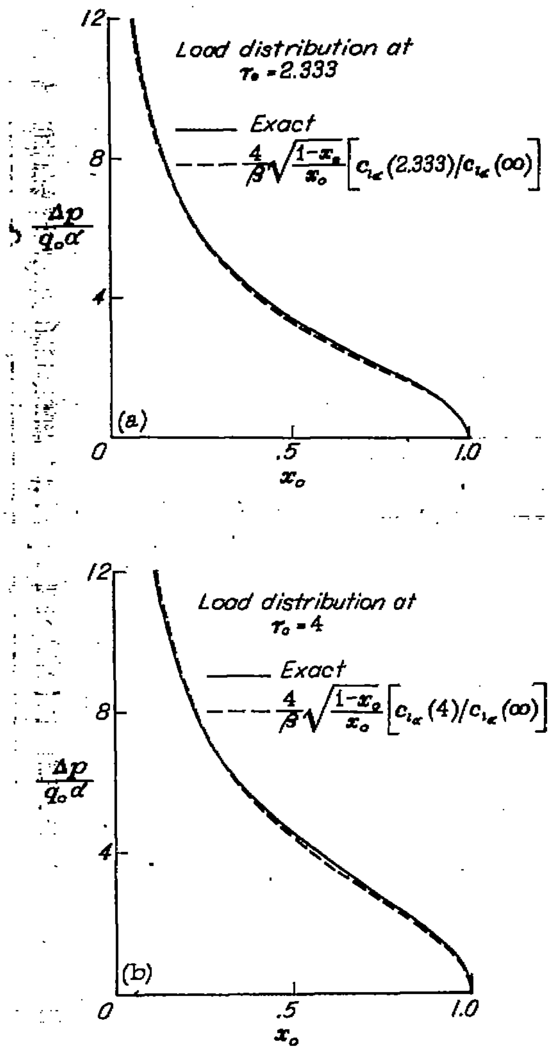

(a) $M_0=0.5$.
(b) $M_0=0.8$.

FIGURE 27.—Load distribution at end of early stage.

[15] A similar result was noted in the study of the load distribution on swept-back wings with subsonic leading edges (reference 17).

the figure that the calculations must be extended beyond this early stage since the asymptotic values are not even closely approached.

Before studying the nature of these curves for large values of time, however, it is useful to examine them with reference to the discussion in the previous section on incompressible flow. For example, it was pointed out that the indicial center of pressure on the sinking wing remained at the quarter-chord point for time greater than zero. Hence, let us consider the location of the center of pressure on the sinking wing when the Mach number lies between 0 and 1. By means of the indicial curves for c_{l_α} and c_{m_α}' and by the relationship

$$c_{m_\alpha}'=-(x/c)_{c.p.}c_{l_\alpha}$$

the variation of $(x/c)_{c.p.}$ is easily evaluated ($(x/c)_{c.p.}$ is the distance between the leading edge and the center of pressure divided by the total wing chord). This variation is shown for the two Mach numbers in figure 28. It is apparent that the center of pressure is very close to the quarter-chord position for values of time greater than those for which the exact calculations were carried out. In other words the significant effect of compressibility on the location of the center of pressure is limited to the interval $0<t_0<2$ for $M_0=0.5$ and to the interval $0<t_0<5$ for $M_0=0.8$.

Likewise, it is apparent from the discussion of the incompressible case that the indicial functions for the pitching wing can also be expressed in a more convenient form by shifting the axis of rotation from the leading edge to the three-quarter-chord point. The values of $\left(c_{l_q}\right)_{3/4}$ and $\left(c_{m_q}'\right)_{3/4}$ for $M_0=0.8$ were calculated from the definitions given in equations (57) and are shown in figure 29. Inspection of this figure again shows that at a Mach number equal to 0.8 the compressibility effects are limited to the interval $0<t_0<5$.

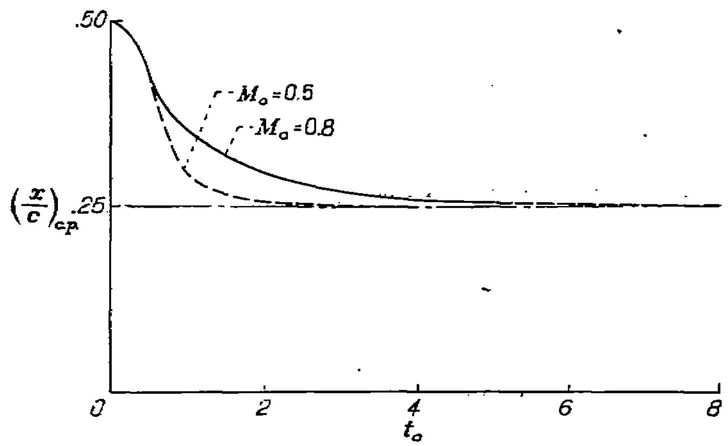

FIGURE 28.—Center-of-pressure variation on sinking wing during early stage.

The later stage.—It follows from the preceding discussion that when t_0 is large, the values of the indicial functions c_{m_α}', c_{l_q}', and c_{m_q}' for compressible flow can be expressed in terms of c_{l_α} by equations similar to equations (58) which were derived for incompressible flow. Thus, after several

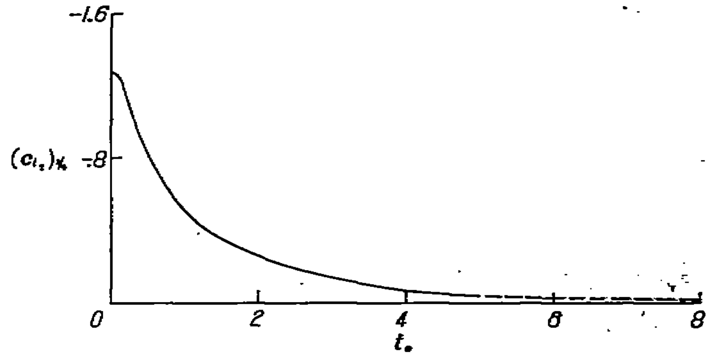

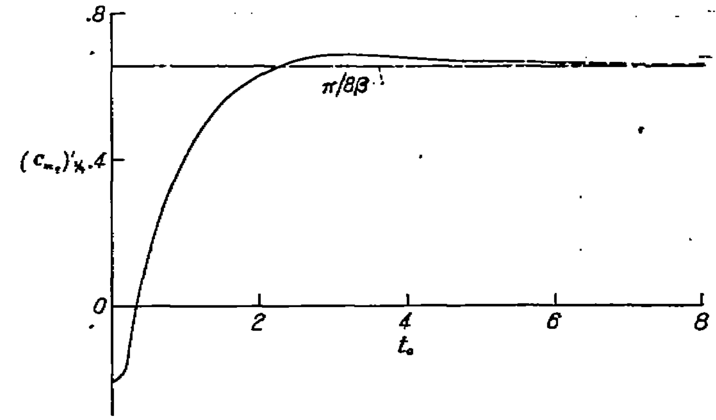

FIGURE 29.—Variation of lift and moment on pitching wing during early stage; $M_0=0.8$

chord lengths have been traveled, one can write, on the basis of the asymptotic values shown in figures 28 and 29,

$$\left.\begin{aligned}c_{m_\alpha}'&=-c_{l_\alpha}/4\\c_{l_q}'&=3c_{l_\alpha}/4\\c_{m_q}'&=-(3c_{l_\alpha}/16)-(\pi/8\beta)\end{aligned}\right\}\qquad(64)$$

It remains, therefore, to determine the asymptotic behavior of c_{l_α}.

Consider the steady-state solution for the lift on a two-dimensional, flat lifting surface traveling at a subsonic Mach number. As was pointed out by Wieghardt (reference 18), if the lift on such a surface is represented by placing at the quarter-chord point a vortex which has the same circulation as that developed by the wing, the angle of attack measured at the three-quarter-chord point will be the same as that of the flat plate. Extending this concept to include the unsteady effects, an investigation will be made of the variation with time of the vortex strength which will maintain a constant angle of attack at the three-quarter-chord station following an impulsive start at $t'=0$.

The analogous problem in steady-state theory becomes one of finding the strength of the vortex system, shown in figure 30, which gives a constant value of w along the line CD. In the vicinity of the origin, of course, this representation gives a poor approximation to the original boundary-value problem. On the other hand, in this vicinity the exact values of lift and moment have already been determined.

Each vortex composing this system lies along the line AB, extending from minus infinity toward the origin, and trails back parallel to the x_1 axis to form the trailing vortex sheet. Note that, for convenience, the origin of the axis system has been located at the quarter-chord point. The solution to such a problem in steady-state, lifting-line theory would result from the solution of the integral equation [16] (for a development using the notation adopted here, see reference 19):

$$w=-\frac{\beta^2}{2\pi}\int_\tau dy_1 \fint \frac{\Delta\varphi(y_1)\,dx_1}{[(x-x_1)^2-\beta^2(y-y_1)^2]^{3/2}}$$

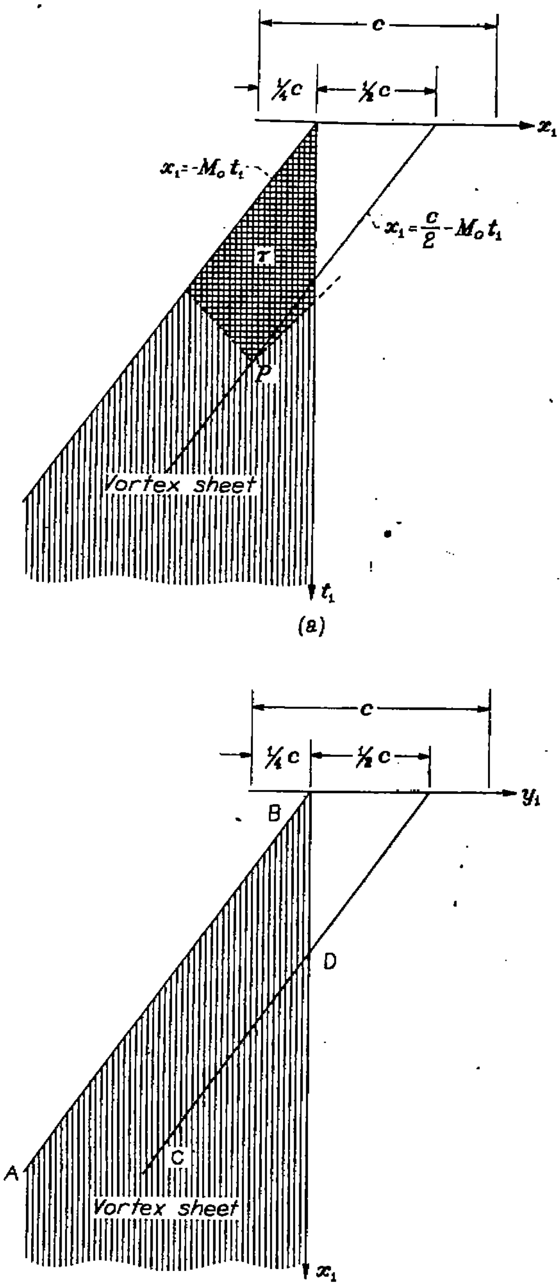

(a) Unsteady case.
(b) Steady-state analog.

FIGURE 30.—Vortex systems for two-dimensional unsteady and analogous three-dimensional, steady-state wings.

where $\Delta\varphi$ is not a function of x_1 since the strength of a trailing vortex is, of course, constant. The area of integration τ is the region within the forecone springing from the point x,y.

If the above equation is transformed by means of the analogy to represent the solution of the unsteady problem (see fig. 30(a)), β, x, and y are replaced by 1, t, and x, respectively; and $\Delta\varphi$, the total jump in potential at a given section, is replaced by the circulation Γ. Hence,

$$w=-\frac{1}{2\pi}\int_\tau dx_1 \fint \frac{\Gamma(x_1)}{[(t-t_1)^2-(x-x_1)^2]^{3/2}}\,dt_1$$

where τ, as indicated in figure 30 (a), is the area in the forecone from the point P which lies always along the line $x=(1/2)c-M_0t$. Integration with respect to t_1 reduces the last equation to

$$w=\frac{1}{2\pi}\fint_{\frac{M_0(x-t)}{1+M_0}}^{0}\frac{\Gamma(x_1)\left(\frac{t+x_1}{M_0}\right)dx_1}{(x-x_1)^2\sqrt{\left(\frac{t+x_1}{M_0}\right)^2-(x-x_1)^2}}$$

which, by means of the substitution $x_1/c=-x_2/2$ becomes along the line $x=\frac{c}{2}-M_0t$

$$w=\frac{1}{c\pi\beta}\fint_0^{\lambda_0}\frac{(\lambda_0+\mu_0-x_2)\,\Gamma(x_2)}{(\mu_2-\lambda_0+x_2)^2\sqrt{(\lambda_0-x_2)(\lambda_0+\mu_1-x_2)}}\,dx_2 \quad (65)$$

where $\lambda_0=2M_0t_0-\mu_0$, $\mu_0=M_0/(1+M_0)$, $\mu_1=2M_0/(1-M_0^2)$, $\mu_2=1/(1+M_0)$, $t_0=t/c$, and where, of course, w is a constant equal to $-V_0\alpha$.

A solution for $\Gamma(x_2)$ in the integral equation (65) may be obtained by expanding Γ in a series of the form

$$\Gamma(x_2)=\frac{\pi c\alpha V_0}{\beta}\left[\sqrt{\frac{x_2}{(a_0+x_2)}}+b_1\sqrt{\frac{x_2}{(a_1+x_2)^3}}+\ldots\right] \quad (66)$$

Place equation (66) into (65) and expand in powers of $1/\lambda_0$. There results the expression

$$-\frac{w}{V_0\alpha}=1+\frac{c_1}{\lambda_0}+\frac{c_2 ln(1/\lambda_0)}{\lambda_0^2}+\frac{c_3}{\lambda_0^3}+\ldots \quad (67)$$

in which

$$c_1=b_1-\frac{a_0}{2}+\frac{1}{\beta^2}$$

Hence if a_0 and b_1 are chosen so that c_1 is zero, an expression for Γ will be obtained which represents the solution to the integral equation (65) correct to the first order in $1/t_0$ (i. e., $1/\lambda_0$) for large values of t_0. Further, if equation (66) is expanded in powers of x_2, there results

$$\Gamma(x_2)=\frac{\pi c\alpha V_0}{\beta}\left[1+\frac{1}{x_2}\left(b_1-\frac{a_0}{2}\right)+\ldots\right]$$

[16] The symbols $\fint$ and $\Xint=$ are used to indicate that the finite part is to be taken. Thus (see reference 19 or 20), $\Xint=_a^b\frac{f(y)\,dy}{(x-y)^2}=-\frac{\partial}{\partial x}\fint_a^b\frac{f(y)\,dy}{(x-y)}=G(x,b)-G(x,a)$ where $G(x,y)$ is the indefinite integral of $f(y)/(x-y)^2$. Further, $\fint_a^x\frac{f(y)\,dy}{(x-y)^{3/2}}=-2\frac{\partial}{\partial x}\int_a^x\frac{f(y)}{\sqrt{x-y}}\,dy$.

which becomes, using the condition for c_1 and relating x_2 and t_0 by the equation of the leading edge, $x_2=2M_0t_0-1=(2V_0t'/c)-1$,

$$\Gamma(\tau_0)=\frac{\pi c\alpha V_0}{\beta}\left[1-\frac{1}{2\beta^2\tau_0}+\ldots\right] \tag{68}$$

By choosing the values of a_0, a_1, and b_1 given as follows:

M_0	a_0	a_1	$b_1=(a_0/2)-(1/\beta^2)$
0.5	56	28	26.67
.8	36	27	15.22

(69)

and placing the resulting expression for $\Gamma(x_2)$ as given by equation (66) into equation (65), the values of $-w/V_0\alpha$ shown in figure 31 were obtained. This figure demonstrates the accuracy to which the first two terms of the series expansion for $\Gamma(x_2)$ yields a constant value of w for the constants given in equation (69).

The relation between circulation and lift has been derived and presented as equation (48). This expression can be written

$$l=\rho_0V_0\Gamma+\rho_0c\frac{d}{dt'}\int_{-\tau_0}^{1-\tau_0}\Delta\varphi(\tau_0,x_0)dx_0$$

where $x_0=x/c$. In order to obtain a complete expression for the section lift, it is necessary to know the chordwise variation of $\Delta\varphi$. Since equation (66) gives only the total vorticity and not its chordwise distribution, some assumption as to such distribution must be made. In lieu of this, the result presented in figure 27 suggests that for large values of time the value of $\Delta\varphi(\tau_0,x_0)$ used in the equation for section lift

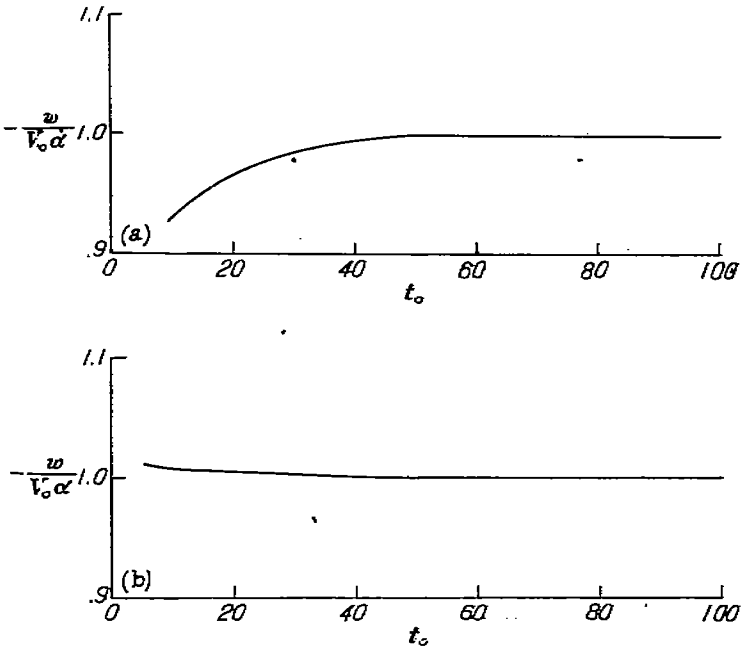

(a) $M_0=0.5$.
(b) $M_0=0.8$.
FIGURE 31.—Variation of downwash at three-quarter-chord position.

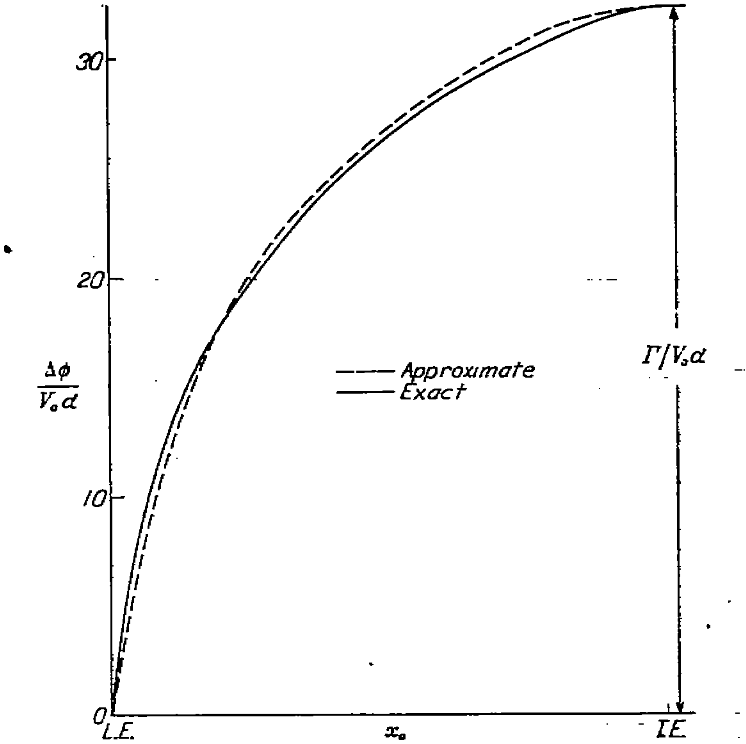

FIGURE 32.—Chordwise variation of circulation at end of early stage; $M_0=0.8$.

can be expressed by the product of $\Delta\varphi(\infty,x_0)$ and $\Gamma(\tau_0)/\Gamma(\infty)$. In other words, for large values of τ_0, the shape of the chordwise distribution of vorticity is the same as the two-dimensional, steady-state value. An indication of the accuracy of such an approximation is shown in figure 32 for a Mach number equal to 0.8 where the precise value of $\Delta\varphi(\tau_0,x_0)$ is compared with the approximation at $\tau_0=4$.

Since $\Gamma(\infty)=\pi\alpha V_0c/\beta$, the substitution of

$$\Delta\varphi(\tau_0,x_0)=\Delta\varphi(\infty,x_0)\Gamma(\tau_0)/\Gamma(\infty)$$

gives for the section lift coefficient

$$c_l=\frac{2\Gamma}{V_0c}+\frac{3}{2}\frac{1}{V_0^2}\frac{d\Gamma}{dt'} \tag{70}$$

By means of equations (66) and (70) and the values of the constants given in (69), an expression for c_{l_α} can be written which is valid for large values of τ_0. This expression is somewhat cumbersome, however, and it is difficult to apply in subsequent analysis. Hence, it has been replaced by a simpler equation that is equivalent [17] to three decimal places for values of τ_0 greater than about 10 for both Mach numbers 0.5 and 0.8. These equations are given by the following: for $M_0=0.5$

$$c_{l_\alpha}=\frac{2\pi}{\beta}\left[1-\frac{4}{3}\frac{1}{5+2\tau_0}-\frac{44.218}{(5+2\tau_0)^2}\right] \tag{71}$$

and for $M_0=0.8$ [18]

$$c_{l_\alpha}=\frac{2\pi}{\beta}\left[1-\frac{1.736}{11+5\tau_0/4}-\frac{70.83}{(11+5\tau_0/4)^2}\right] \tag{72}$$

[17] In order to facilitate fairing the initial portion of the indicial lift curve into the approximate solution obtained for the subsequent variation, the latter results were shifted slightly in terms of V_0t'/c. This did not affect the asymptotic behavior of the curve.

[18] The value for c_{l_α} given by equation (72) disagrees slightly with the value given in the superseded TN 2403 (see footnote 1). The methods for calculating the results are somewhat different, and the value given here is considered to be more accurate.

272483—54——28

The equations for c_{m_α}', c_{l_q}', and c_{m_q}' for $\tau_0 > 10$ can be calculated from these expressions by means of the relations given in equations (64). Equations (71) and (72) will be considered valid for values of τ_0 greater than 10 for both Mach numbers. Values of the indicial functions between $\tau_0=10$ and the highest τ_0 calculated by the exact method were approximated by interpolating between the two results. Tabular values of all the indicial functions calculated for the interval $0\leq\tau_0\leq 10$ are given in tables I and II and curves are given in Part IV.

TABLE I.—INDICIAL LIFT AND MOMENT FOR TWO-DIMENSIONAL SINKING WING. $M_0=0.5$

Vt'/c	$\beta c_{l_\alpha}/2\pi$	$-2\beta c_{m_\alpha}'/\pi$
0.0	1.103	2.205
.1	.995	1.954
.2	.882	1.632
.3	.772	1.246
.4	.691	.904
.5	.656	.766
.6	.634	.663
.7	.618	.602
.8	.604	.561
.9	.588	.540
1.0	.579	.540
1.1	.581	.553
1.2	.597	.572
1.3	.617	.600
1.4	.634	.641
1.5	.642	.652
1.6	.659	.667
1.7	.669	.682
1.8	.677	.691
1.9	.685	.699
2.0	.693	.706
2.5	.724	.727
3.0	.746	.744
3.5	.765	.758
4.0	.781	.772
4.5	.795	.784
5.0	.806	.795
5.5	.816	.805
6.0	.825	.815
6.5	.832	.824
7.0	.840	.832
7.5	.848	.840
8.0	.854	.850
8.5	.860	.858
9.0	.866	.864
9.5	.871	.870
10.0	.877	.875

TABLE II.—INDICIAL LIFT AND MOMENT FOR TWO-DIMENSIONAL SINKING OR PITCHING WING. $M_0=0.8$

Vt'/c	$\beta c_{l_\alpha}/2\pi$	$-2\beta c_{m_\alpha}'/\pi$	$2\beta c_{l_q}'/3\pi$	$-2\beta c_{m_q}'/\pi$
0.0	0.478	0.955	0.318	0.637
.1	.466	.920	.314	.614
.2	.454	.880	.313	.595
.3	.442	.830	.316	.581
.4	.430	.750	.326	.575
.5	.423	.680	.339	.582
.6	.426	.650	.355	.595
.7	.433	.632	.367	.608
.8	.442	.620	.385	.621
.9	.451	.615	.397	.633
1.0	.461	.611	.411	.644
1.5	.507	.612	.473	.688
2.0	.546	.619	.525	.715
2.5	.581	.628	.566	.729
3.0	.610	.641	.598	.737
3.5	.632	.655	.625	.746
4.0	.652	.670	.648	.755
4.5	.670	.684	.665	.765
5.0	.687	.693	.681	.778
6.0	.714	.721	.710	.790
7.0	.738	.743	.736	.806
8.0	.760	.763	.760	.821
9.0	.779	.782	.780	.835
10.0	.798	.798	.798	.849
∞	1.000	1.000	1.000	1.000

INDICIAL FUNCTIONS FOR A TWO-DIMENSIONAL FLAT PLATE, $M_0=1.0$

The general results, obtained in the preceding section for the early stages of the motion and presented in appendix A, for the indicial loading over the sinking and pitching wing may be extended to the sonic case. Furthermore, the two intervals for which analytic results in a closed form were presented in appendix A now cover the complete time range since $0\leq\tau_0\leq M_0/(1+M_0)$ becomes $0\leq\tau_0\leq 0.5$ and $M_0/(1+M_0)\leq\tau_0\leq M_0/(1-M_0)$ becomes $0.5\leq\tau_0\leq\infty$. Hence, by an appropriate limiting process, equations (A8), (A9), (A10), and (A11) become for $0\leq\tau_0\leq 0.5$

$$\left.\begin{aligned}
c_{l_\alpha}&=4\\
c_{m_\alpha}'&=-2+\tau_0^2\\
c_{l_q}'&=2+\tau_0^2\\
c_{m_q}'&=-(4/3)-(2/3)\ \tau_0^3
\end{aligned}\right\}\tag{73a}$$

and for $0.5\leq\tau_0\leq\infty$

$$\left.\begin{aligned}
c_{l_\alpha}&=(4/\pi)\left(2\sqrt{2\tau_0-1}+\text{arc cos}\,\frac{\tau_0-1}{\tau_0}\right)\\
c_{m_\alpha}'&=-(2/\pi)\left[\frac{3+\tau_0}{2}\sqrt{2\tau_0-1}+\left(1-\frac{\tau_0^2}{2}\right)\text{arc cos}\,\frac{\tau_0-1}{\tau_0}\right]\\
c_{l_q}'&=(2/\pi)\left[\frac{5\tau_0}{2}\sqrt{2\tau_0-1}+\left(1+\frac{\tau_0^2}{2}\right)\text{arc cos}\,\frac{\tau_0-1}{\tau_0}\right]\\
c_{m_q}'&=(4/3\pi)\left[\frac{14-\tau_0-3\tau_0^2}{6}\sqrt{2\tau_0-1}+\right.\\
&\qquad\left.\left(1+\frac{\tau_0^3}{2}\right)\text{arc cos}\,\frac{\tau_0-1}{\tau_0}\right]
\end{aligned}\right\}\tag{73b}$$

Since the magnitude of the functions in equations (73b) grows indefinitely with increasing time, the assumptions of linear theory are eventually violated. However, for moderate values of τ_0, these functions have the same order of magnitude as similar indicial curves for Mach numbers other than 1. These effects are illustrated in Part IV.

INDICIAL FUNCTIONS FOR A TWO-DIMENSIONAL FLAT PLATE, $M_0=1.2$

The method of obtaining solutions for the indicial functions at supersonic Mach numbers parallels the development presented for the subsonic Mach numbers. The steady-state analog to the supersonic unsteady wing problem is a constant-chord wing tip with a supersonic trailing edge. (See figs. 33 (a) and 33 (b).) It is well known that the problem of finding the loading over wing plan forms with all supersonic edges is one of the simplest in three-dimensional, lifting-surface theory. In fact, since the upper and lower surfaces are noninteracting, the solution is determined by integrating sources within the Mach forecone. The analysis for c_{l_α} has already been carried out in reference 21.

The analysis used to calculate the loading in terms of $x_0=x/c$ and $t_0=t/c$ over the three regions shown in figure 34 is outlined in appendix B. An example of the manner in which the loading varies with time over a sinking or pitching wing traveling at a Mach number equal to 1.2 is given in figure 35.

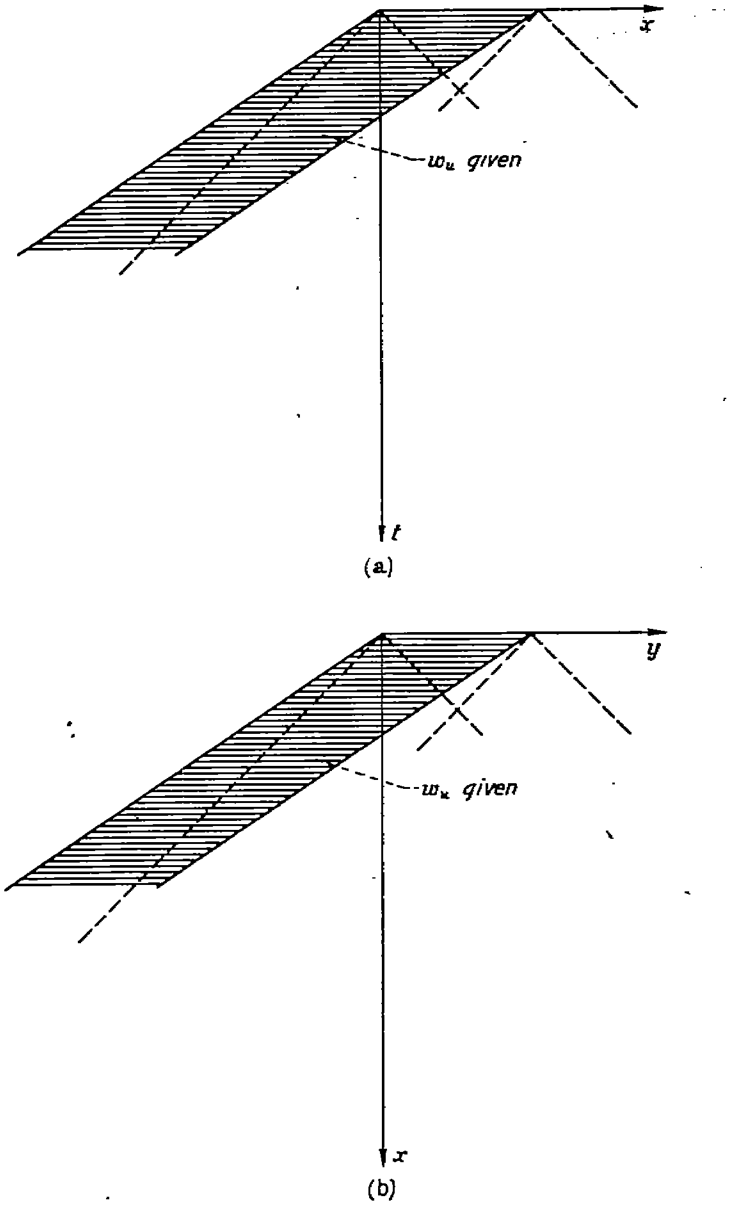

(a) Unsteady case.
(b) Steady-state case.

FIGURE 33.—Boundary conditions for a two-dimensional unsteady wing moving at supersonic speed and the analogous three-dimensional, steady-state wing.

The expressions for the indicial lift and pitching-moment coefficients are given analytically in appendix B, and plotted in Part IV. It can be shown that the results given in appendix B reduce to the expressions given by equations (73) when M_0 is allowed to approach 1, so that there is no discontinuity in the theory in passing through the sonic range.

SUPERSONIC STEADY-STATE LIFT

Since the next section contains a problem involving a complicated acoustic plan form, it may be helpful to consider first a problem involving a very simple acoustic plan form but otherwise similar to the subsequent analysis. Hence let us inspect, using Kirchhoff's formula, the problem of finding the steady-state loading on a two-dimensional flat plate traveling at a constant speed (equation (15)).

Since the upper and lower surfaces are noninteracting, we can use the special form of Kirchhoff's formula given as

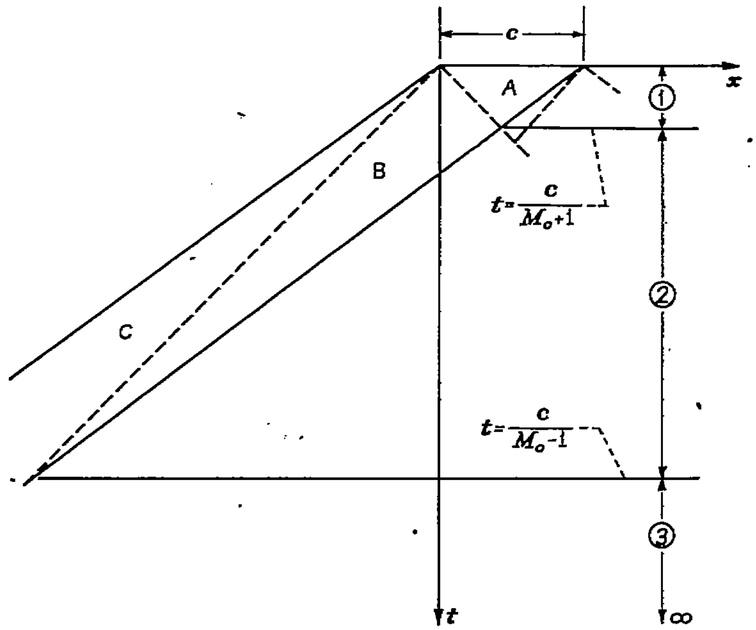

FIGURE 34.—Regions used in analysis of supersonic unsteady wing.

equation (28). In the plane of the wing this equation becomes

$$\varphi=-\frac{1}{2\pi}\int_{S_a}\int\frac{w_u dx_1 dy_1}{\sqrt{(x-x_1)^2+(y-y_1)^2}} \tag{74}$$

Figure 36 shows the positions of the wing in the xy plane. The wing has constant speed for $t>0$. The point $P(x,y)$ is chosen on the wing and ahead of the wave which started at time zero; therefore, $P(x,y)$ lies in the region which has attained its steady-state value. Further, the value of w_u is constant over the acoustic plan form in such a region. This constancy reduces the problem to one of integrating $[(x-x_1)^2+(y-y_1)^2]^{-1/2}$ over the ellipse representing the acoustic plan form.

The equation for S_a can be determined from equations (20) and (21). In this case, equation (21) becomes simply

$$x_1=-M_0\tau$$

Eliminate τ between this equation and equation (20) and there results in the $z=0$ plane

$$(x-x_1)^2+(y-y_1)^2=\left(t+\frac{x_1}{M_0}\right)^2 \tag{75}$$

That equation (75) is the equation of an ellipse with one focal point at x,y can be readily verified. It is more convenient, however, to change to a polar coordinate system with origin at P. Hence set

$$x-x_1=r\cos\theta$$

$$y-y_1=r\sin\theta$$

$$dy_1\,dx_1=rdrd\theta$$

Then equation (75) becomes

$$M_0r=M_0t+x-r\cos\theta$$

or

$$r=\frac{x+M_0t}{M_0+\cos\theta} \tag{76}$$

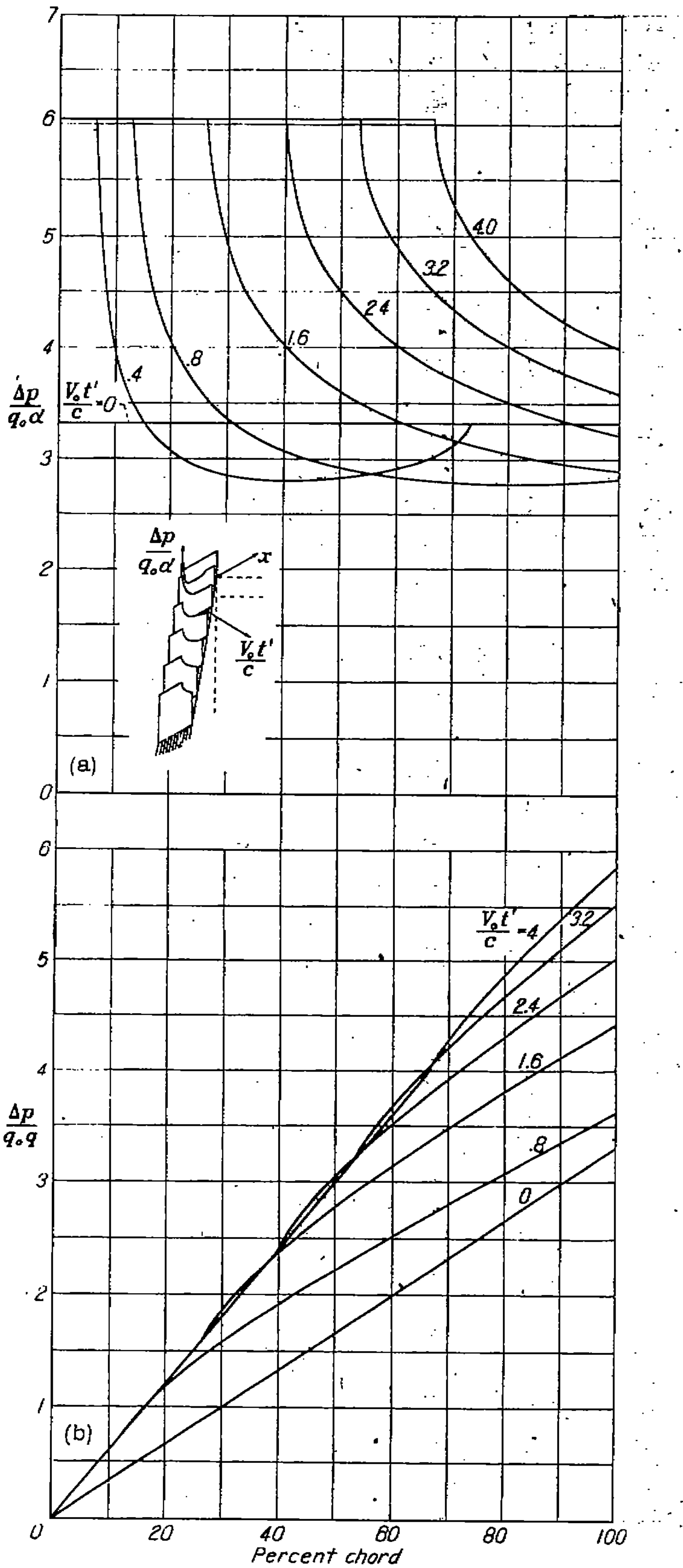

(a) Sinking wing.
(b) Wing pitching about its leading edge.

FIGURE 35.—Variation of two-dimensional indicial load distribution with percent chord for a Mach number equal to 1.2.

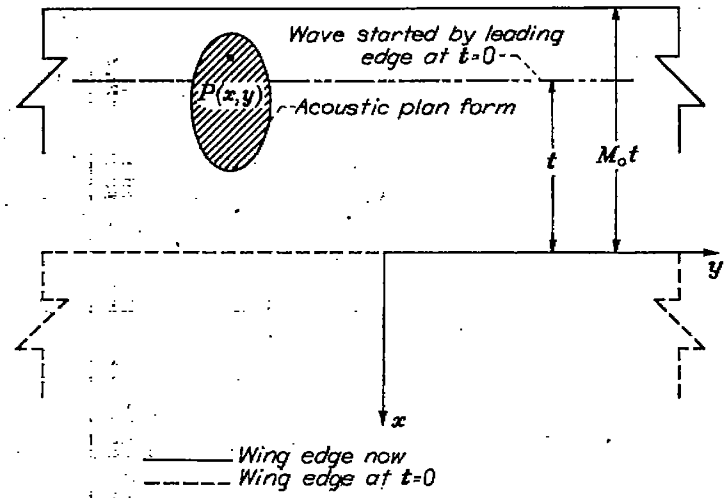

FIGURE 36.—Acoustic plan form for point in steady-state region of two-dimensional unsteady wing flying at a supersonic speed.

and, therefore, equation (74) becomes simply

$$\varphi=-\frac{w_u}{2\pi}\int_0^{2\pi}d\theta\int_0^{\frac{x+M_0t}{M_0+\cos\theta}}dr$$

$$=-\frac{w_u}{2\pi}(x+M_0t)\int_0^{2\pi}\frac{d\theta}{M_0+\cos\theta}$$

The integral is not difficult to evaluate so

$$\varphi=-\frac{w_u}{2\pi}(x+M_0t)\left(\frac{2\pi}{\sqrt{M_0^2-1}}\right)$$

and, finally, by equation (12)

$$\frac{\Delta p}{q}=\frac{4}{V_0M_0}\left(-\frac{w_uM_0}{\sqrt{M_0^2-1}}\right)=\frac{4\alpha}{\sqrt{M_0^2-1}} \tag{77}$$

which is the familiar Ackeret value for the loading on a two-dimensional flat plate. The lift coefficient, of course, follows immediately as

$$c_l=\frac{4\alpha}{\sqrt{M_0^2-1}} \tag{78}$$

INDICIAL LOADING FOR SINKING TRIANGULAR WING WITH SUPERSONIC EDGES

The seven regions.—The analytic expression for the indicial loading over the triangular wing has a different form in each of seven regions. These regions are determined by the positions of the various wave fronts relative to the wing plan form (fig. 37). For $t<0$ the wing is motionless, its leading edge lying along lines represented by the dashed lines in figure 37. The trailing edge is considered to be supersonic and hence its position is immaterial, since the solution can be cut off wherever desired. At $t=0$ the wing starts suddenly to move, and for $t>0$, travels forward at a constant speed V_0. After a certain time t has elapsed, the wing has traveled to a new position, also shown in the figure.

In this same interval of time, pressure impulses have traveled out in spherical waves from every point of the region which the wing has occupied. The trace on the wing of the sphere starting from the wing apex at $t=0$ forms the external boundary of region 7. The area outside this circle and within the traces of the cylindrical waves (the envelopes of the spherical waves) generated by the leading edges at $t=0$ forms region 4. Region 5 is formed by the overlappping of these cylindrical waves, and the solution for loading within it can be found by a suitable superposition of the solutions for regions 3 and 4. Region 1 lies between the cylinder trace on the wing and the leading-edge position at time t; the loading in this region cannot be affected by the manner in which the wing started its motion since it lies outside the starting cylindrical waves. Hence, the loading in region 1 is the same as that on a swept wing flying at a steady supersonic speed. The solution in region 2 can also be obtained from steady-state lifting-surface theory, but, whereas in region 1 the field is two-dimensional (i. e., invariant with distance measured parallel to the leading edge), in region 2 the field is conical. Region 6 is formed by the overlapping of regions 2 and 4. Finally, region 3 is that area completely unaffected by waves from the wing edges. In the following subdivisions the analysis of each of the separate regions will be discussed.

Region 1: The loading in region 1 of figure 37 is equal to the loading on a two-dimensional flat plate moving at a constant velocity given by the component of stream velocity normal to the leading edge of the triangular wing. Since this component is supersonic, the loading is of the Ackeret type and is given by

$$\left(\frac{\Delta p}{q_n}\right)_1=\frac{4\alpha_n}{\beta_n}$$

But since $V_n=V_o \cos \Lambda$ where Λ is the angle of sweep (see fig. 38),

$$q_n=q_0 \cos^2 \Lambda$$

$$\alpha_n=\alpha \sec \Lambda$$

$$M_n=M_0 \cos \Lambda$$

$$\beta_n=\sqrt{M_0^2 \cos^2 \Lambda-1}$$

and

$$\left(\frac{\Delta p}{q_0}\right)_1=\frac{4\alpha}{\sqrt{M_0^2-\sec^2 \Lambda}}$$

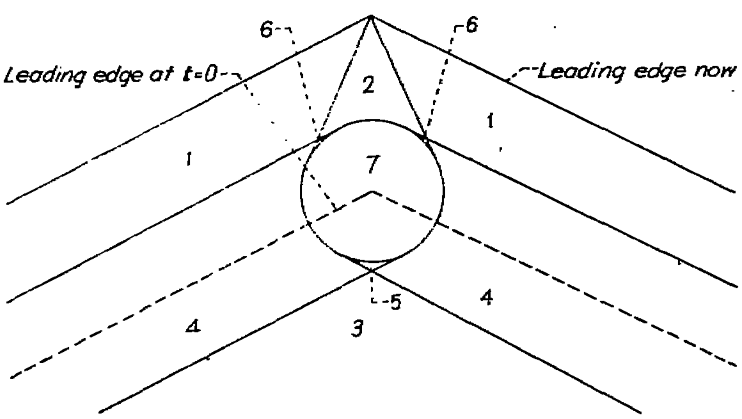

FIGURE 37.—The seven regions used in the analysis of the triangular wing with supersonic leading edges.

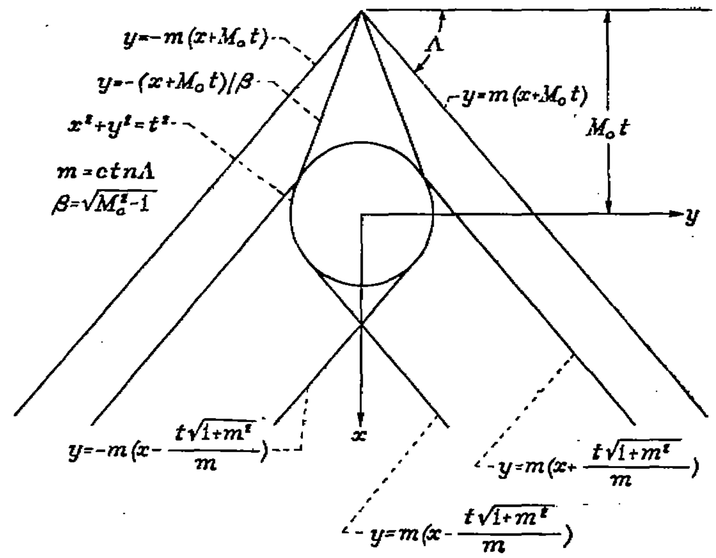

FIGURE 38.—Equations of lines used in the analysis of the triangular wing with supersonic leading edges.

Finally, if $\operatorname{ctn} \Lambda=m$

$$\left(\frac{\Delta p}{q_0}\right)_1=\frac{4\alpha m}{\sqrt{\beta^2m^2-1}} \tag{79}$$

where $\beta=\sqrt{M_0^2-1}$.

Region 2: The steady-state loading on a triangular wing with supersonic edges has been given by several authors (see, for convenience, reference 22) so the expression for the loading in region 2 can be written immediately for the coordinate system shown in figure 38 as

$$\left(\frac{\Delta p}{q_0}\right)_2=\frac{4\alpha m}{\pi\sqrt{\beta^2m^2-1}}\left\{\pi+\text{arc sin}\,\frac{\beta^2my-(x+M_0t)}{\beta[m(x+M_0t)-y]}-\text{arc sin}\,\frac{\beta^2my+(x+M_0t)}{\beta[m(x+M_0t)+y]}\right\} \tag{80}$$

Region 3: Since region 3 is unaffected by the edges of the wing the solution for the loading therein can be written as in reference 21

$$\left(\frac{\Delta p}{q_0}\right)_3=\frac{4\alpha}{M_0} \tag{81}$$

Region 4: The solution for loading in region 4 can be obtained from consideration of a two-dimensional wing starting from rest and moving with velocity V_n normal to its leading edge. This problem has been treated in reference 21 and the solution written there can be written for the right-hand side of figure 37 as

$$\left(\frac{\Delta p}{q_n}\right)_4=\frac{4\alpha_n}{\pi\beta_n}\left[\text{arc cos}\,\frac{M_nx_n+t}{x_n+M_nt}+\frac{\sqrt{M_n^2-1}}{M_n}\left(\frac{\pi}{2}+\text{arc sin}\,\frac{x_n}{t}\right)\right]$$

where the notation, as defined by figure 39, is

$$x_n=x \cos \Lambda-y \sin \Lambda$$

$$y_n=x \sin \Lambda+y \cos \Lambda$$

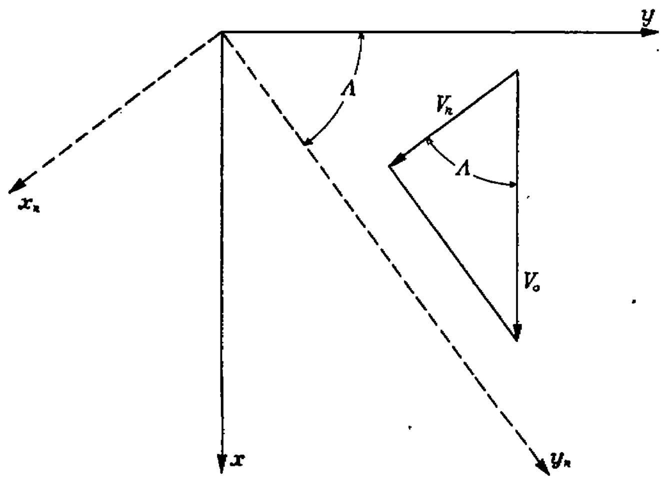

FIGURE 39.—The x_ny_n coordinate system.

and since

$$\text{ctn}\ \Lambda=m,\ \sin\Lambda=\frac{1}{\sqrt{1+m^2}}$$

$$\cos\Lambda=\frac{m}{\sqrt{1+m^2}}$$

Then

$$x_n=\frac{mx-y}{\sqrt{1+m^2}}$$

$$y_n=\frac{x+my}{\sqrt{1+m^2}}$$

The equation for loading now becomes, in the coordinate system of figure 38,

$$\left(\frac{\Delta p}{q_0}\right)_4=\frac{4\alpha m}{\pi\sqrt{\beta^2m^2-1}}\left[\text{arc cos}\,\frac{mM_0(mx-|y|)+t(1+m^2)}{\sqrt{1+m^2}(mx-|y|+mM_0t)}+\frac{\sqrt{\beta^2m^2-1}}{mM_0}\left(\frac{\pi}{2}+\text{arc sin}\,\frac{mx-|y|}{t\sqrt{1+m^2}}\right)\right] \quad (82)$$

Region 5: The solution for loading in region 5 can be obtained by superposition of the solutions for regions 3 and 4. (See fig. (40).) If the solutions for the two sides of region 4 (obtained from equation (82)) are added, the result gives twice the required value of w_u on the wing, as well as undesirable pressures off the wing. However, subtraction from this sum of the solution for region 3 (equation (81)) reduces the downwash w_u to the proper value, and also cancels the excess pressures. The resulting expression can be written

$$\left(\frac{\Delta p}{q_0}\right)_5=\frac{4\alpha m}{\pi\sqrt{\beta^2m^2-1}}\left[\text{arc cos}\,\frac{mM_0(mx-y)+(1+m^2)t}{\sqrt{1+m^2}(mx-y+mM_0t)}+\text{arc cos}\,\frac{mM_0(mx+y)+(1+m^2)t}{\sqrt{1+m^2}(mx+y+mM_0t)}+\frac{\sqrt{\beta^2m^2-1}}{mM_0}\left(\text{arc sin}\,\frac{mx+y}{t\sqrt{1+m^2}}+\text{arc sin}\,\frac{mx-y}{t\sqrt{1+m^2}}\right)\right] \quad (83)$$

Region 6: The loading in region 6 can also be calculated by superposition. To find the loading in this case, add the

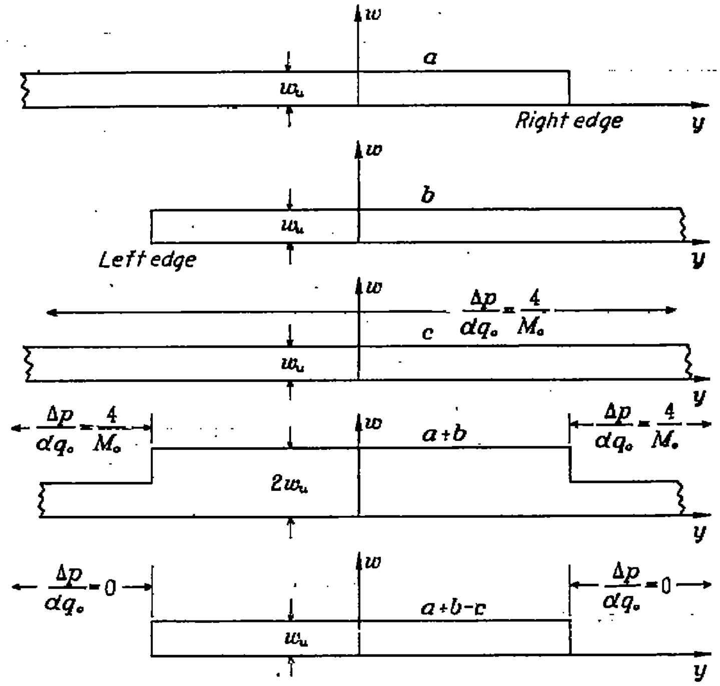

FIGURE 40.—Solutions superimposed to obtain equation (83).

solutions for regions 2 and 4 (equations (80) and (82)) and subtract the solution for region 1 (equation (79)). There results

$$\left(\frac{\Delta p}{q_0}\right)_6=\frac{4\alpha m}{\pi\sqrt{\beta^2m^2-1}}\left\{\text{arc sin}\,\frac{\beta^2my-(x+M_0t)}{\beta[m(x+M_0t)-y]}-\text{arc sin}\,\frac{\beta^2my+(x+M_0t)}{\beta[m(x+M_0t)+y]}+\text{arc cos}\,\frac{mM_0(mx-|y|)+t(1+m^2)}{(mx-|y|+mM_0t)\sqrt{1+m^2}}+\frac{\sqrt{\beta^2m^2-1}}{mM_0}\left(\frac{\pi}{2}+\text{arc sin}\,\frac{mx-|y|}{t\sqrt{1+m^2}}\right)\right\} \quad (84)$$

Region 7: The solution for the loading in region 7 can be obtained by means of equation (28). The analysis used in finding the solution in this region is not difficult but the algebra is rather involved. It is useful at this point to introduce polar coordinates (see fig. 41) such that

$$\left.\begin{aligned}x-x_1&=r\cos\theta\\ y-y_1&=r\sin\theta\\ dx_1dy_1&=r\,dr\,d\theta\end{aligned}\right\} \quad (85)$$

From equation (85), equation (28) can be written in the form

$$\varphi=\frac{V_0\alpha}{2\pi}\int_{S_a}\int dr\,d\theta \quad (86)$$

The acoustic plan form for points in region 7 is the region bounded by three curves as indicated in figure 42. The arc between θ_1 and θ_2 is determined by eliminating T between the equations

$$r^2=(t-T)^2$$

(the equation for the inverse sound waves) and the equation for the left leading edge

$$y_1 = -m(x_1 + M_0 T)$$

The arc between θ_3 and θ_1 is found by determining the acoustic intersection (eliminating T) of the right leading edge with the inverse sound wave; and, finally, the arc between θ_2 and θ_3 is given by the equation $r=t$. The equations of these arcs can be written in polar coordinates as

$$r = \frac{m(x+M_0 t)+y}{m\cos\theta + mM_0 + \sin\theta};\ \theta_1 \leq \theta \leq \theta_2$$

$$r = t;\ \theta_2 \leq \theta \leq \theta_3$$

$$r = \frac{m(x+M_0 t)-y}{m\cos\theta + mM_0 - \sin\theta};\ \begin{cases} 0 \leq \theta \leq \theta_1 \\ \theta_3 \leq \theta \leq 2\pi \end{cases}$$

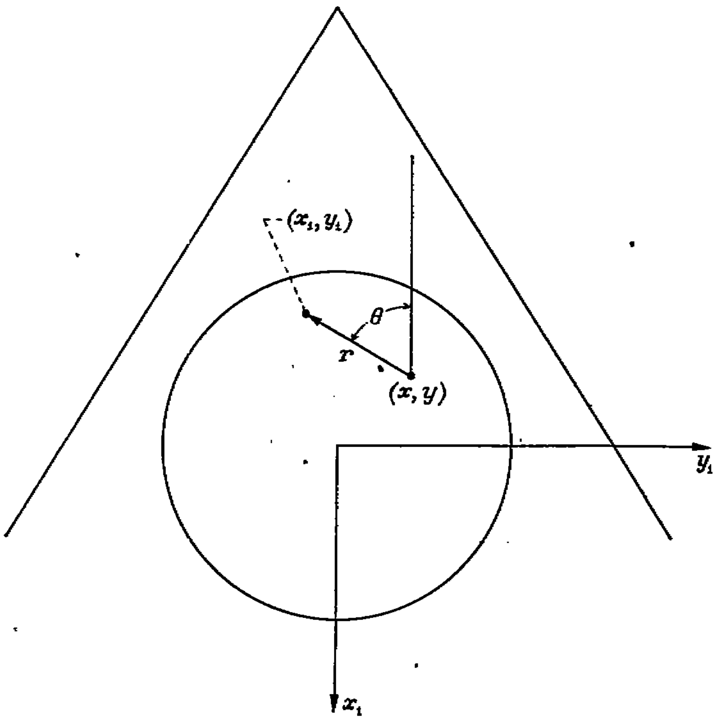

FIGURE 41.—The $r\theta$ coordinate system.

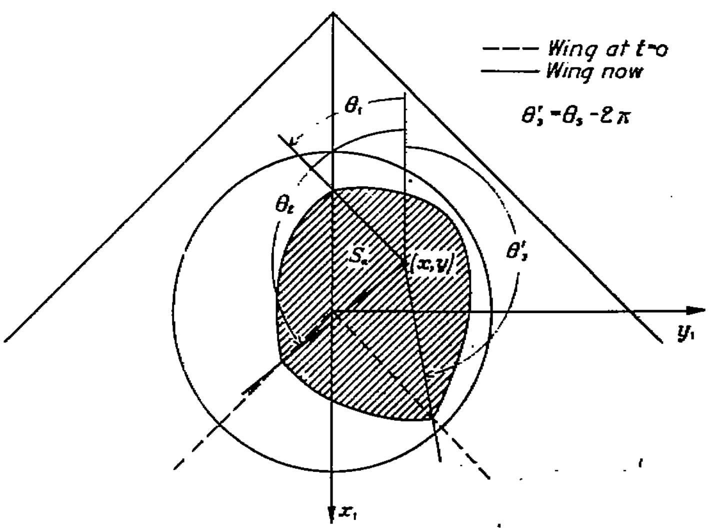

FIGURE 42.—Acoustic plan form for point in region 7.

Using these expressions, equation (86) reduces to

$$\varphi = \frac{V_0\alpha}{2\pi}\int_{\theta_1}^{\theta_2} \frac{m(x+M_0 t)+y}{m\cos\theta + mM_0 + \sin\theta}\, d\theta + \frac{V_0\alpha}{2\pi}\int_{\theta_2}^{\theta_3} t\, d\theta + \frac{V_0\alpha}{2\pi}\int_{\theta_3}^{\theta_1} \frac{m(x+M_0 t)-y}{m\cos\theta + mM_0 - \sin\theta}\, d\theta$$

and taking the partial derivative with respect to t (to determine the loading according to equation (12)) one finds [19]

$$\left(\frac{\Delta p}{q_0}\right)_7 = \frac{2\alpha m}{\pi}\int_{\theta_1}^{\theta_2} \frac{d\theta}{mM_0 + m\cos\theta + \sin\theta} + \frac{2\alpha}{\pi M_0}\int_{\theta_2}^{\theta_3} d\theta + \frac{2\alpha m}{\pi}\int_{\theta_3}^{\theta_1} \frac{d\theta}{mM_0 + m\cos\theta - \sin\theta} \tag{87}$$

In evaluating this equation, the following integral is used: for $-\pi \leq \theta \leq \pi$

$$\int \frac{d\theta}{mM_0 + m\cos\theta \pm \sin\theta} = \frac{2}{\sqrt{\beta^2 m^2 - 1}} \arctan \frac{m(M_0-1)\tan(\theta/2) \pm 1}{\sqrt{\beta^2 m^2 - 1}} \tag{88}$$

Since equation (88) is valid only in the interval $-\pi \leq \theta \leq \pi$, care must be exercised in applying it because the angle θ_3 may be greater than π (as in fig. 42). In case $\pi \leq \theta_3$, it is convenient to introduce the angle $\theta_3' = \theta_3 - 2\pi$. The expression for $\Delta p/q_0$ can then be written in two forms, according to whether θ_3 is less than or greater than π:

for $y \geq 0$, $\theta_3 \leq \pi$

$$\left(\frac{\Delta p}{q_0}\right)_7 = \frac{4\alpha m}{\pi\sqrt{\beta^2 m^2 - 1}}\left[\pi + \arctan \frac{m(M_0-1)\tan(\theta_1/2)-1}{\sqrt{\beta^2 m^2 - 1}} - \arctan \frac{m(M_0-1)\tan(\theta_1/2)+1}{\sqrt{\beta^2 m^2 - 1}} + \arctan \frac{m(M_0-1)\tan(\theta_2/2)+1}{\sqrt{\beta^2 m^2 - 1}} - \arctan \frac{m(M_0-1)\tan(\theta_3/2)-1}{\sqrt{\beta^2 m^2 - 1}}\right] + \frac{2\alpha}{\pi M_0}(\theta_3 - \theta_2) \tag{89a}$$

for $y \geq 0$, $\pi \leq \theta_3$

$$\left(\frac{\Delta p}{q_0}\right)_7 = \frac{4\alpha m}{\pi\sqrt{\beta^2 m^2 - 1}}\left[\arctan \frac{m(M_0-1)\tan(\theta_1/2)-1}{\sqrt{\beta^2 m^2 - 1}} - \arctan \frac{m(M_0-1)\tan(\theta_1/2)+1}{\sqrt{\beta^2 m^2 - 1}} + \arctan \frac{m(M_0-1)\tan(\theta_2/2)+1}{\sqrt{\beta^2 m^2 - 1}} - \arctan \frac{m(M_0-1)\tan(\theta_3'/2)-1}{\sqrt{\beta^2 m^2 - 1}}\right] + \frac{2\alpha}{\pi M_0}(\theta_3' - \theta_2 + 2\pi) \tag{89b}$$

[19] The limits θ_1, θ_2, and θ_3 are all functions of t but in moving the partial derivative through the integral sign the terms involving $\partial\theta_1/\partial t$, $\partial\theta_2/\partial t$, and $\partial\theta_3/\partial t$ all cancel one another.

where

$$\theta_1 = \text{arc cos} \frac{-M_0 y^2 + (x+M_0 t)\sqrt{(x+M_0 t)^2 - \beta^2 y^2}}{y^2 + (x+M_0 t)^2}$$

$$(0 < \theta_1 < \pi)$$

$$\theta_2 = \text{arc cos} \frac{m(y+mx) - \sqrt{(1+m^2)t^2 - (y+mx)^2}}{(1+m^2)t}$$

$$(0 < \theta_2 < \pi)$$

$$\theta_3 = \text{arc cos} \frac{-m(y-mx) - \sqrt{(1+m^2)t^2 - (y-mx)^2}}{(1+m^2)t}$$

$$\theta_3' = \theta_3 - 2\pi (\text{if } \pi \leq \theta_3)$$

The limitation on θ_3 can be given both an analytic and geometric interpretation. Thus, equation (89a) applies for $0 \leq m(x+t) \leq y$ and equation (89b) applies for $0 \leq y \leq m(x+t)$. These regions are shown in figure 43. Because of the geometrical symmetry about the x axis, equations (89) suffice for the determination of loading throughout region 7.

An isometric drawing of the load distribution on the right panel of a triangular wing with supersonic edges is shown in figure 44. The positions of the spanwise sections were chosen so that each of the regions 1 through 7 is represented. It is to be noted that the results for region 7 show no unusual characteristics and, in general, the distribution is similar to the steady-state loading on a triangular wing.

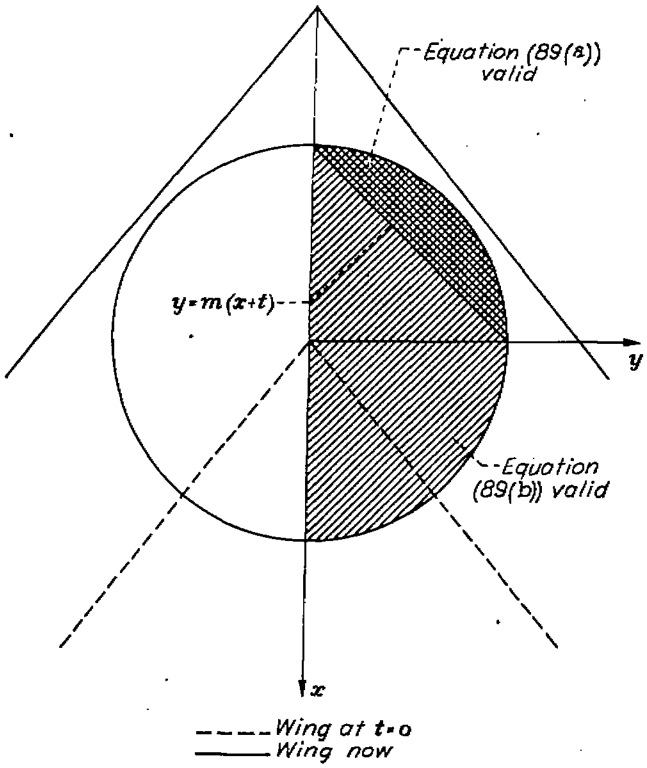

FIGURE 43.—Regions in which equations (89a) and (89b) are valid.

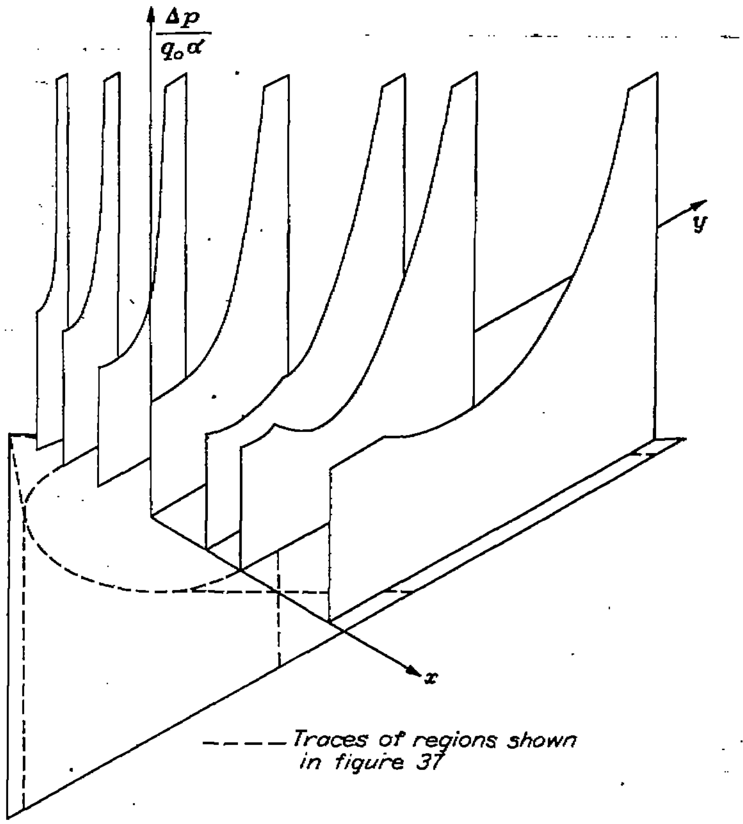

FIGURE 44.—Distribution of indicial loading on right panel of supersonic-edged, triangular wing.

INDICIAL LIFT AND PITCHING MOMENT ON A TRIANGULAR WING WITH SUPERSONIC EDGES

The indicial lift and moment could be obtained, of course, by integrating load distributions calculated by the method presented above. However, it is far simpler to use the methods outlined in the section entitled "Boundary-Value Problems Involving Noninteracting Surfaces" in Part II. In particular the second of the two methods outlined therein will be applied.

It was seen in the above-mentioned section that the lift and moment coefficients for a supersonic-edged triangular wing could be found by solving a related steady-state lifting-surface problem. For the cases of indicial sinking and pitching, the boundary conditions for this related problem can be found readily from equation (34). Since y_r and y_l become, for $z=0$, the right and left leading edges, respectively the boundary conditions are given by

$$\left(\frac{\partial \Phi}{\partial z}\right)_{z=0} = -2V_0 \alpha m(x+M_0 t) \tag{90}$$

for the sinking wing, and

$$\left(\frac{\partial \Phi}{\partial z}\right)_{z=0} = -2\dot{\theta} m(x+M_0 t)^2 \tag{91}$$

for the pitching wing. In addition, it was shown that the lift and moment coefficients for the wing in unsteady motion are obtainable by integration of the quantity $\partial \Phi / \partial t$. For convenience, this quantity is expressed as a chordwise loading factor in terms of the following notation:

$$P_0 = \frac{M_0}{2s\alpha} \int_{-s}^{s} \frac{\Delta p}{q_0} dy \text{ (sinking wing)} \tag{92a}$$

$$P_1 = \frac{m M_0 V_0}{2s^2 \dot{\theta}} \int_{-s}^{s} \frac{\Delta p}{q_0} dy \text{ (pitching wing)} \tag{92b}$$

where

$$s=m(x+M_0t) \tag{93}$$

It is found that (equation (35))

$$P_0=\frac{4m}{\pi s}\frac{\partial}{\partial t}\int_\sigma\int\frac{(x_1+M_0t_1)\,dx_1dt_1}{\sqrt{(t-t_1)^2-(x-x_1)^2}} \tag{94}$$

$$P_1=\frac{4m^2}{\pi s^2}\frac{\partial}{\partial t}\int\int\frac{(x_1+M_0t_1)^2\,dx_1dt_1}{\sqrt{(t-t_1)^2-(x-x_1)^2}} \tag{95}$$

The lift and moment of sinking and pitching wings will now be obtained by the use of P_0 and P_1.

Wing with constant angle of attack (sinking wing).—The solution for the chord loading on a flat, supersonic-edged, triangular wing starting from rest at $t=0$ and flying at a constant speed and angle of attack is given by equation (94). With the transformations

$$x-x_1=x_2$$

$$t-t_1=t_2$$

this becomes

$$P_0=\frac{4m}{\pi s}\frac{\partial}{\partial t}\int_\sigma\int dt_2dx_2\,\frac{\frac{s}{m}-x_2-M_0t_2}{\sqrt{t_2^2-x_2^2}}$$

This integral can be evaluated and gives for $x<t$ (region A)

$$P_0=4 \tag{96a}$$

for $-t\leq x\leq t$ (region B)

$$P_0=\frac{4}{\pi}\left[\frac{\sqrt{t^2-x^2}}{x+M_0t}+\text{arc cos}\left(-\frac{x}{t}\right)+\frac{M_0}{\beta}\text{ arc cos }\frac{t+M_0x}{x+M_0t}\right] \tag{96b}$$

and for $x<-t$ (region C)

$$P_0=\frac{4M_0}{\beta} \tag{96c}$$

where the regions are shown in figure 13. As has been pointed out, equations (96) can also be obtained by integrating the equations for the loading given in the preceding section. These integrations were carried out (in some regions numerically) and the results were found to agree with those of the present analysis.

It is now possible to write the indicial functions C_{L_α} and $C_{m_\alpha}{}'$ in the form

$$C_{L_\alpha}=\frac{2}{S\,M_0}\int_{-M_0t}^{c_0-M_0t}m(x+M_0t)P_0dx \tag{97}$$

$$C_{m_\alpha}{}'=-\frac{2}{Sc_0M_0}\int_{-M_0t}^{c_0-M_0t}m(x+M_0t)^2P_0dx \tag{98}$$

where c_0 is the root chord, S is the wing area (equal to mc_0^2) and the prime indicates that the pitching moment is measured about the apex, the positive moment being one which causes the trailing edge to sink relative to the apex.

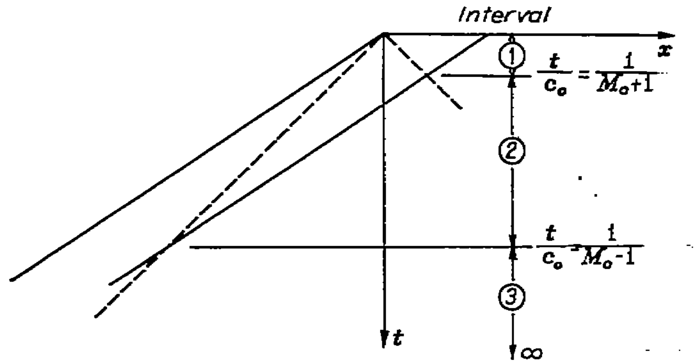

FIGURE 45.—Time intervals used in expressing lift and moment on unsteady, supersonic-edged, triangular wing.

Combining equations (96) and (97) one finds for the first interval shown in figure 45

$$C_{L_\alpha}=\frac{2}{M_0c_0^2}\left\{\int_{-M_t}^{-t}\frac{4M_0}{\beta}(x+M_0t)dx+\right.$$

$$\frac{4}{\pi}\int_{-t}^{t}(x+M_0t)\left[\frac{\sqrt{t^2-x^2}}{x+M_0t}+\text{arc cos}\left(-\frac{x}{t}\right)+\right.$$

$$\left.\left.\frac{M_0}{\beta}\text{ arc cos}\frac{t+M_0x}{x+M_0t}\right]dx+\int_t^{c_0-M_0t}4(x+M_0t)dx\right\}$$

This equation integrates to give, if $t_0=t/c_0$,

for $0\leq t_0\leq\frac{1}{M_0+1}$ (first interval)

$$C_{L_\alpha}=\frac{4}{M_0}\left(1+\frac{1}{2}t_0^2\right) \tag{99a}$$

Similarly for $\frac{1}{M_0+1}\leq t_0\leq\frac{1}{M_0-1}$ (second interval)

$$C_{L_\alpha}=\frac{4}{\pi M_0}\left(1+\frac{1}{2}t_0^2\right)\text{arc cos }\frac{M_0t_0-1}{t_0}+$$

$$\frac{4}{\pi\beta}\text{arc cos }(M_0-t_0\beta^2)+$$

$$2\,\frac{3-M_0t_0}{\pi M_0}\sqrt{t_0^2-(1-M_0t_0)^2} \tag{99b}$$

and for $\frac{1}{M_0-1}\leq t_0$ (third interval)

$$C_{L_\alpha}=\frac{4}{\beta} \tag{99c}$$

In the same manner the values for $C_{m_\alpha}{}'$ in the various intervals can be determined by combining equations (96) and (98). There results

for $0\leq t_0\leq\frac{1}{M_0+1}$ (first interval)

$$C_{m_\alpha}{}'=-\frac{8}{3M_0}\left(1+\frac{1}{2}M_0t_0^3\right) \tag{100a}$$

for $\frac{1}{M_0+1}\leq t_0\leq\frac{1}{M_0-1}$ (second interval)

$$C_{m_\alpha}'=-\frac{8}{\pi M_0}\left[\frac{1}{18}(8-M_0t_0-M_0^2t_0^2-2t_0^2)\sqrt{t_0^2-(1-M_0t_0)^2}+\frac{1}{6}(2+M_0t_0^3)\arccos\frac{M_0t_0-1}{t_0}+\frac{M_0}{3\beta}\arccos(M_0-\beta^2t_0)\right] \tag{100b}$$

and for $\frac{1}{M_0-1}\leq t_0$ (third interval)

$$C_{m_\alpha}'=-\frac{8}{3\beta} \tag{100c}$$

Numerical results will be presented in Part IV.

Wing with linear angle-of-attack variation (pitching wing).—The solution for the average load on a flat, supersonic-edged, triangular wing flying at a constant speed and pitching at a uniform rate $\dot{\theta}$ about its apex is given by equation (95). With the transformation

$$x-x_1=x_2$$

$$t-t_1=t_2$$

this equation becomes

$$P_1=\frac{4m^2}{\pi s^2}\frac{\partial}{\partial t}\int_\tau\int_\sigma\frac{\left(\frac{s}{m}-x_2-M_0t_2\right)^2}{\sqrt{t_2^2-x_2^2}}dt_2dx_2$$

and the evaluation of this gives (for the intervals defined in fig. 13)
for $x\leq t$ (region A)

$$P_1=4\left[1+\frac{1}{2}\left(\frac{t}{x+M_0t}\right)^2\right] \tag{101a}$$

for $-t\leq x\leq t$ (region B)

$$P_1=\frac{4}{\pi}\left[\frac{1}{2}\frac{t^2+(x+M_0t)^2}{(x+M_0t)^2}\arccos\left(-\frac{x}{t}\right)+\frac{M_0}{\beta}\arccos\frac{t+M_0x}{x+M_0t}+\frac{1}{2}\frac{3x+2M_0t}{(x+M_0t)^2}\sqrt{t^2-x^2}\right] \tag{101b}$$

and for $x\leq -t$ (region C)

$$P_1=\frac{4M_0}{\beta} \tag{101c}$$

The equations for the indicial functions C_{L_q}' and C_{m_q}' can be obtained from the equations

$$\frac{C_L'}{\left(\frac{c_0\dot{\theta}}{V_0}\right)}=C_{L_q}'=\frac{2}{Sc_0M_0}\int_{-M_0t}^{c_0-M_0t}m(x+M_0t)^2P_1\,dx \tag{102}$$

$$\frac{C_m'}{\left(\frac{c_0\dot{\theta}}{V_0}\right)}=C_{m_q}'=-\frac{2}{Sc_0^2M_0}\int_{-M_0t}^{c_0-M_0t}m(x+M_0t)^3P_1\,dx \tag{103}$$

where the primes indicate the wing is pitching about and the moments are measured about the leading edge.

A combination of equations (101) and (102) gives for the lift coefficient
for $0\leq t_0\leq\frac{1}{M_0+1}$ (first interval)

$$C_{L_q}'=\frac{8}{3M_0}\left(1+\frac{3}{2}t_0^2-M_0t_0^3\right) \tag{104a}$$

for $\frac{1}{M_0+1}\leq t\leq\frac{1}{M_0-1}$ (second interval)

$$C_{L_q}'=\frac{8}{\pi M_0}\left[\left(\frac{1}{2}t_0^2-\frac{1}{3}M_0t_0^3+\frac{1}{3}\right)\arccos\frac{M_0t_0-1}{t_0}+\frac{M_0}{3\beta}\arccos(M_0-\beta^2t_0)+\left(\frac{2}{9}t_0^2+\frac{1}{9}M_0^2t_0^2-\frac{7}{18}M_0t_0+\frac{11}{18}\right)\sqrt{t_0^2-(1-M_0t_0)^2}\right] \tag{104b}$$

and for $\frac{1}{M_0-1}\leq t_0$ (third interval)

$$C_{L_q}'=8/3\beta \tag{104c}$$

Similarly a combination of equations (101) and (103) yields, for the pitching moment about the apex, the results

for $0\leq t_0\leq\frac{1}{M_0+1}$ (first interval)

$$C_{m_q}'=-\frac{2}{M_0}\left[1+t_0^2-\frac{1}{8}t_0^4(1+4M_0^2)\right] \tag{105a}$$

for $\frac{1}{M_0+1}\leq t_0\leq\frac{1}{M_0-1}$ (second interval)

$$C_{m_q}'=-\frac{1}{\pi M_0}\left\{\left[2(1+t_0^2)-\frac{1}{4}t_0^4(1+4M_0^2)\right]\arccos\frac{M_0t_0-1}{t_0}+\frac{2M_0}{\beta}\arccos(M_0-\beta^2t_0)+\frac{1}{12}[42-22M_0t_0+(2M_0^2+3)t_0^2+(2M_0^2+13)M_0t_0^3]\sqrt{t_0^2-(1-M_0t_0)^2}\right\} \tag{105b}$$

and for $\frac{1}{M_0-1}\leq t_0$ (third interval)

$$C_{m_q}'=-\frac{2}{\beta} \tag{105c}$$

Numerical results are presented in Part IV.

INDICIAL LOADING FOR SINKING TRIANGULAR WING WITH SUBSONIC LEADING EDGES

The six regions.—As in the study of supersonic-edged triangular wings, there are also in the case of triangular wings with subsonic leading edges various regions in which the analytical form of the loading equation is different. Figure 46 shows the regions into which the subsonic-edged triangular wing can be most conveniently divided, where the trailing edges are again assumed to be supersonic and the solutions are cut off appropriately. Most of these regions have counterparts on the supersonic-edged wing shown in figure 37.

To begin with, region 6 lies within the spherical wave which started at $t=0$ from the wing apex. Region 1 is within the cylindrical wave which was started at $t=0$ by one edge of the wing, but outside the wave started by the other edge. Region 4 is the area formed by the overlapping of the two cylindrical waves from the opposite edges, but outside the region influenced by the reflection of one of these waves on the opposite edge (secondary wave fronts shown in the figure). Region 5 is the area between regions 4 and 6 where the flow is influenced by secondary (and higher order) wave reflections. Finally, regions 2 and 3 are similar to regions 2 and 3 in the supersonic-edged case; region 2 being that uninfluenced by the starting phenomena and therefore having a loading already at its steady-state value, and region 3 being that which is unaffected by the disturbances emanating from the edges.

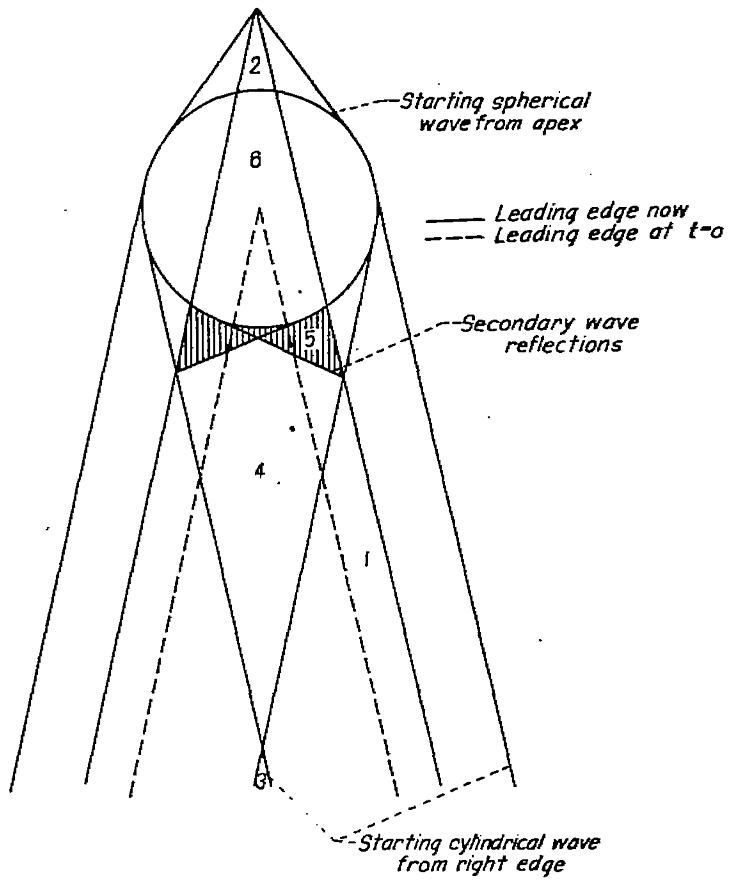

FIGURE 46.—The six regions used in the analysis of the triangular wing with subsonic leading edges.

Region 1: The solution for the load distribution in region 1 is the same as that for a two-dimensional wing starting suddenly from rest and moving with a steady subsonic velocity V_n normal to the leading edge. A solution to the latter problem for the initial part of the motion is presented as equation (A6(b)) in appendix A. In terms of the normal components of velocity and distance, therefore, the loading coefficient for the right-hand side of figure 46 can be written immediately:

$$\left(\frac{\Delta p}{q_n}\right)_1=-\frac{8w_0}{\pi V_n M_n}\left(\frac{M_n}{1+M_n}\sqrt{\frac{t-x_n}{M_n t+x_n}}+\text{arc tan}\sqrt{\frac{M_n t+x_n}{t-x_n}}\right)$$

The equations which relate the normal components to those in the free-stream direction have already been given in the section on region 4 of the supersonic-edged wing. Use of these relations leads to the following expression for loading in region 1 (in the coordinate system of fig. 47):

$$\left(\frac{\Delta p}{q_0}\right)_1=\frac{8\alpha}{\pi M_0}\left(\frac{mM_0}{mM_0+\sqrt{1+m^2}}\sqrt{\frac{t\sqrt{1+m^2}+|y|-mx}{mM_0t-|y|+mx}}+\text{arc tan}\sqrt{\frac{mM_0t-|y|+mx}{t\sqrt{1+m^2}+|y|-mx}}\right) \tag{106}$$

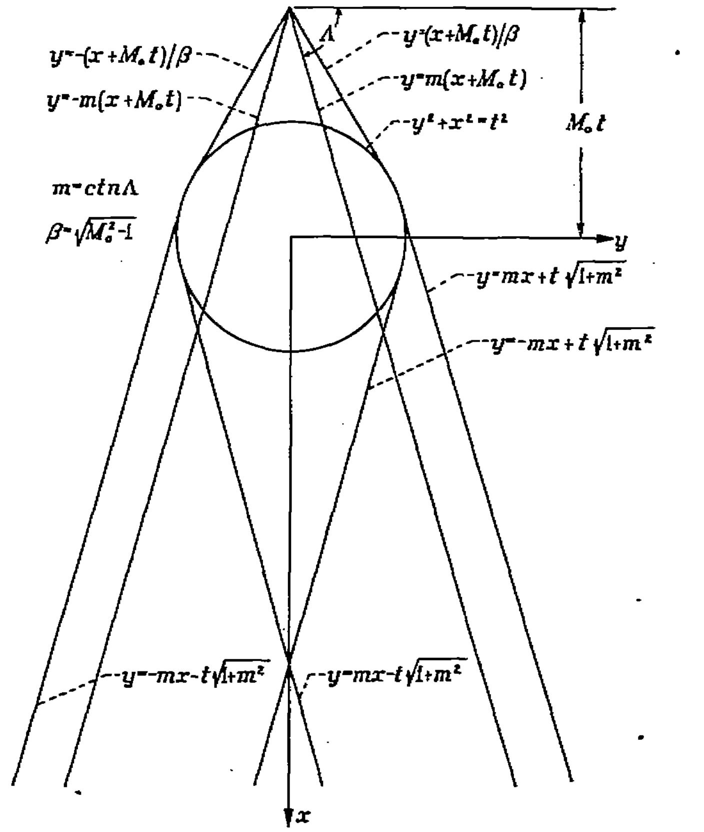

FIGURE 47.—Equations of lines used in the analysis of the triangular wing with subsonic leading edges.

Region 2: The loading on region 2, being the steady-state loading on a triangular wing with subsonic edges, is well known. The solution for region 2 of figure 46 is therefore given by (see, for convenience, reference 22)

$$\left(\frac{\Delta p}{q_0}\right)_2=\frac{4\alpha m^2(x+M_0t)}{E\sqrt{m^2(x+M_0t)^2-y^2}} \tag{107}$$

where E is the complete elliptic integral of the second kind with modulus $\sqrt{1-\beta^2m^2}$.

Region 3: The loading in region 3 follows from reference 21 and is

$$\left(\frac{\Delta p}{q_0}\right)_3=\frac{4\alpha}{M_0} \tag{108}$$

Region 4: The loading in region 4 of figure 46 is calculated by superposition, just as the solution for region 5 of the wing with supersonic edges was obtained. The solution in region 4 is the sum of the solutions for the right and left halves of region 1, minus the result for region 3. Thus

$$\left(\frac{\Delta p}{q_0}\right)_4=\frac{8\alpha}{\pi M_0}\left[\frac{mM_0}{mM_0+\sqrt{1+m^2}}\left(\sqrt{\frac{t\sqrt{1+m^2}-y-mx}{mM_0t+y+mx}}+\sqrt{\frac{t\sqrt{1+m^2}+y-mx}{mM_0t-y+mx}}\right)+\arctan\sqrt{\frac{mM_0t+y+mx}{t\sqrt{1+m^2}-y-mx}}+\arctan\sqrt{\frac{mM_0t-y+mx}{t\sqrt{1+m^2}+y-mx}}-\frac{\pi}{2}\right] \tag{109}$$

Regions 5 and 6: In these regions the exact solution for the loading has not been determined. As was shown in the section on homogeneous boundary-value problems, such solutions would require the solution of a three-dimensional elliptic-type partial differential equation. A later section will contain an approximate solution for these regions when the wing plan form is slender.

Discussion.—An isometric drawing of the load distribution, for the regions in which it is known, is shown in figure 48. Comparing the results for the loading on this wing to the one with supersonic edges (fig. 44), it is apparent that the principal difference in the two distributions is in the behavior around the leading edges; the loading being finite at the supersonic edge, whereas it becomes infinite at the subsonic edge. In view of the known steady-state results this difference was to be expected. Elsewhere the loadings are quite similar.

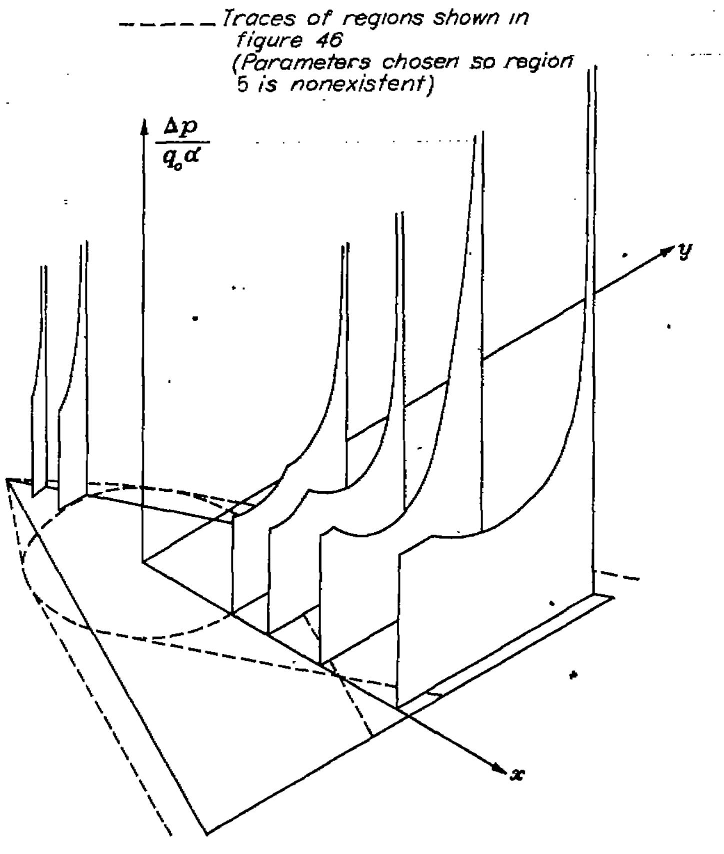

FIGURE 48.—Distribution of indicial loading on right panel of subsonic-edged triangular wing.

The results presented in equations (106) through (109) will next be examined in a different light. Choose a given spanwise section on the wing and watch this section as time progresses from $t=0$. This amounts to fixing the axis on the body and can be accomplished simply by using the quantity s introduced in equation (93),

$$s=m(x+M_0t).$$

It is clear that s is the semispan of a given spanwise sections and that if equations (106) through (109) are written in term, of s, y, and t, for a fixed s they represent the variation of loading on a given section as time progresses.

If the notation is further simplified by introducing the parameter β_e where

$$\beta_e=\frac{1}{mM_0+\sqrt{1+m^2}} \tag{110}$$

equations (106) through (109) can be written in the following way:

$$\left(\frac{\Delta p}{q_0}\right)_1=\frac{8\alpha}{\pi M_0}\left(mM_0\beta_e\sqrt{\frac{(t/\beta_e)-s+|y|}{s-|y|}}+\arctan\sqrt{\frac{s-|y|}{(t/\beta_e)-s+|y|}}\right) \tag{111}$$

$$\left(\frac{\Delta p}{q_0}\right)_2=\frac{4\alpha ms}{E\sqrt{s^2-y^2}} \tag{112}$$

$$\left(\frac{\Delta p}{q_0}\right)_3=\frac{4\alpha}{M_0} \tag{113}$$

$$\left(\frac{\Delta p}{q_0}\right)_4=\frac{8\alpha}{\pi M_0}\left(mM_0\beta_e\sqrt{\frac{(t/\beta_e)+y-s}{s-y}}+mM_0\beta_e\sqrt{\frac{(t/\beta_e)-y-s}{s+y}}+\arctan\sqrt{\frac{s-y}{(t/\beta_e)+y-s}}+\arctan\sqrt{\frac{s+y}{(t/\beta_e)-y-s}}-\frac{\pi}{2}\right) \tag{114}$$

The load distribution across any section is given by equations (111), (113), and (114) from the time $t/\beta_e=0$ to $(t/\beta_e)_1$, where the term $(t/\beta_e)_1$ is equal to $2s$ or $s/m(M_0+1)\beta_e$, whichever is smaller. (At $t/\beta_e=2s$ the secondary waves shown in fig. 46 have just reached the spanwise section, and at $t/\beta_e=s/m\beta_e(M_0+1)$ the spherical wave which started from the apex has just reached the spanwise section.) From $(t/\beta_e)_1$ to $(t/\beta_e)_2=s/m\beta_e(M_0-1)$, the loading has not been determined and from $t/\beta_e=(t/\beta_e)_2$ to $t=\infty$ the loading is the steady-state value given by equation (112). Figure 49 shows this initial and final load variation plotted as a function of the parameter t/β_e. At the beginning of the motion the loading is constant across the span, but this type of distribution is quickly modified and the shape of the curve tends toward the steady-state loading given by equation (112) and shown in the figure as the distribution at $t/\beta_e=(t/\beta_e)_2$. In fact, if the span is crossed first by the secondary waves rather than the spherical wave, when this span has traveled a distance such that

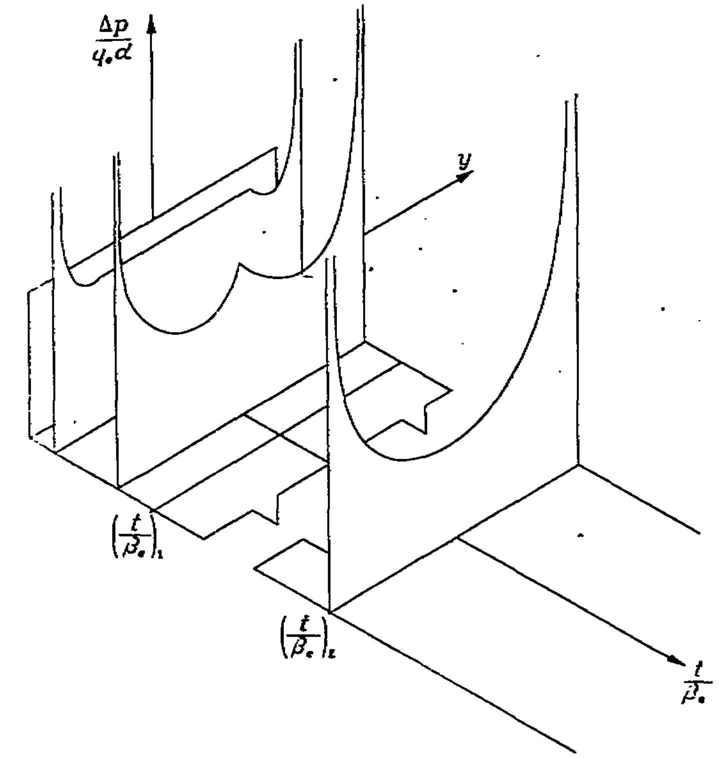

FIGURE 49.—Variation of indicial loading with t/β_e at a fixed spanwise section.

$t/\beta_e=2s$, the expression for the loading given by equation (114) becomes

$$\left(\frac{\Delta p}{q_0}\right)_{\frac{t}{\beta_e}=2s}=\frac{16m\beta_e s\alpha}{\pi\sqrt{s^2-y^2}} \tag{115}$$

which differs from the value given by equation (112) only by a constant of proportionality. Both before and after the time $t/\beta_e=2s$ the shape of the loading curve varies from the simple type represented by equation (115), but the trend is established.

The average chord loading factor P_0, introduced by equation (92a), can now be determined for certain regions. Hence, if the notation

$$\left.\begin{aligned} \tau&=t/s \\ P_0&=\frac{M_0}{2s\alpha}\int_{-s}^{s}\frac{\Delta p}{q_0}\,dy \end{aligned}\right\} \tag{116}$$

is adopted, there results for the early part of the motion, that is, for $0\leq\tau/\beta_e\leq(\tau/\beta_e)_1$

$$P_0=2\left(2-\frac{\tau}{\beta_e}\right)+4m\beta_e M_0(\tau/\beta_e) \tag{117}$$

Equation (117) was derived by integrating equations (111), (113), and (114). For values of $\tau/\beta_e\geq 1/\beta_e m(M_0-1)=\left(\frac{\tau}{\beta_e}\right)_2$ equation (112) is valid. Hence for $\frac{\tau}{\beta_e}\geq\left(\frac{\tau}{\beta_e}\right)_2$

$$P_0=\frac{2\pi m M_0}{E} \tag{118}$$

Figure 50 indicates the magnitude of this average load for both large and small values of τ/β_e. Notice that for small values of τ/β_e it is sufficient for the establishment of the curve to specify the parameter $mM_0\beta_e$, but for large values an additional parameter must be given (such as M_0 in the figure). Notice, further, that in spite of the large variation in the distribution of the loading, as shown in the previous sketch, the average value P_0 varies linearly throughout the intervals considered. This result is similar to the one obtained for triangular wings with supersonic edges.

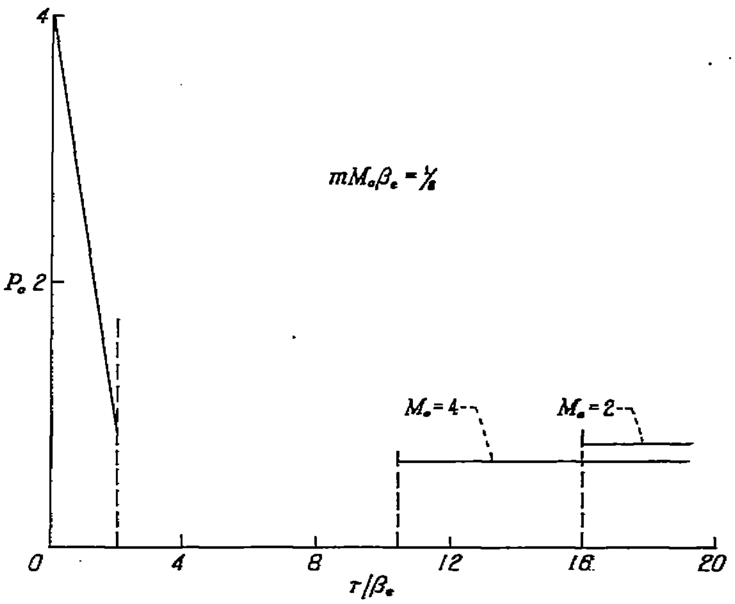

FIGURE 50.—Variation of P_0 with t/β_e at a fixed spanwise section.

INDICIAL LOADING ON VERY SLENDER TRIANGULAR WINGS

In Part II of this report it was pointed out that if the wing is slender (i. e., has a small ratio of span to chordwise length) the governing partial differential equation simplified to the form

$$\varphi_{tt}-\varphi_{yy}-\varphi_{zz}=0 \tag{119}$$

where the independent variables refer to a coordinate system that is either fixed on the wing or is fixed with respect to the still air at infinity. The boundary conditions that apply when the axes are fixed on the wing will now be considered in some detail. (In Part II the variables x_1, y_1, z_1 and t_1 were used to denote this coordinate system. In order to avoid a cumbersome notation, however, the subscript 1 will be deleted in the following.)

Just as in the previous sections of this report, consider a triangular wing which is at rest for $t<0$, starts suddenly to move at a forward velocity equal to V_0 at $t=0$, and continues at this same velocity for $t>0$. In this case, the triangular wing can be considered as having a finite chord, since spanwise sections act independently in slender wing theory, and the final integration in the x direction can be stopped at any desired chord length. It should be emphasized that in this case, V_0 may be either subsonic or supersonic. A section in the spanwise direction, as for instance section AA in figure 51 has a trace in the yt plane which is a narrow rectangular

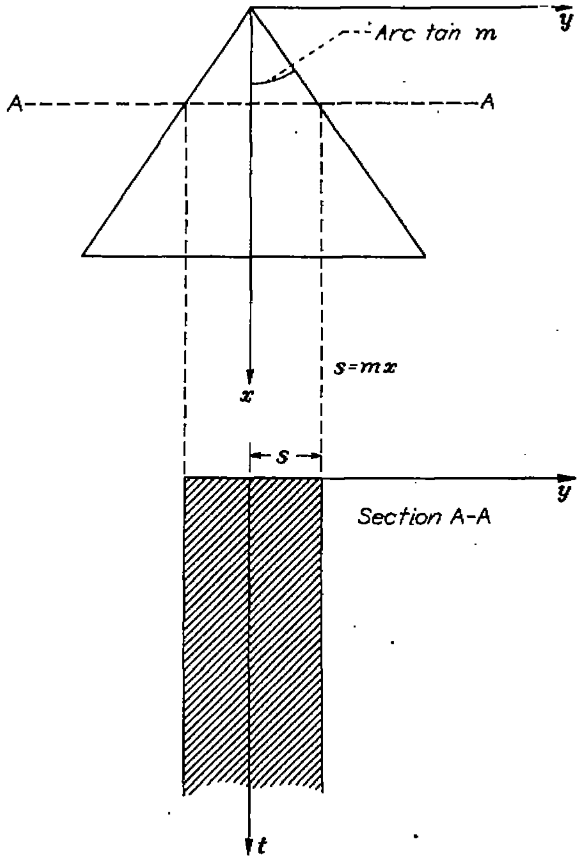

FIGURE 51.—Slender wing in xy plane and trace of section in yt plane.

strip along the t axis. Since equation (119) has been derived on the assumption that the velocity gradients in the y, z, and t directions are independent of the gradient in the x direction, the boundary conditions along the strip shown in the figure are independent of those on other strips corresponding to traces from spanwise sections along the wing. Hence, the problem is to find a solution to equation (119) which will make φ_z constant over the strip (since a given spanwise section experiences constant downwash whether the slender triangular wing is undergoing sinking or pitching motion) and at the same time will satisfy the other conditions listed under equation (2). In the lifting-surface analog this corresponds to the problem of finding the velocity potential over a flat rectangular wing of low aspect ratio situated in a free stream moving at a Mach number equal to $\sqrt{2}$. Solutions to the latter problem can be obtained by various techniques, and so the procedure will be first, to find the potential for the steady-state, flat, rectangular wing, and then, by analogy, to convert this to the solution for either the sinking or pitching slender triangular wing.

The steady-state, lifting-surface problem.—Lifting-surface solutions for the loading on a rectangular wing traveling at supersonic speeds have been developed for regions 1, 2, and 3 of figure 52 (by Busemann and others), and by means of these solutions the load distribution on a spanwise section of the triangular wing can be determined to a time necessary for sound to travel that span length. For $t>2s$, however, the solution becomes considerably complicated by the increasing number of reflections from the edges. Reference 24 gives solutions for the loading on a rectangular wing in region 4 and indicates methods for extending the solution to

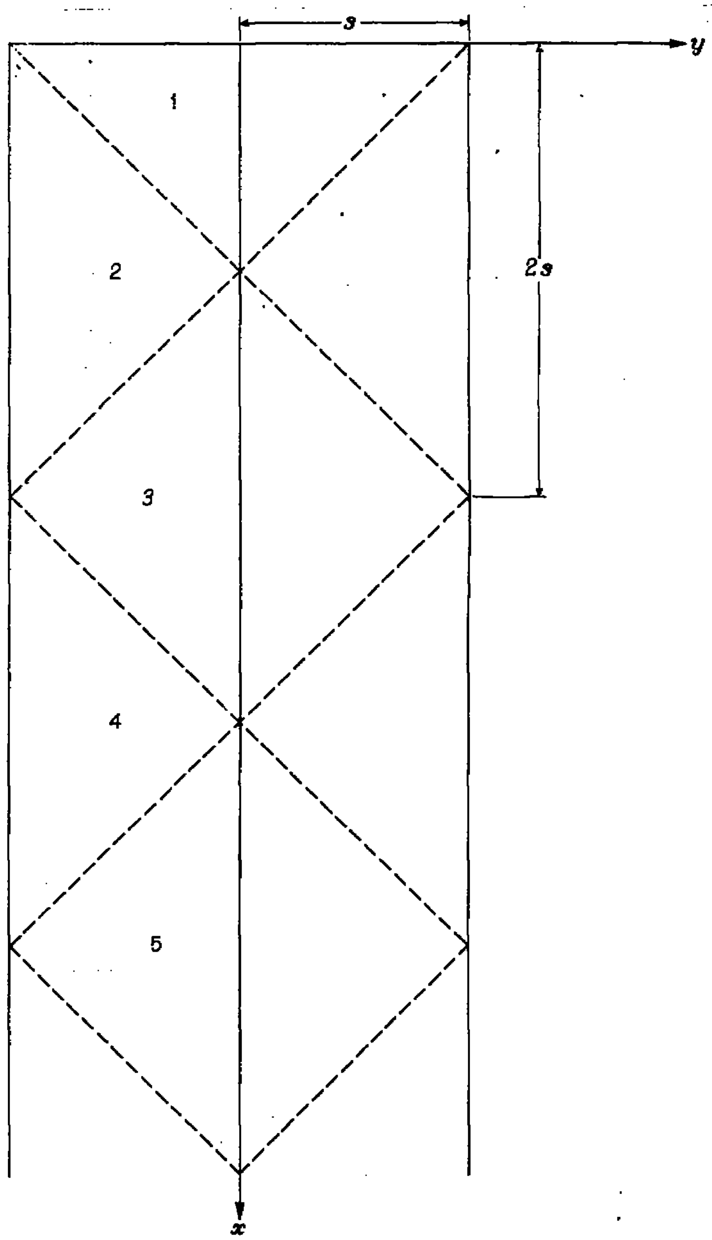

FIGURE 52.—Regions used in the discussion of the low-aspect-ratio rectangular wing.

regions farther along the wing. Already in region 4, however, the expression is cumbersome and in higher-numbered regions the expressions become difficult to manipulate. These methods, therefore, will be discarded in favor of a more approximate but simpler analysis.

If x is the distance along the chord, y the distance along the span, and s the semispan, then the solution for regions 1, 2, and 3 of figure 52 can be written (for convenience, see reference 22):

Region 1

$$\frac{\Delta p}{q_0}=-4\,\frac{w}{V_0} \tag{120a}$$

Region 2

$$\frac{\Delta p}{q_0}=-\frac{8w}{\pi V_0}\arctan\sqrt{\frac{s-|y|}{x-s+|y|}} \tag{120b}$$

Region 3

$$\frac{\Delta p}{q_0}=-\frac{8w}{\pi V_0}\left(\arctan\sqrt{\frac{s+y}{x-s-y}}+\arctan\sqrt{\frac{s-y}{x-s+y}}-\frac{\pi}{2}\right) \tag{120c}$$

As x increases (i. e., for higher-numbered regions in fig. 52) it is reasonable to assume that the spanwise variation of loading is virtually invariant with x, that it is "smooth," and that it falls to zero at the side edges. Assume, therefore, that the loading is given by the relation

$$\frac{\Delta p}{q_0}=-4\frac{w}{V_0}f\left(\frac{x}{s}\right)\sqrt{1-\left(\frac{y}{s}\right)^2} \tag{121}$$

Spanwise, this has the variation shown in figure 53; chordwise it is as yet arbitrary. To fix the chordwise distribution the value of $f(x/s)$ will be determined so that the vertical induced velocity along the center line is constant and equal to w.

The solution to this somewhat artificial problem approaches the exact solution to the steady-state lifting-surface problem for a flat rectangular wing along sections far behind the leading edge; closer to the leading edge it only approximates the exact solution; and, of course, in the vicinity of the leading edge it will be least representative. But, on the other hand, the exact solution is known in the vicinity of the leading edge and it turns out that the solution of the problem posed above forms a reasonable continuation over the remainder of the wing.

The velocity potential for the problem which has been set can be readily expressed in terms of an integration of elementary horseshoe vortices over the plan form. Since the Mach number equals $\sqrt{2}$, then according to reference 19,

$$\varphi=\frac{V_0z}{4\pi}\int_A\int\frac{(x-x_1)(\Delta p/q_0)dx_1dy_1}{(y_1^2+z^2)\sqrt{(x-x_1)^2-y_1^2-z^2}}$$

where A is the area on the wing within the forecone from the point $P(x,y,z)$, at which φ is to be determined (the shaded area in fig. 53).

The simplification of the last expression is given in reference 19. The result is the integral equation

$$1=f(\eta)+\frac{2}{\pi}\int_0^\eta f(\eta_1)G(\eta-\eta_1)d\eta_1 \tag{122}$$

where $\eta=x/s$ and G is given by

$$G(\eta-\eta_1)=\begin{cases} E_1 & 1\leq\eta-\eta_1 \\ \dfrac{E_2-(1-k_2^2)K_2}{k_2} & \eta-\eta_1\leq 1\end{cases}$$

$$k_1=\frac{1}{\eta-\eta_1};\ k_2=\eta-\eta_1$$

The modulus of E_1 is k_1 and the modulus of K_2 and E_2 is k_2.

The solution of equation (122) for $f(\eta)$ is not difficult when numerical methods are used. For intervals of η_1 equal to 0.2, the result is given in tabular form in table III, and also in figure 54. As mentioned previously, the function $f(\eta)$ determined by this approximate method will be least representative of the exact solution in the region near the leading edge. However, since the exact solution is known for $x/s=\eta\leq 2$, a compromise can be effected. If the spanwise average of the loading is calculated from equations (120), it is found to be a linear function of η, starting at $4/\pi$ for $\eta=0$ and falling to zero at $\eta=2$. On the other hand, the spanwise average of loading given by equation (121) is $-\pi\frac{w}{V_0}f(\eta)$. Therefore, an improved solution for $f(\eta)$ consists in taking $f(\eta)$ as the value given by

$$f(\eta)=\frac{2}{\pi}(2-\eta)$$

in the region $0\leq\eta\leq 2$, and then fairing this curve into that given by the solution of equation (122) for $\eta>2$. The two curves are shown in figure 54.

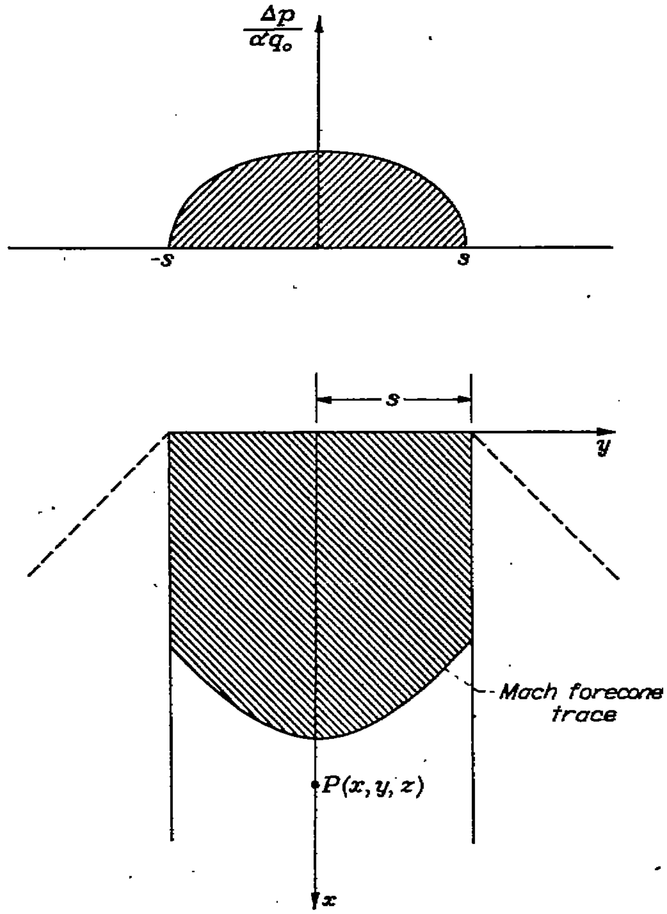

FIGURE 53.—Spanwise loading and region of integration used in the analysis of the low-aspect-ratio rectangular wing.

By using the results listed in table III, the loading over a low-aspect-ratio rectangular wing flying at a Mach number equal to $\sqrt{2}$ can be estimated. Of particular interest is the damped oscillatory nature of the load, as shown in figure 54, falling to zero at one span length behind the leading edge and taking alternately negative and positive values beyond this point. (See reference 25.) A somewhat different approach to this problem (reference 26) has led to a solution very like the one given here.

TABLE III.—SOLUTION OF EQUATION (122)

η	$f(\eta)$	$\int_0^\eta f(\eta_1)d\eta_1$	η	$f(\eta)$	$\int_0^\eta f(\eta_1)d\eta_1$
0.0	1.0000	0.0000	4.0	−0.1307	1.0124
.2	.9899	.1990	4.2	−.1008	.9893
.4	.9597	.3940	4.4	−.0716	.9720
.6	.9087	.5808	4.6	−.0446	.9604
.8	.8356	.7552	4.8	−.0207	.9539
1.0	.7339	.9122	5.0	−.0008	.9517
1.2	.6032	1.0459	5.2	.0149	.9531
1.4	.4597	1.1522	5.4	.0265	.9578
1.6	.3188	1.2300	5.6	.0340	.9633
1.8	.1880	1.2807	5.8	.0379	.9705
2.0	.0724	1.3067	6.0	.0388	.9782
2.2	−.0245	1.3115	6.2	.0373	.9858
2.4	−.1008	1.2990	6.4	.0338	.9929
2.6	−.1562	1.2733	6.6	.0292	.9992
2.8	−.1919	1.2385	6.8	.0237	1.0045
3.0	−.2098	1.1983	7.0	.0180	1.0087
3.2	−.2126	1.1561	7.2	.0124	1.0117
3.4	−.2031	1.1145	7.4	.0072	1.0137
3.6	−.1843	1.0758	7.6	.0026	1.0146
3.8	−.1593	1.0414	7.8	−.0012	1.0148

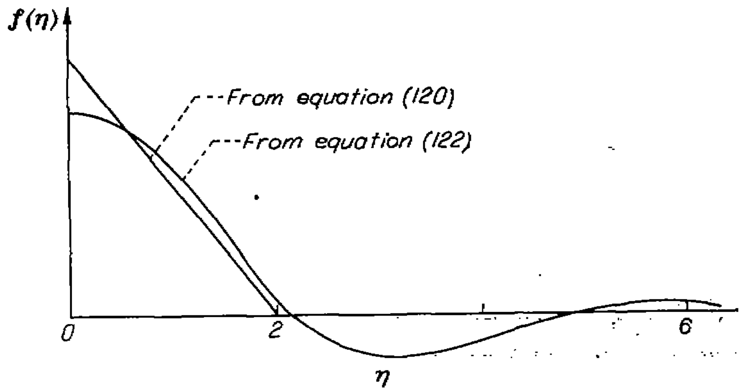

FIGURE 54.—Variation of $f(\eta)$ with η.

The unsteady-analog, sinking wing.—The first step in deriving the unsteady-flow results for the sinking wing from the steady solution is to replace x with t. In equation (122) this corresponds to replacing η with τ where τ is equal to t/s (equations (116)). The second step is to replace w/V_0 with $-\alpha$ and to rederive the expression for loading coefficient since in the time-varying problem it is expressed in a somewhat different manner than in the steady-state analog. In the unsteady case, as the triangular wing moves through a fixed reference plane the local span intersecting this plane grows as a function of time and equation (12), which represents the partial derivative with respect to time with x fixed, must be expanded to the form

$$\frac{\Delta p}{q_0}=\frac{2}{V_0M_0}\left[\frac{\partial\Delta\varphi}{\partial t}\right]_x=\frac{2}{V_0M_0}\left(\left[\frac{\partial\Delta\varphi}{\partial t}\right]_s+\left[\frac{\partial\Delta\varphi}{\partial s}\right]_t\frac{\partial s}{\partial t}\right)$$

where $\left[\frac{\partial\Delta\varphi}{\partial t}\right]_s$ and $\left[\frac{\partial\Delta\varphi}{\partial s}\right]_t$ indicate derivatives taken at constant s and t, respectively. Since s is equal to $m(x+M_0t)$, $\partial s/\partial t$ equals mM_0, and there results

$$\frac{\Delta p}{q_0}=\frac{2}{V_0M_0}\left(\left[\frac{\partial\Delta\varphi}{\partial t}\right]_s+mM_0\left[\frac{\partial\Delta\varphi}{\partial s}\right]_t\right) \tag{123}$$

In the steady-state problems an analog to the term involving $\left[\frac{\partial\Delta\varphi}{\partial s}\right]_t$ is missing, and the loading coefficient is given entirely by an operation equivalent to $\left[\frac{\partial\Delta\varphi}{\partial t}\right]_s$. It is necessary, therefore, to operate further on the solution given for the loading in the steady-state problem to obtain the solution for the loading in the unsteady problem. But

$$\left[\frac{\partial\Delta\varphi}{\partial s}\right]_t=\frac{\partial}{\partial s}\int_0^t\left[\frac{\partial\Delta\varphi}{\partial t}\right]_s dt_1$$

so that if the notation

$$\left[\frac{\partial\Delta\varphi}{\partial t}\right]_s=\frac{V_0}{2}\left(\frac{\Delta p}{q_0}\right)_s$$

is adopted (where $\left(\frac{\Delta p}{q_0}\right)_s$ represents the loading in the analogous steady-state problem), then the expression for the unsteady loading can be given in terms of $\left(\frac{\Delta p}{q_0}\right)_s$ by the equation

$$\frac{\Delta p}{q_0}=\frac{1}{M_0}\left[\left(\frac{\Delta p}{q_0}\right)_s+mM_0\frac{\partial}{\partial s}\int_0^t\left(\frac{\Delta p}{q_0}\right)_s dt_1\right] \tag{124}$$

By the application of equation (124) to equations (120), the loading for the various regions in the yt plane of the unsteady wing can be found. For region 2 in figure 55 there results

$$\frac{\Delta p}{q_0}=\frac{1}{M_0}\left[\frac{8\alpha}{\pi}\arctan\sqrt{\frac{s-|y|}{t-s+|y|}}+mM_0\frac{\partial}{\partial s}\left(\int_0^{s-|y|}4\alpha\,dt_1+\int_{s-|y|}^{t}\frac{8\alpha}{\pi}\arctan\sqrt{\frac{s-|y|}{t_1-s+|y|}}\,dt_1\right)\right]$$

which becomes

$$\frac{\Delta p}{q_0}=\frac{8\alpha}{\pi M_0}\left[mM_0\sqrt{\frac{t-s+|y|}{s-|y|}}+\arctan\sqrt{\frac{s-|y|}{t-s+|y|}}\right]$$

The loading coefficient can be similarly derived in the other regions so that finally, for the regions shown in figure 55,

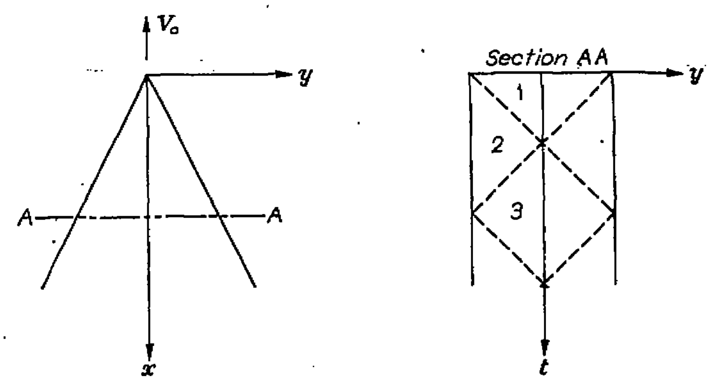

FIGURE 55.—Regions used to express loading on section of unsteady, subsonic-edged, triangular wing.

Region 1

$$\frac{\Delta p}{q_0}=\frac{4\alpha}{M_0} \tag{125a}$$

Region 2

$$\frac{\Delta p}{q_0}=\frac{8\alpha}{\pi M_0}\left(mM_0\sqrt{\frac{t-s+|y|}{s-|y|}}+\arctan\sqrt{\frac{s-|y|}{t-s+|y|}}\right) \tag{125b}$$

Region 3

$$\frac{\Delta p}{q_0}=\frac{8\alpha}{\pi M_0}\left(mM_0\sqrt{\frac{t-s+y}{s-y}}+mM_0\sqrt{\frac{t-s-y}{s+y}}+\right.$$
$$\left.\text{arc tan}\sqrt{\frac{s-y}{t-s+y}}+\text{arc tan}\sqrt{\frac{s+y}{t-s-y}}-\frac{\pi}{2}\right) \tag{125c}$$

For the interval $t\geq 2s$ equation (121) must be considered. By means of equation (124), the expression for the loading coefficient can be written

$$\frac{\Delta p}{q_0}=\frac{1}{M_0}\left[4\alpha f(\tau)\sqrt{1-\left(\frac{y}{s}\right)^2}+mM_0\frac{\partial}{\partial s}\int_0^t 4\alpha f\left(\frac{t_1}{s}\right)\sqrt{1-\left(\frac{y}{s}\right)^2}dt_1\right]$$

which becomes

$$\frac{\Delta p}{q_0}=\frac{4\alpha}{M_0}\left[(1-mM_0\tau)\sqrt{1-\left(\frac{y}{s}\right)^2}f(\tau)+\frac{mM_0}{\sqrt{1-\left(\frac{y}{s}\right)^2}}\int_0^\tau f(\tau_1)d\tau_1\right] \tag{126}$$

where $f(\tau)$ is the solution to equation (122). Notice that for large τ (when the loading has reached its steady state), $f(\tau)$ is zero and $\int_0^\tau f(\tau_1)d\tau_1$ is unity. (See table III.) Hence, the loading is given by the equation

$$\frac{\Delta p}{q_0}=\frac{4\alpha ms}{\sqrt{s^2-y^2}}$$

which is the steady-state value for a slender triangular wing (equation (112) when $E=1$).

It is now possible to derive the chord loading factor P_0 as defined by equation (92a), thus

$$P_0=\frac{M_0}{2s\alpha}\int_{-s}^{s}\frac{\Delta p}{q_0}dy$$

Placing equations (125) and (126) in this expression, it is found that for $0\leq\tau\leq 2$

$$P_0=2(2-\tau)+4mM_0\tau \tag{127a}$$

and for $\tau\geq 2$

$$P_0=\pi(1-mM_0\tau)f(\tau)+2mM_0\pi\int_0^\tau f(\tau_1)d\tau_1 \tag{127b}$$

Since the values of P_0 given by equations (127a) and (127b) were derived using different methods, their magnitudes at $\tau=2$ are not equal. The final curve for P_0 must be constructed by fairing the solution for $\tau\leq 2$ into that for $\tau>2$. Figure 56 shows these results together with the final curve chosen (solid line).

The unsteady-analog, pitching wing.—When the wing is pitching at a steady rate about its apex, the equation for the vertical induced velocity on the plan form is

$$w_a=-(x+M_0t)\dot{\theta}$$

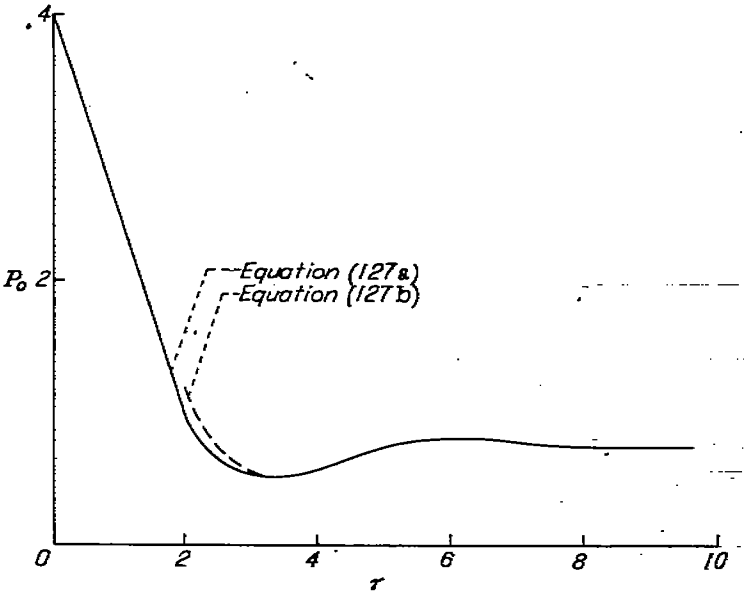

FIGURE 56.—Variation of P_0 with τ.

so that $-w/V_0$ in the steady-state equations (120) and (121) becomes $\dot{\theta}s/mV_0$. Since the loading coefficient is still given by equation (124), there results for the conversion of equation (121) the expression

$$\frac{\Delta p}{q_0}=\frac{4\dot{\theta}}{mM_0V_0}\left[\sqrt{s^2-y^2}f(\tau)+mM_0\frac{\partial}{\partial s}s\sqrt{s^2-y^2}\int_0^{t/s}f(\tau_1)d\tau_1\right]$$

and this can be reduced to the form

$$\frac{\Delta p}{q_0}=\frac{4\dot{\theta}}{mM_0V_0}(1-mM_0\tau)\sqrt{s^2-y^2}f(\tau)+$$
$$\frac{4\dot{\theta}}{V_0}\left(\frac{2s^2-y^2}{\sqrt{s^2-y^2}}\right)\int_0^\tau f(\tau_1)d\tau_1 \tag{128}$$

As in the discussion of equations (127), it can be seen that equation (128) becomes for the steady state (τ large)

$$\frac{\Delta p}{q_0}=\frac{4\dot{\theta}}{V_0}\left(\frac{2s^2-y^2}{\sqrt{s^2-y^2}}\right)$$

and this can be shown to agree with the steady-state slender-wing results given in reference 27.

It is now possible to derive the chord loading factor P_1 as defined by equation (92b)

$$P_1=\frac{mM_0V_0}{2s^2\dot{\theta}}\int_{-s}^{s}\frac{\Delta p}{q_0}dy$$

Using equation (128), one finds for $\tau>2$

$$P_1=\pi(1-mM_0\tau)f(\tau)+3mM_0\pi\int_0^\tau f(\tau_1)d\tau_1 \tag{129a}$$

and a similar analysis based on equation (120) yields for $0\leq\tau\leq 2$

$$P_1=\frac{2s}{m}\left(2-\tau+4mM_0\tau-\frac{1}{2}mM_0\tau^2\right) \tag{129b}$$

As in the case for P_0, the two equations for P_1 do not join at $\tau=2$ and the final curve must be constructed by fairing the solution for $\tau\leq 2$ into that for $\tau\geq 2$ (see fig. 57).

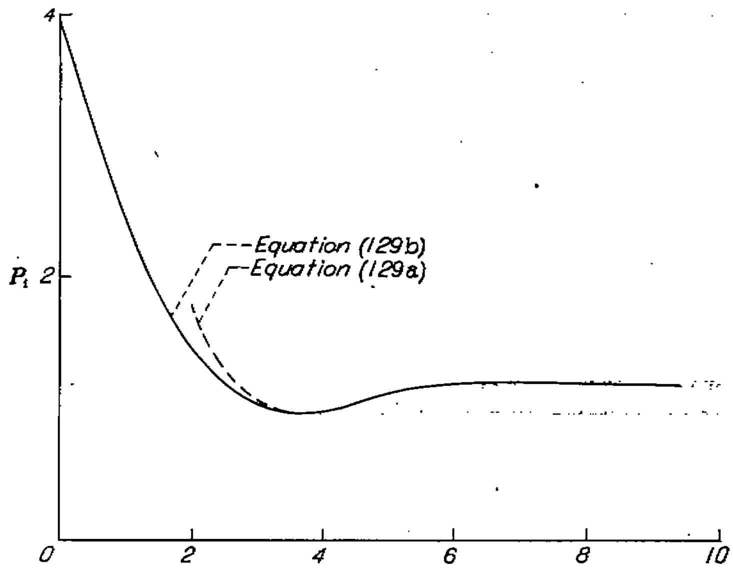

FIGURE 57.—Variation of P_1 with τ.

Discussion.—It is now possible to assess the accuracy of the solution for very slender wings in the interval $0\leq\tau\leq 2$ by comparing the values of loading given by slender wing theory (equations (125)) with the exact loadings given by equations (111), (113), and (114), and also by comparing the slender wing value of the chord loading factor P_0 (equation (127 a)) with the exact value given by equation (117). It is apparent that the approximate solution differs from the exact only by a stretching factor in the t direction. Hence, if τ is replaced by τ/β_e and m (note m is proportional to y/t) by $m\beta_e$, where β_e is given by equation (110), then equations (125a), (b), and (c) are identical with equations (113), (111), and (114), respectively, and, of course, equation (127a) corresponds to equation (117).

This rather remarkable result can be enlarged upon from another viewpoint. Suppose that in the steady-state analog problem the wing had been flying at some Mach number other than $\sqrt{2}$, say M_e. The solution to such a new problem could be obtained from the old one merely by applying the Prandtl-Glauert correction, that is, by stretching all distances in the x direction by the factor $1/\beta_e$ where $\beta_e^2=|1-M_e^2|$. Such a procedure would convert, for example, equation (127a) to the form

$$P_0\beta_e=2(2-\tau/\beta_e)+4m\ \beta_e M_0\ \tau/\beta_e$$

Finally, if P_0 is adjusted so that $P_0=4$ at $\tau=0$, there results

$$P_0=2(2-\tau/\beta_e)+4mM_0\tau$$

which is exactly the answer given by equation (117). It is possible to simplify the statement of the procedure by simply remarking: The exact results for $\Delta p/q_0$ or P_0 in the interval $0\leq\tau/\beta_e\leq 2$ can be obtained from the approximate results for a very slender wing by making an effective Mach number correction to the right-hand side of equation (125) or (127a), respectively.

It is interesting to pursue this concept even further. Consider a spanwise section of a triangular wing as time increases from the starting impulse. The primary wave fronts emanating from either side pass across the section, forming the Mach lines in the steady-state rectangular-wing analogy. For very slender wings these lines make a 45° angle with the trace of the side edge and are used to divide the plan form into regions as in figure 58. Now find the actual position of these primary wave fronts as they form a trace on the section in the $y\tau$ plane. A straightforward calculation shows that these lines actually make an angle equal to arc tan $1/\beta_e$ with the trace of the side edges. Hence the effective Mach number which is used to correct the slender-wing results in the interval $0\leq\tau\leq 2\beta_e$ is that which makes the Mach lines of the steady-state analogy coincide with the actual trace of the primary wave fronts.

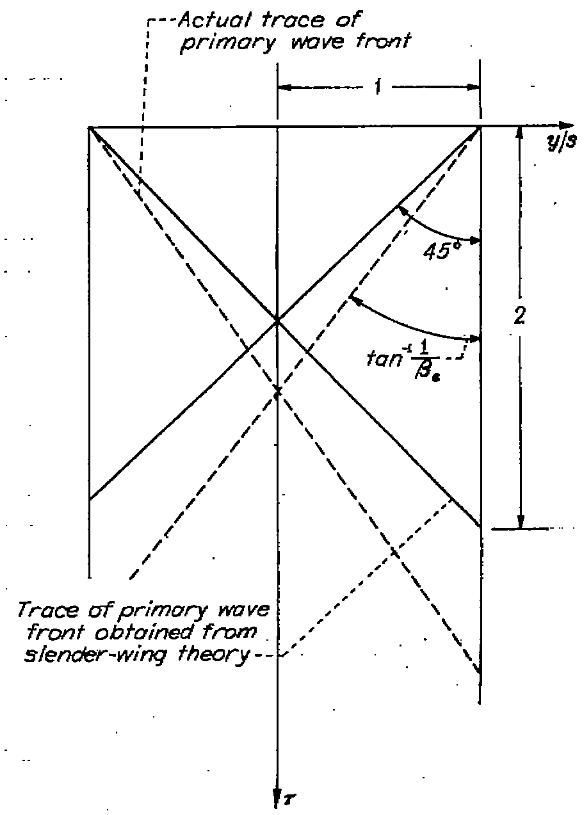

FIGURE 58.—Wave traces on spanwise section of slender wing.

INDICIAL LIFT AND PITCHING MOMENT ON VERY SLENDER TRIANGULAR WINGS

The lift coefficient for the sinking wing is given in the notation introduced in equation (92a) by the equation

$$C_L=\frac{\alpha}{mc_0^2}\int_0^{c_0}\frac{2s}{M_0}P_0dx$$

where P_0 has been determined in the last section as a function of $\tau=t/s$ and c_0 is the root chord. Consider the situation at a certain fixed time and let the x coordinate in the above formula be fixed in the wing. Then set

$$\zeta=\frac{x}{c_0}=\frac{s}{mc_0} \tag{130}$$

and as before

$$\tau_0 = \frac{M_0 t}{c_0} = m M_0 \zeta \tau \tag{131}$$

where τ_0 is the number of wing-chord lengths traveled. In this way it is possible to obtain the expression

$$M_0 C_{L_\alpha} = 2\int_0^1 \zeta P_0 \left(\frac{\tau_0}{m M_0 \zeta}\right) d\zeta \tag{132}$$

and similarly

$$M_0 C_{m_\alpha}{}' = -2\int_0^1 \zeta^2 P_0 \left(\frac{\tau_0}{m M_0 \zeta}\right) d\zeta \tag{133}$$

The equation for the lift and pitching-moment responses (where again the pitching moment is taken about the apex) on a pitching wing are

$$M_0 C_{L_q}{}' = \frac{M_0 C_L}{\left(\frac{c_0 \theta}{V_0}\right)} = 2\int_0^1 \zeta^2 P_1 \left(\frac{\tau_0}{m M_0 \zeta}\right) d\zeta \tag{134}$$

and

$$M_0 C_{m_q}{}' = \frac{M_0 C_m{}'}{\left(\frac{c_0 \theta}{V_0}\right)} = -2\int_0^1 \zeta^3 P_1 \left(\frac{\tau_0}{m M_0 \zeta}\right) d\zeta \tag{135}$$

The values of P_0 and P_1 were taken from curves similar to figures 56 and 57 in the last section (using the faired curves in the vicinity of $\tau=2$) and the results for the indicial lift and pitching moment in terms of τ_0, the number of chord lengths traveled, are shown in Part IV.

PART IV—RESULTS AND DISCUSSION

TWO-DIMENSIONAL RESULTS

The methods presented in the previous sections have been used to calculate the indicial lift and moment curves for two-dimensional wings flying at Mach numbers equal to 0, 0.5, 0.8, 1.0, 1.2, and 2.0. These results are presented in figure 59.

Figures 59 (a) and (b) show the variation of the indicial lift and moment on a sinking wing. The initial value of the lift is given by the expression $4\alpha/M_0$. When the free-stream Mach number goes to zero this expression still is valid, the initial value being a pulse of force that occurs at $t=0$. The final values of the lift are simply the two-dimensional, steady-state results given by the Prandtl-Glauert rule. Figures 59 (c) and (d) show the lift and moment variation on a wing pitching about its leading edge. These functions were not computed for $M_0=0.5$. The results are, of course, subject to the restrictions of linearized, compressible-flow theory and, for example, the calculated responses given in figure 59 for sonic speeds must be considered as being outside the realm of validity within a few chord lengths of travel. In application to high-frequency oscillations, however, the initial portions of the indicial curves dominate the response characteristics of the airfoil and calculations near M_0 equal to one need not be invalid.

More accurate values of the indicial curves are given in tables I and II for the subsonic Mach numbers 0.5 and 0.8. These tables can be extended to larger values of τ_0 by means of equations (71) and (72).

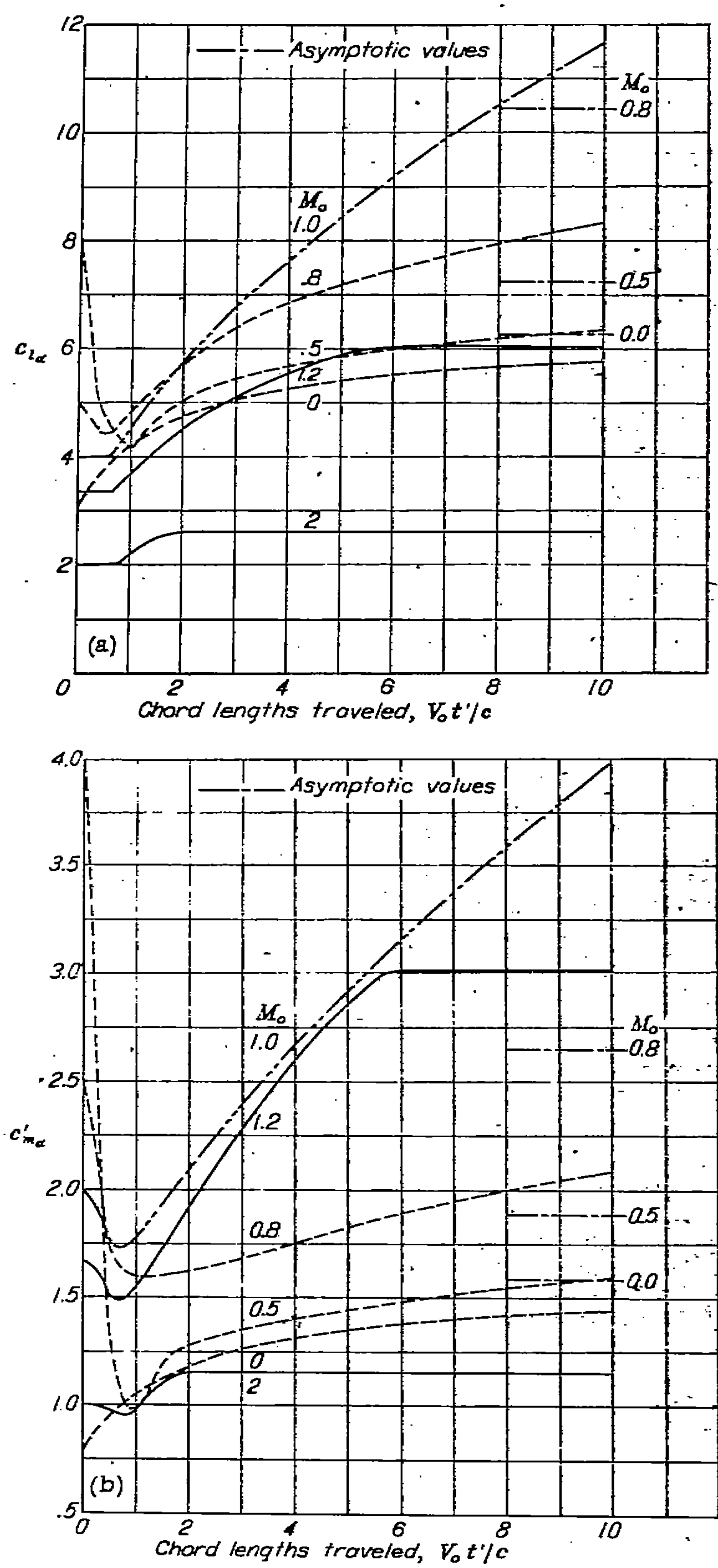

(a) Lift on a sinking wing.

(b) Pitching moment (about leading edge) on a sinking wing.

FIGURE 59.—Variation of two-dimensional indicial lift and pitching-moment coefficients with chord lengths traveled for several Mach numbers.

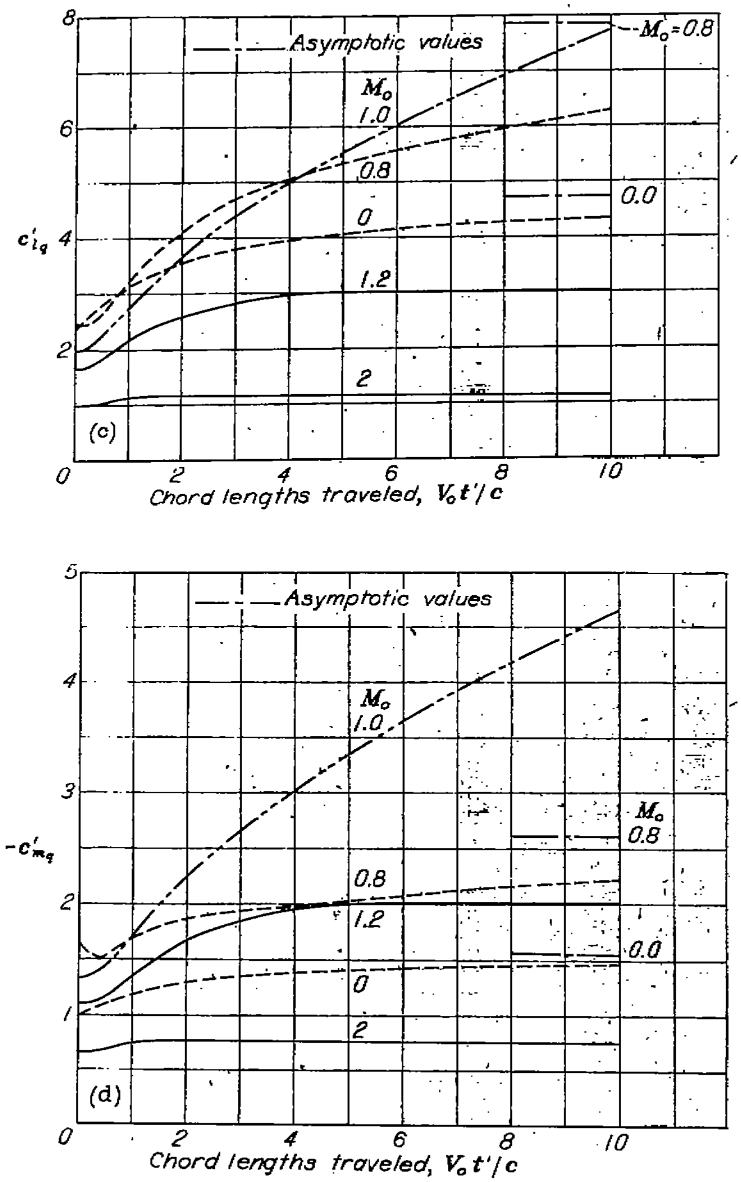

(c) Lift on wing pitching about its leading edge.
(d) Pitching moment (about leading edge) on a wing pitching about its leading edge.

FIGURE 59.—Concluded.

TRIANGULAR WINGS WITH SUPERSONIC EDGES

Curves of the indicial lift and moment on sinking and pitching triangular wings with all supersonic edges are shown in figures 60 and 61 for Mach numbers 1.2 and 2.0, respectively. For the purpose of comparison, the curves for a two-dimensional wing flying at the same Mach number have been included in each figure, as well as the curves for the same triangular wing in reversed flow.

Several conclusions can be drawn from these results. First, notice that the total indicial lift on the triangular sinking wing is the same at every instant as that on the same wing in reversed flow (both wings, of course, having started with the same velocity at the same time), and that the value of this lift is the same as the total indicial lift on the two-dimensional wing only at the beginning of the motion and again when the steady state has been attained.

Second, notice that, since all the characteristics for the triangular wings are independent of the angle of sweep, they are valid for any unyawed triangular wing as long as the edges are supersonic.

Third, it is apparent that the transition of the total indicial lift from its initial to its final value is less abrupt for the triangular than for the two-dimensional wing. The initial and final values of C_{L_α} depend on $1/M_0$ and $1/\beta$, respectively, so that as the Mach number is increased the variation dies out altogether since β and M_0 approach one another. The same remark applies to all the other coefficients.

SLENDER TRIANGULAR WINGS

The results for the lift and moment on a slender triangular wing that is sinking or pitching about its apex are shown in figure 62. The analysis by which the results were obtained is valid when both m, the tangent of the semiapex angle, and mM_0 are small; the results are given for $mM_0=1/8$. The curves are all qualitatively alike, in each case the response falls from its high initial value to a minimum at about $\tau_0=1/3$ and then recovers and practically attains its asymptotic value at $\tau_0=1$.

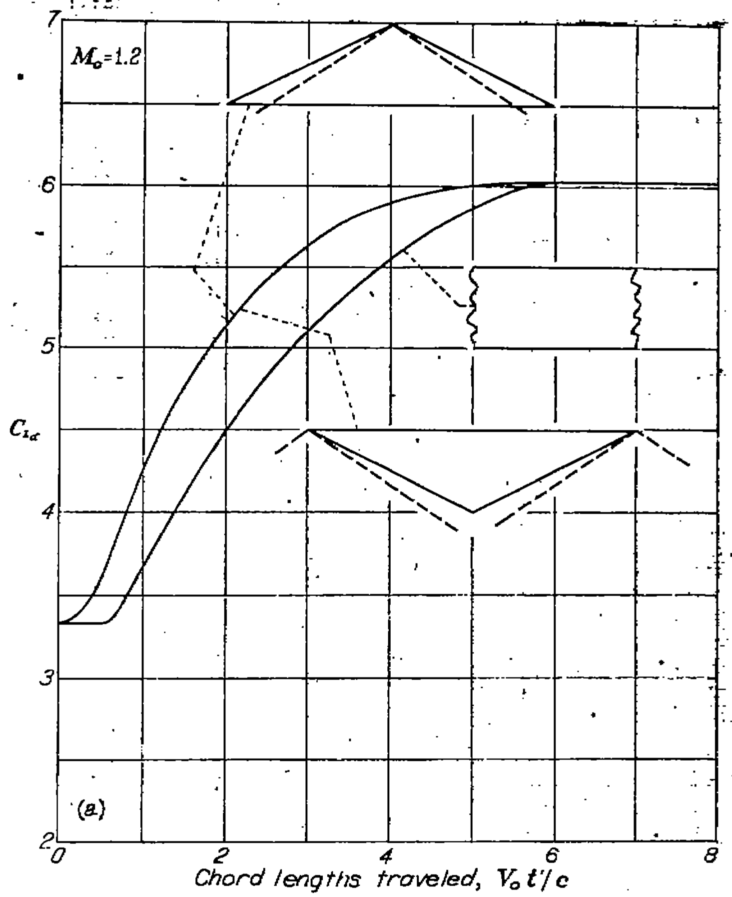

(a) Lift on sinking wings.

FIGURE 60.—Indicial aerodynamic characteristics of triangular wings with supersonic edges; $M_0=1.2$.

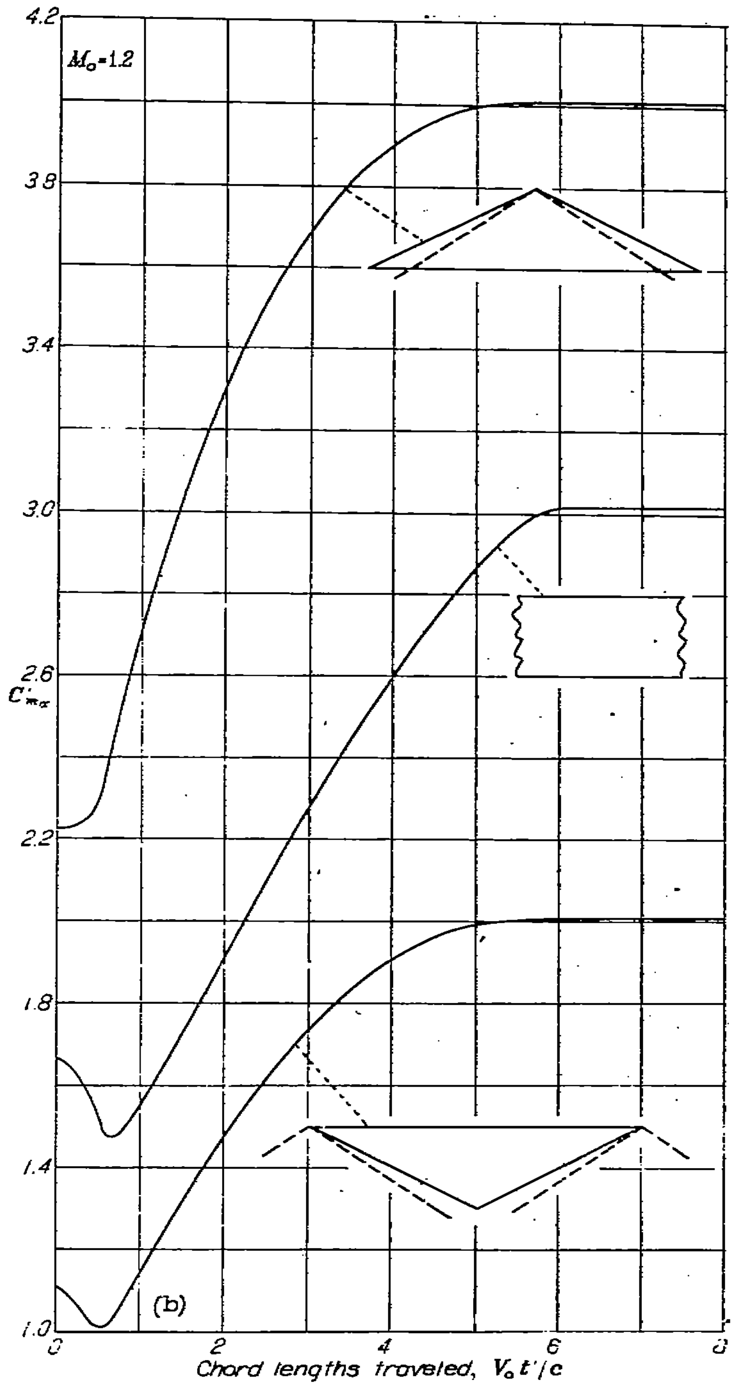

(b) Pitching moment (about leading edge or apex) on sinking wings.

FIGURE 60.—Continued.

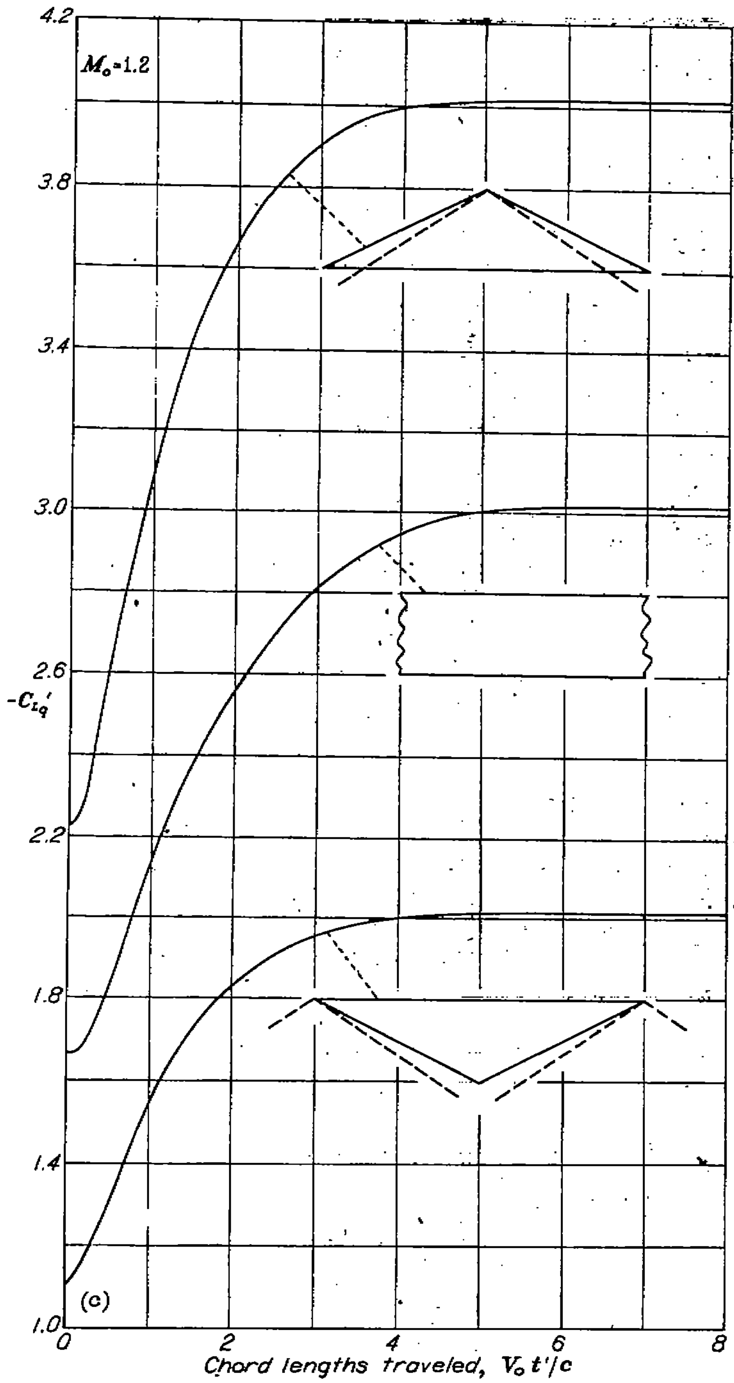

(c) Lift on wings pitching about their leading edge or apex.

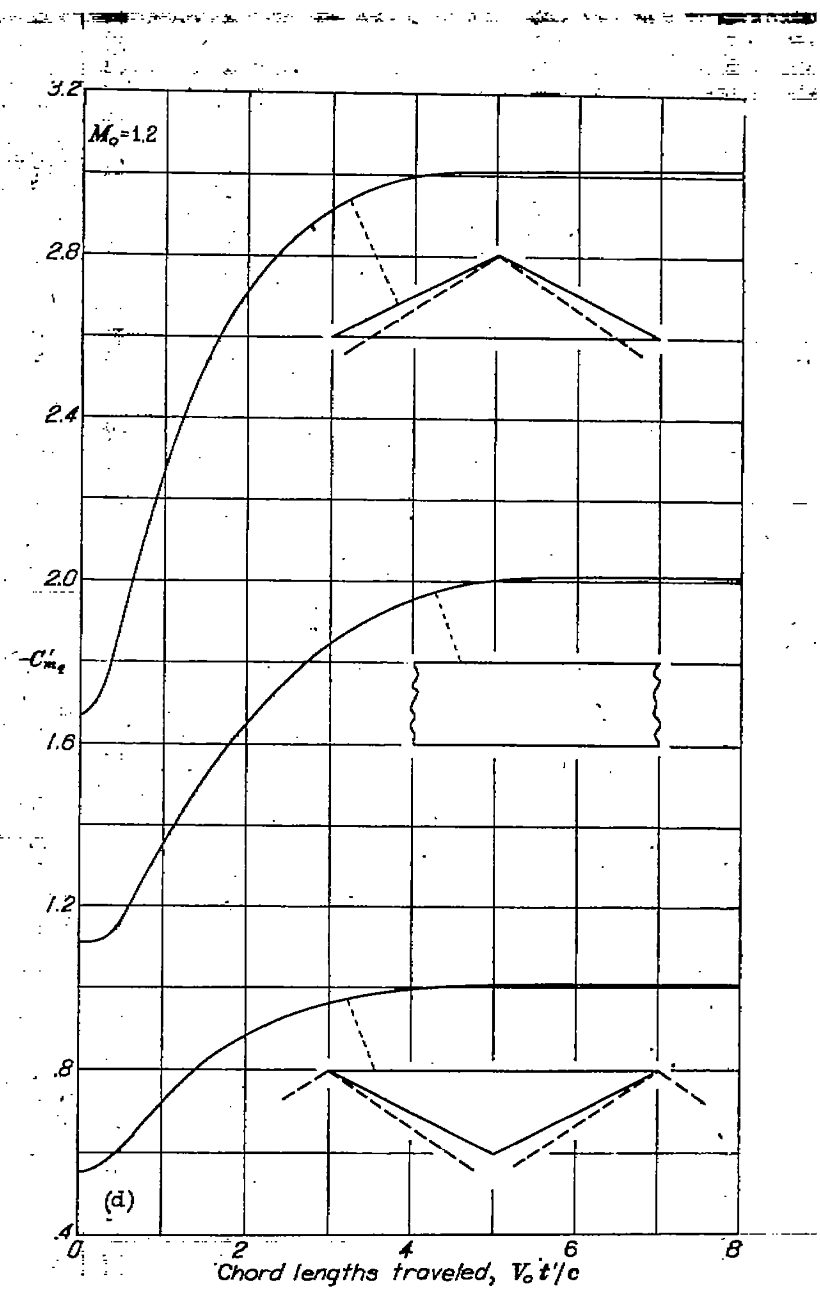

(d) Pitching moment (about leading edge or apex) on wings pitching about their leading edge or apex.

FIGURE 60.—Concluded.

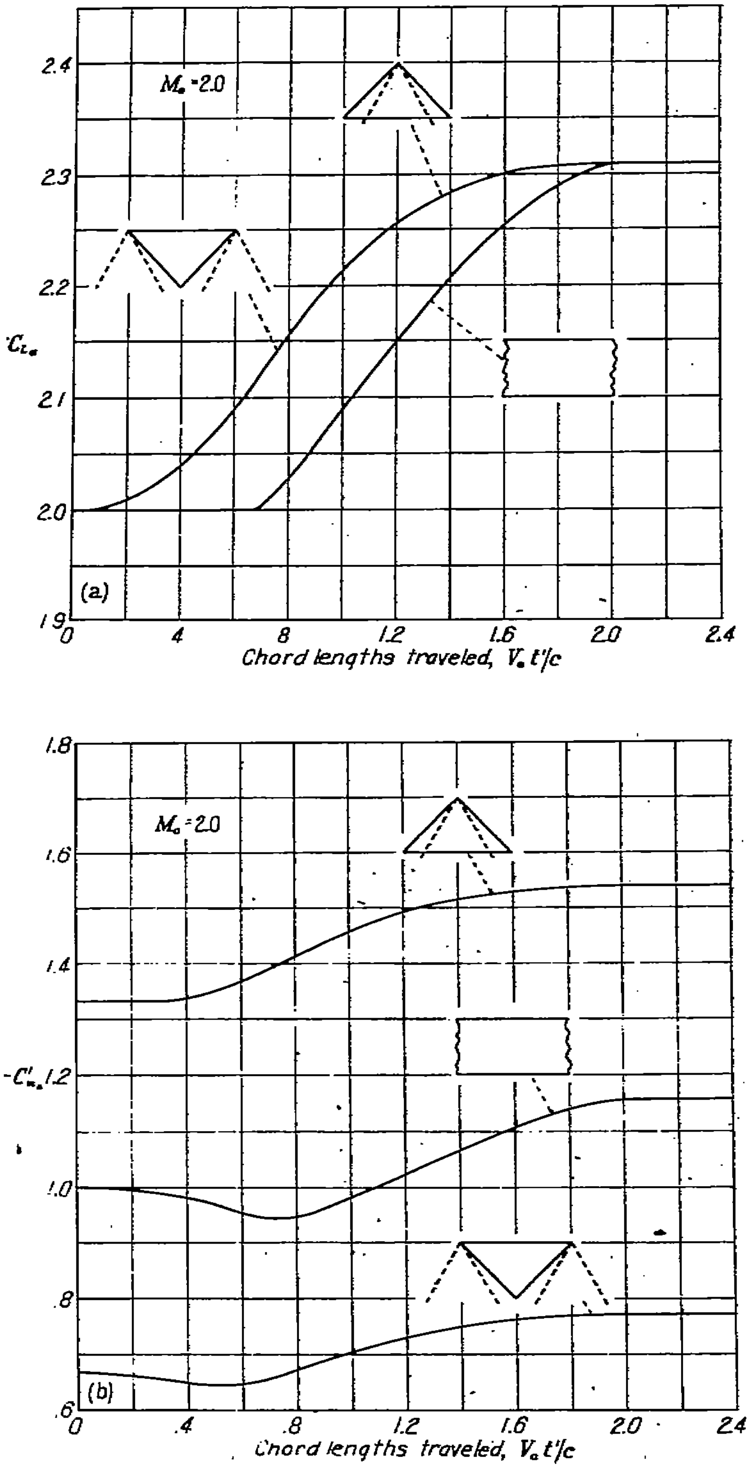

(a) Lift on sinking wings.
(b) Pitching moment (about leading edge or apex) on sinking wings.

FIGURE 61.—Indicial aerodynamic characteristics of triangular wings with supersonic edges; $M_0=2.0$.

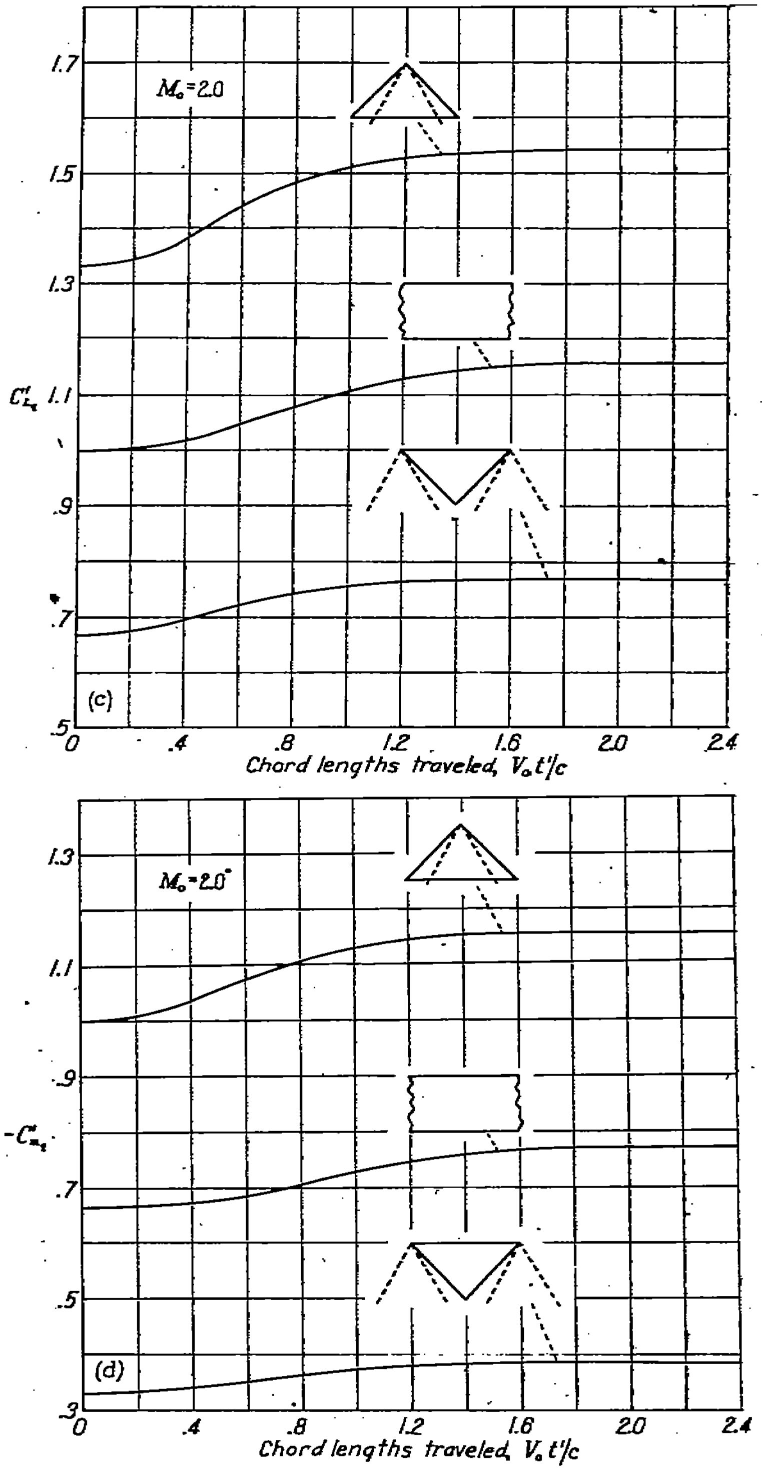

(c) Lift on wings pitching about their leading edge or apex.
(d) Pitching moment (about leading edge or apex) on wings pitching about their leading edge or apex.

FIGURE 61.—Concluded.

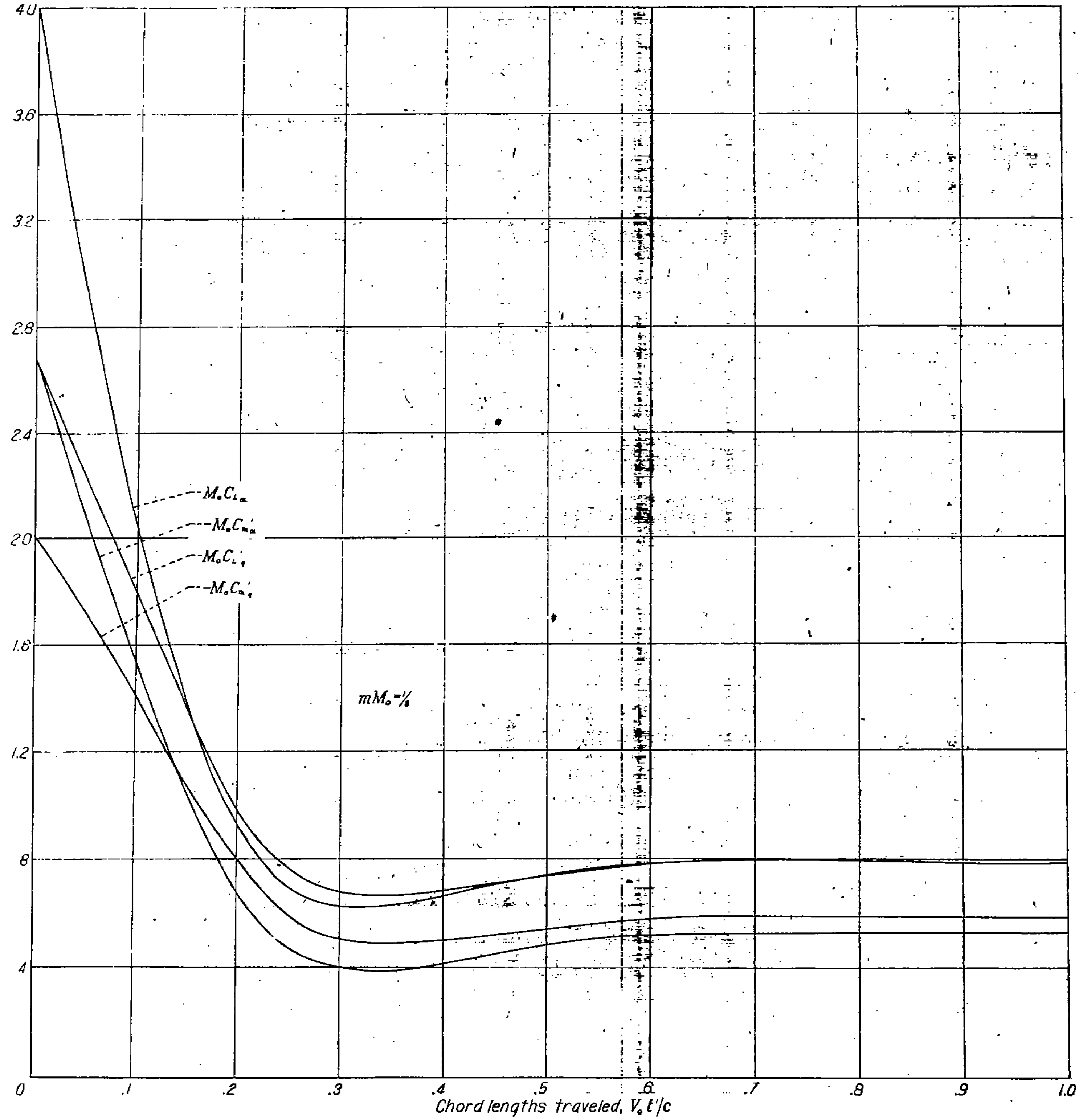

FIGURE 62.—Indicial aerodynamic characteristics of sinking and pitching triangular wings with slender plan forms.

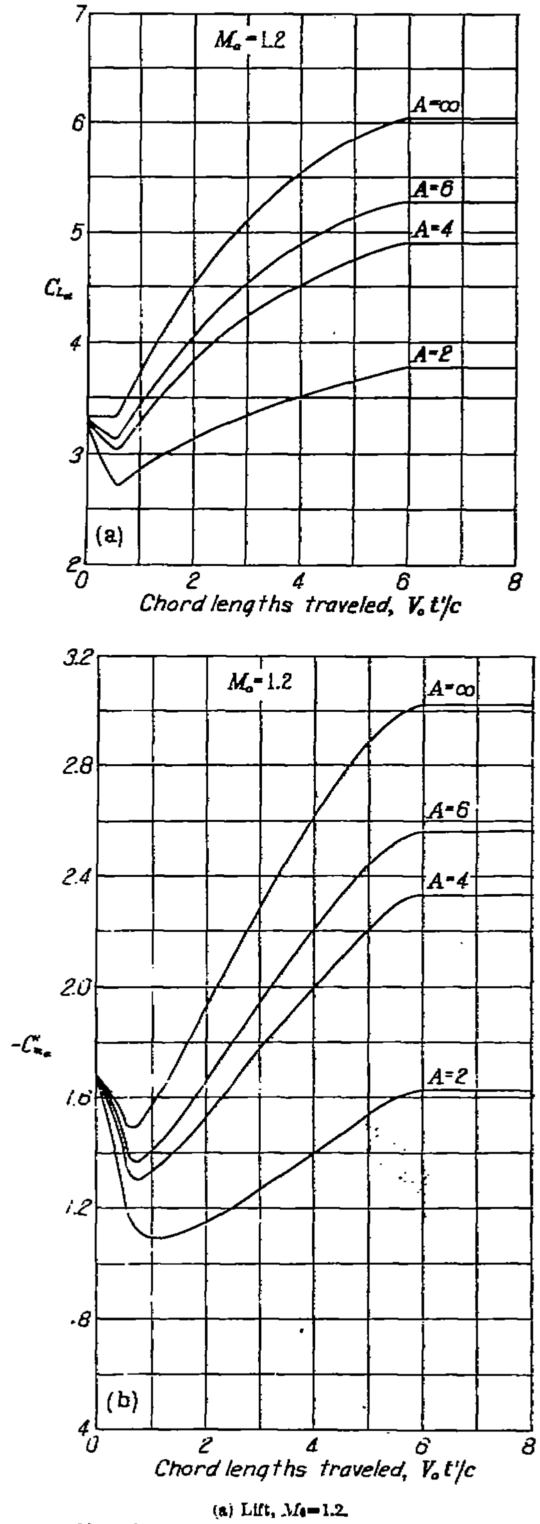

(a) Lift, $M_0=1.2$.
(b) Pitching moment (about leading edge), $M_0=1.2$.
FIGURE 63.—Indicial lift and moment on sinking rectangular wings flying at supersonic speeds.

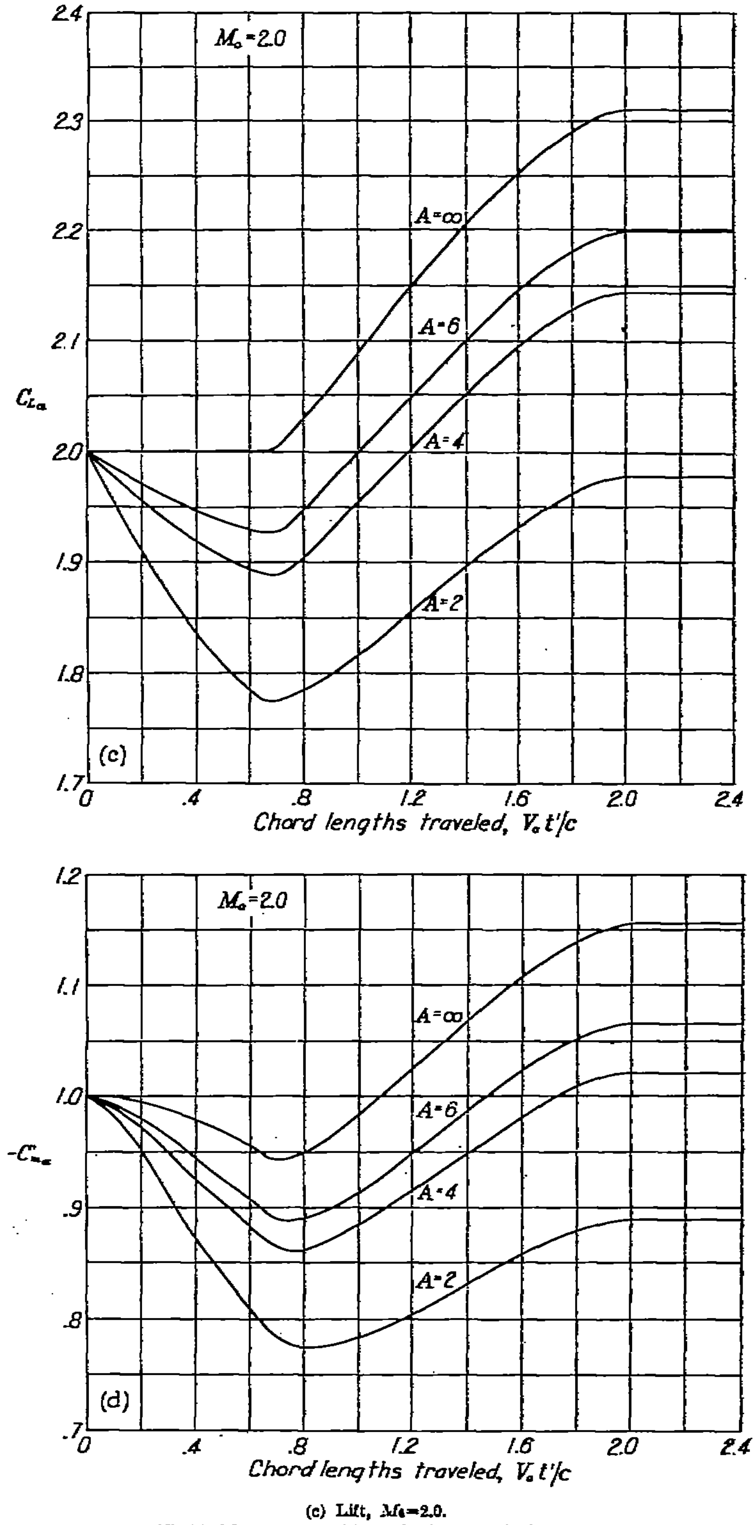

(c) Lift, $M_0=2.0$.
(d) Pitching moment (about leading edge), $M_0=2.0$.
FIGURE 63.—Concluded.

RECTANGULAR WINGS

By means of the analysis and curves presented by J. W. Miles in reference 2, the indicial results for a two-dimensional, sinking wing can be compared with those for a rectangular, sinking wing flying at supersonic speeds. This comparison is given in figure 63 for Mach numbers equal to 1.2 and 2.0 and aspect ratios equal to 2, 4, 6, and infinity. It can be seen that the modification in the shape of the indicial curves brought about by the decrease in aspect ratio is similar to that caused by a decrease in Mach number from supersonic to subsonic magnitudes.

AMES AERONAUTICAL LABORATORY
NATIONAL ADVISORY COMMITTEE FOR AERONAUTICS
MOFFETT FIELD, CALIF., *October 12, 1950.*

272483—54——29

APPENDIX A

DETERMINATION OF SUBSONIC, INDICIAL, SECTION LIFT AND PITCHING-MOMENT CURVES

THE LOAD DISTRIBUTION

The following results for the indicial load distribution on sinking or pitching wings can be obtained in two ways. One of these methods will be outlined in the subsequent paragraphs. The other is outlined in references 28 and 29 and is referred to as the lift-cancellation technique. The latter method has been used to check the load distributions originally obtained by the former so that an independent check of these results has been carried out.

It was shown in Part II, Two-Dimensional Boundary-Value Problems, that the lifting-surface analog to the solution for load distribution over an unsteady, two-dimensional wing traveling at a constant subsonic speed involved the calculation of load distribution over a swept-forward wing tip with subsonic edges. Figure A1 indicates the geometry associated with the boundary conditions. Solutions are given only for the loading in the five regions shown. As has been discussed in the text, for $M_0=0.8$ this was considered adequate to define the behavior of the indicial responses in the early stage of motion. For $M_0=0.5$ the loading in regions farther down the wing had to be calculated; and in all, for this Mach number, the loading was analyzed in the 11 regions shown in figure 25. However, the latter analysis was carried out by a numerical application of the lift-cancellation technique and none of the details will be presented here.

In the notation of the unsteady problem the expression for the velocity potential can be written

$$\varphi=-\frac{1}{\pi}\int_\tau\int\frac{w_u dt_1 dx_1}{\sqrt{(t-t_1)^2-(x-x_1)^2}} \qquad \text{(A1)}$$

where τ is the area on the wing plan form included in the Mach forecone from the point (t,x). Equation (A1) is applicable only for cases in which w_u is known at all points within the forecone, as is the case when the edge of the wing within the forecone is everywhere supersonic (i. e., region 1 in fig. A1). However, Evvard (reference 30) has extended the solution provided by equation (A1) to include cases such

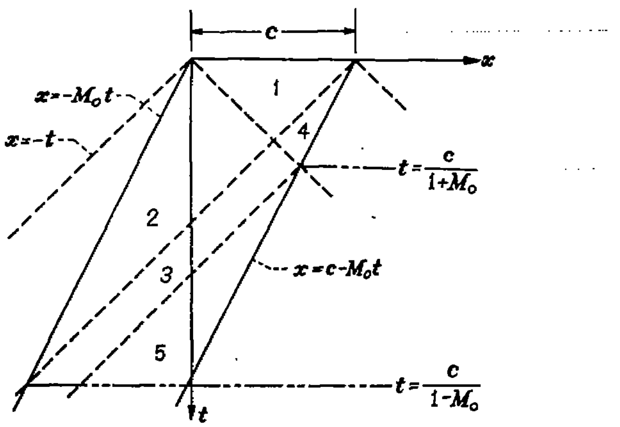

FIGURE A1.—Regions used in analysis of unsteady, two-dimensional wing flying at subsonic speed.

as shown in figures A2 and A3 in which the forecone intersects a subsonic edge and includes a region of unknown upwash. As was pointed out in reference 30, equation (A1) applies in these instances if the area of integration τ is limited to the shaded regions shown in the figures. It is apparent, therefore, that the potential (and thus the loading) over a sinking or pitching wing can readily be determined for regions 1, 2, and 4, in figure A1.

Points in regions 3 and 5 have forecones which intersect two subsonic edges, and the method just discussed can no longer be directly applied. In reference 30, however, a method was given of evaluating the upwash in the region between the Mach cone from the apex and the leading edge (region 6 in fig. A4). Thus, the plan form has become,

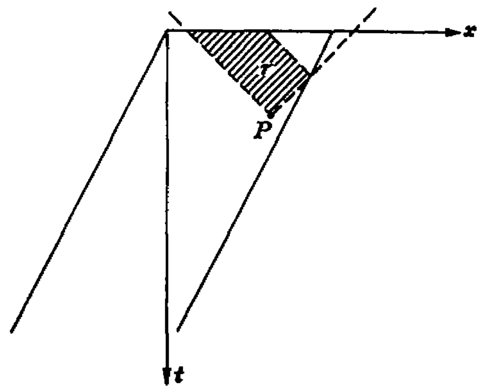

FIGURE A2.—Area of integration when Mach forecone intersects subsonic trailing edge.

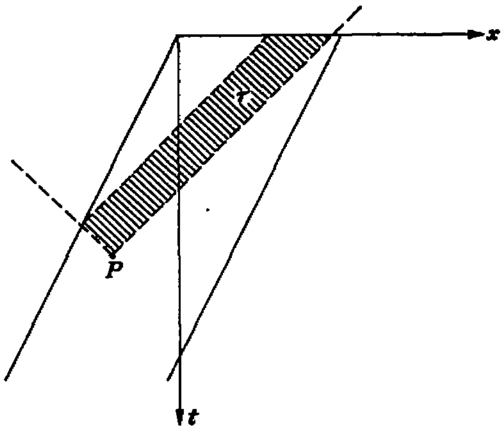

FIGURE A3.—Area of integration when Mach forecone intersects subsonic leading edge.

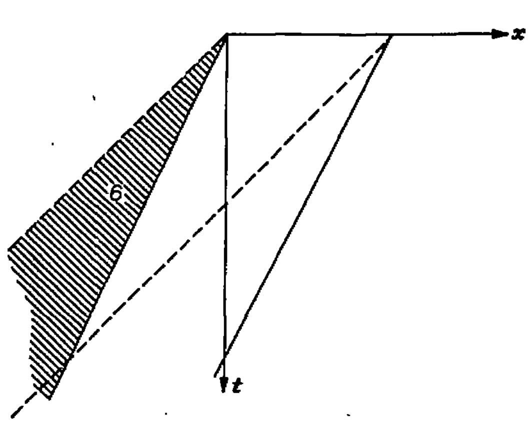

FIGURE A4.—Region 6, area between wing leading edge and trace of foremost Mach cone.

effectively, one such as shown in figure A5 in which only one edge is subsonic. This reduces the problem of finding the potential in these regions to the same problem as was involved in region 4. The analysis used in finding the loading over the various regions will now be considered.

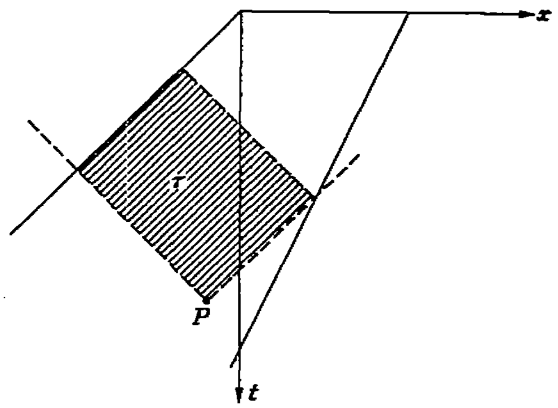

FIGURE A5.—Region of integration for mixed sonic and supersonic leading edge and subsonic trailing edge.

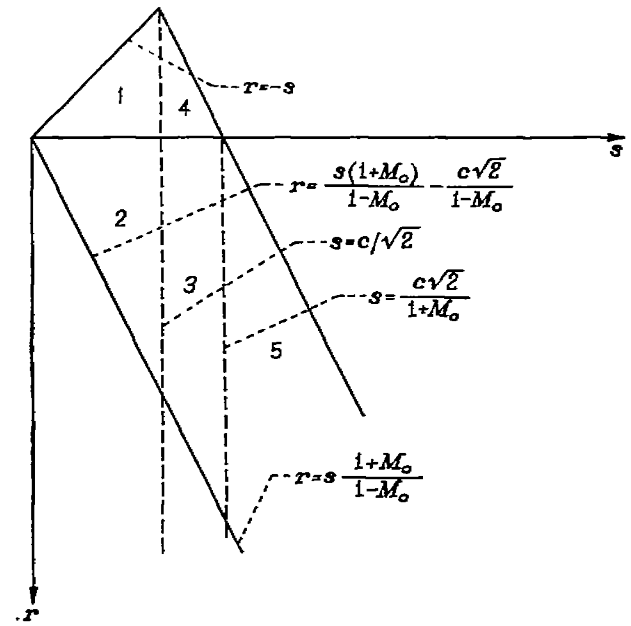

FIGURE A6.—Regions of figure A1 in the *rs* plane.

First, introduce a new coordinate system in which the lines $x=-t$ and $x=t$ are taken as the r and s axes, respectively. (See fig. A6). This amounts to a rotation of the original system of axes through an angle of 45°. The transformations relating the r,s to the x,y system are

$$r=\frac{1}{\sqrt{2}}(t-x) \quad t=\frac{1}{\sqrt{2}}(r+s)$$

$$s=\frac{1}{\sqrt{2}}(t+x) \quad x=\frac{1}{\sqrt{2}}(s-r)$$

In the new coordinate system equation (A1) is written

$$\varphi=-\frac{1}{\pi\sqrt{2}}\int_{\tau}\int\frac{w_u(r_1,s_1)dr_1ds_1}{\sqrt{(r-r_1)(s-s_1)}} \tag{A2}$$

The vertical induced velocity w_u over the wing plan form is given in equations (2) and (3) of the text for the sinking wing and pitching wing, respectively. The method developed in reference 30 was used to obtain the value of w_u over the area between the lines $s=0$ and $r=s(1+M_0)/(1-M_0)$ (region 6 in fig. A4). The results for the sinking and pitching wing are respectively,

$$\left.\begin{aligned}
w_u&=\frac{2V_0\alpha}{\pi}\left[\sqrt{\frac{2s}{(r-s)-M_0(r+s)}}-\right.\\
&\qquad\left.\arctan\sqrt{\frac{2s}{(r-s)-M_0(r+s)}}\right]\\
w_u&=\frac{2\dot{\theta}}{\pi}\frac{1}{\sqrt{2}}\left\{\left[(r-s)-M_0(r+s)-\frac{2s}{3}\right]\sqrt{\frac{2s}{(r-s)-M_0(r+s)}}-\right.\\
&\qquad\left.[(r-s)-M_0(r+s)]\arctan\sqrt{\frac{2s}{(r-s)-M_0(r+s)}}\right\}
\end{aligned}\right\} \tag{A3}$$

In the r,s coordinate system, if the subsonic trailing edge is not included in the forecone from the point at which the loading is being determined, the expression for the loading coefficient can be written

$$\frac{\Delta p}{q_0}=\frac{-2}{\pi V_0M_0}\left(\frac{\partial}{\partial r}+\frac{\partial}{\partial s}\right)\int_{\tau}\int\frac{w_u(r_1,s_1)dr_1ds_1}{\sqrt{(r-r_1)(s-s_1)}} \tag{A4}$$

However, if the trailing edge is included in the forecone, and if the Kutta condition is to apply along such an edge, it can be shown that the equation for the loading coefficient assumes the form

$$\frac{\Delta p}{q_0}=-\frac{2}{\pi V_0M_0}\int_{\tau}\frac{dr}{\sqrt{r-r_1}}\left(\frac{\partial}{\partial r_1}+\frac{\partial}{\partial s}\right)\int\frac{w_u(r_1,s_1)ds_1}{\sqrt{s-s_1}} \tag{A5}$$

SINKING WING

The preceding method can be applied to the sinking wing to obtain the following integral relationship for the loading over the various regions. The subscripts on $\left(\frac{\Delta p}{q_0}\right)$ indicate the region for which the particular equation applies.

$$\frac{1}{\alpha}\left(\frac{\Delta p}{q_0}\right)_1=\frac{2}{\pi M_0}\left(\frac{\partial}{\partial r}+\frac{\partial}{\partial s}\right)\int_{-s}^{r}\frac{dr_1}{\sqrt{r-r_1}}\int_{-r}^{s}\frac{ds_1}{\sqrt{s-s_1}}$$

$$\frac{1}{\alpha}\left(\frac{\Delta p}{q_0}\right)_2=\frac{2}{\pi M_0}\left(\frac{\partial}{\partial r}+\frac{\partial}{\partial s}\right)\int_{\frac{r(1-M_0)}{(1+M_0)}}^{s}\frac{ds_1}{\sqrt{s-s_1}}\int_{-s_1}^{r}\frac{dr_1}{\sqrt{r-r_1}}$$

$$\frac{1}{\alpha}\left(\frac{\Delta p}{q_0}\right)_3=\frac{2}{\pi M_0}\left\{\int^{r}\frac{dr_1}{\sqrt{r-r_1}}\left(\frac{\partial}{\partial r_1}+\frac{\partial}{\partial s}\right)\int_{\frac{r_1(1-M_0)}{(1+M_0)}}^{s}\frac{ds_1}{\sqrt{s-s_1}}+\right.$$

$$\int_{0}^{r}\frac{dr_1}{\sqrt{r-r_1}}\left(\frac{\partial}{\partial r_1}+\frac{\partial}{\partial s}\right)\int^{\frac{r_1(1-M_0)}{(1+M_0)}}-$$

$$\frac{2}{\pi}ds_1\left[\frac{\sqrt{\frac{2s_1}{(r_1-s_1)-M_0(r_1+s_1)}}-\arctan\sqrt{\frac{2s_1}{(r_1-s_1)-M_0(r_1+s_1)}}}{\sqrt{s-s_1}}\right]+$$

$$\left.\int_{r_d}^{0}\frac{dr_1}{\sqrt{r-r_1}}\left(\frac{\partial}{\partial r_1}+\frac{\partial}{\partial s}\right)\int_{-r_1}^{s}\frac{ds_1}{\sqrt{s-s_1}}\right\}$$

$$\frac{1}{\alpha}\left(\frac{\Delta p}{q_0}\right)_4=\frac{2}{\pi M_0}\int_{r_d}^{r}\frac{dr_1}{\sqrt{r-r_1}}\left(\frac{\partial}{\partial r_1}+\frac{\partial}{\partial s}\right)\int_{-r_1}^{s}\frac{ds_1}{\sqrt{s-s_1}}$$

$$\frac{1}{\alpha}\left(\frac{\Delta p}{q_0}\right)_5=\frac{2}{\pi M_0}\left\{\int_{r_d}^{r}\frac{dr_1}{\sqrt{r-r_1}}\left(\frac{\partial}{\partial r_1}+\frac{\partial}{\partial s}\right)\int_{\frac{r_1(1-M_0)}{(1+M_0)}}^{s}\frac{ds_1}{\sqrt{s-s_1}}+\right.$$

$$\int_{r_d}^{r}\frac{dr_1}{\sqrt{r-r_1}}\left(\frac{\partial}{\partial r_1}+\frac{\partial}{\partial s}\right)\int_{0}^{\frac{r_1(1-M_0)}{(1+M_0)}}-$$

$$\left.\frac{2}{\pi}ds_1\left[\frac{\sqrt{\frac{2s_1}{(r_1-s_1)-M_0(r_1+s_1)}}-\arctan\sqrt{\frac{2s_1}{(r_1-s_1)-M_0(r_1+s_1)}}}{\sqrt{s-s_1}}\right]\right\}$$

where

$$r_d=\frac{s(1+M_0)-c\sqrt{2}}{1-M_0}$$

Most of these integrals can be readily evaluated to give

$$\frac{1}{\alpha}\left(\frac{\Delta p}{q_0}\right)_1=\frac{4}{M_0} \tag{A6a}$$

$$\frac{1}{\alpha}\left(\frac{\Delta p}{q_0}\right)_2=\frac{8}{\pi M_0}\left(\frac{M_0}{1+M_0}\sqrt{\frac{t_0-x_0}{M_0t_0+x_0}}+\arctan\sqrt{\frac{M_0t_0+x_0}{t_0-x_0}}\right) \tag{A6b}$$

$$\frac{1}{\alpha}\left(\frac{\Delta p}{q_0}\right)_3=\frac{8}{\pi(1+M_0)}\sqrt{\frac{t_0-x_0}{M_0t_0+x_0}}+\frac{4}{\pi M_0}\left[\arcsin\frac{2x_0-t_0(1-M_0)}{(1+M_0)t_0}+\arcsin\frac{2(1-x_0)-t_0(1+M_0)}{t_0(1-M_0)}\right] \tag{A6c}$$

$$\frac{1}{\alpha}\left(\frac{\Delta p}{q_0}\right)_4=\frac{8}{\pi M_0}\arcsin\sqrt{\frac{x_0-1+M_0t_0}{t_0(M_0-1)}} \tag{A6d}$$

$$\frac{1}{q}\left(\frac{\Delta p}{q_0}\right)_5=\frac{16}{\pi^2(1+M_0)}\sqrt{\frac{t_0-x_0}{M_0t_0+x_0}}\left[\frac{\pi}{2}-EF(\psi,k')-KE(\psi,k')+KF(\psi,k')\right]-\frac{2}{\pi M_0}\arcsin\frac{x_0}{t_0}+\frac{4}{\pi M_0}\arcsin\frac{2x_0-t_0(1-M_0)}{(1+M_0)t_0}+\frac{32K}{\pi^2(1+M_0)}\sqrt{\frac{1-x_0-M_0t_0}{(1-M_0^2)(x_0+t_0)}}-\frac{2}{\pi M_0}\arcsin\frac{2-t_0(1+M_0)}{t_0(1+M_0)}+G_1 \tag{A6e}$$

where

$$k'=\sqrt{1-k^2}$$

$$k=\sqrt{1-\frac{2}{(t_0+x_0)(1+M_0)}}$$

$$\psi=\arcsin\sqrt{x_0+M_0t_0}$$

$$G_1=\frac{4}{\pi^2M_0}\int_0^{s-\frac{c\sqrt{2}}{1+M_0}}\left[\frac{ds_1}{\sqrt{(s-s_1)(r+s_1)}}\right]\arcsin\left\{\frac{(r+s_1)(1-M_0)[(s-s_1)(1+M_0)-c\sqrt{2}]+2s_1[s(1+M_0)-c\sqrt{2}-r(1-M_0)]}{[s(1+M_0)-c\sqrt{2}+s_1(1-M_0)][r(1-M_0)-s_1(1+M_0)]}\right\}$$

PITCHING WING

A similar analysis of the pitching wing yields the following results for the loading coefficient:

$$\frac{1}{q}\left(\frac{\Delta p}{q_0}\right)_1=\frac{4}{M_0}(M_0t_0+x_0) \tag{A7a}$$

$$\frac{1}{q}\left(\frac{\Delta p}{q_0}\right)_2=\frac{8}{3\pi M_0}\left[\frac{M_0(1-M_0)(t_0-x_0)^{3/2}}{(1+M_0)^2\sqrt{M_0t_0+x_0}}+3\sqrt{(t_0-x_0)(M_0t_0+x_0)}+3(M_0t_0+x_0)\arctan\sqrt{\frac{M_0t_0+x_0}{t_0-x_0}}\right] \tag{A7b}$$

$$\frac{1}{q}\left(\frac{\Delta p}{q_0}\right)_3=\frac{8}{\pi M_0}\left\{\sqrt{(t_0-x_0)(M_0t_0+x_0)}+\frac{1}{3}\frac{M_0(1-M_0)}{(1+M_0)^2}\sqrt{\frac{(t_0-x_0)^3}{M_0t_0+x_0}}-\sqrt{[1-(M_0t_0+x_0)][(t_0+x_0)-1]}+(M_0t_0+x_0)\left[\arctan\sqrt{\frac{1-(M_0t_0+x_0)}{(t_0+x_0)-1}}-\arctan\sqrt{\frac{t_0-x_0}{M_0t_0+x_0}}\right]\right\} \tag{A7c}$$

$$\frac{1}{q}\left(\frac{\Delta p}{q_0}\right)_4=\frac{8}{\pi M_0}\left\{(M_0t_0+x_0)\arctan\sqrt{\frac{1-(M_0t_0+x_0)}{t_0+x_0-1}}-\sqrt{(t_0+x_0-1)[1-(M_0t_0+x_0)]}\right\} \tag{A7d}$$

$$\frac{1}{q}\left(\frac{\Delta p}{q_0}\right)_5=\frac{8}{\pi M_0}\left\{\frac{M_0}{\sqrt{1-M_0^2}}\left[\sqrt{1-(M_0t_0+x_0)}+(M_0t_0+x_0)\tanh^{-1}\sqrt{1-(M_0t_0+x_0)}\right]-\frac{\sqrt{(t_0-x_0)(t_0+x_0)}}{2}+\sqrt{(t_0-x_0)(M_0t_0+x_0)}+\frac{M_0(1-M_0)}{3(1+M_0)^2}\sqrt{\frac{(t_0-x_0)^3}{M_0t_0+x_0}}-(M_0t_0+x_0)\left[\arctan\sqrt{\frac{t_0+x_0}{t_0-x_0}}-\arctan\sqrt{\frac{M_0t_0+x_0}{t_0-x_0}}+\frac{M_0}{\sqrt{1-M_0^2}}\tanh^{-1}\sqrt{\frac{(t_0-x_0)(1-M_0)}{(t_0+x_0)(1+M_0)}}\right]\right\}+\frac{1}{c}G_2 \tag{A7e}$$

where

$$G_2=-\frac{4}{\pi^2M_0}\int_0^{\frac{r_d(1-M_0)}{1+M_0}}\frac{ds_1}{\sqrt{s-s_1}}\left\{\left(-2M_0\sqrt{r+s_1}-\frac{2s_1}{\sqrt{r+s_1}}\right)\left[\arctan\frac{-4s_1(r+s_1)+(r_d+s_1)[r(1-M_0)+s_1(1+M_0)+2s_1(1-M_0)]}{2\sqrt{2s_1(r+s_1)(r-r_d)[r_d(1-M_0)-s_1(1+M_0)]}}+\frac{\pi}{2}\right]-4M_0\sqrt{r-r_d}\arctan\sqrt{\frac{2s_1}{r_d(1-M_0)-s_1(1+M_0)}}+\frac{2M_0\pi}{\sqrt{1-M_0}}\sqrt{r(1-M_0)-s_1(1+M_0)}+\frac{2}{3}\frac{M_0}{1+M_0}\left[\frac{(2s_1)^{3/2}}{s-s_1}+6\sqrt{2s_1}\right]\frac{1}{\sqrt{1-M_0}}\arctan\sqrt{\frac{r_d(1-M_0)-s_1(1+M_0)}{(1-M_0)(r-r_d)}}\right\}$$

LIFT AND PITCHING-MOMENT COEFFICIENTS

The lift and pitching-moment coefficients may be obtained by suitable integrations of equations (A6) and (A7) and are given in the time intervals indicated in figure 34 by the following expressions:

Sinking wing

$0 \leq t_0 \leq \frac{1}{1+M_0}$

$$c_{l_\alpha}=\frac{4}{M_0}\left[1-t_0(1-M_0)\right] \tag{A8a}$$

$$c_{m_\alpha}'=-\frac{4}{M_0}\left[\frac{1}{2}-\frac{t_0}{2}(1-M_0)+\frac{t_0^2M_0}{4}(M_0-2)\right] \tag{A9a}$$

$\frac{1}{1+M_0} \leq t_0 \leq \frac{1}{1-M_0}$

$$c_{l_\alpha}=\frac{4}{\pi M_0}\left\{\frac{4-3t_0(1-M_0^2)}{1+M_0}\arctan\sqrt{\frac{2-t_0(1-M_0^2)}{2t_0(1+M_0)-2}}+\pi\left(t_0-\frac{2}{1+M_0}\right)+\frac{1+3M_0}{(1+M_0)^2}\sqrt{[2t_0(1+M_0)-2][2-t_0(1-M_0^2)]}+\frac{4-2t_0(1+M_0)}{1+M_0}\arcsin\sqrt{\frac{t_0(1+M_0)-1}{t_0(1+M_0)}}-\frac{1-M_0}{1+M_0}\sqrt{t_0(1+M_0)-1}+[2-t_0(1+M_0)]\arctan\sqrt{\frac{1}{t_0(1+M_0)-1}}\right\}+\int_{\frac{2}{1+M_0}-t_0}^{1-M_0t_0}\left(\frac{\Delta p}{q_0}\right)_5 dx_0 \tag{A8b}$$

where $\left(\frac{\Delta p}{q_0}\right)_5$ is given by equation (A6e)

$$c_{m_\alpha}'=-\frac{8}{\pi M_0}\left\{\left[\frac{t_0^2(5-18M_0+9M_0^2)}{16}+\frac{2t_0(M_0-1)}{1+M_0}+\frac{2}{(1+M_0)^2}\right]\arctan\sqrt{\frac{2-t_0(1-M_0^2)}{2[t_0(1+M_0)-1]}}+\left[\frac{-5t_0^2(1-M_0)^2}{16}+\frac{t_0(M_0^2-4M_0+3)}{2(1+M_0)}+\frac{M_0^2+2M_0-3}{2(1+M_0)^2}\right]\arctan\frac{1}{\sqrt{t_0(1+M_0)-1}}+\frac{\sqrt{2[2-t_0(1-M_0^2)][t_0(1+M_0)-1]}}{1+M_0}\left[\frac{t_0(1-6M_0+9M_0^2)}{16(1+M_0)}+\frac{1+5M_0}{4(1+M_0)^2}\right]+\frac{1-M_0}{1+M_0}\sqrt{t_0(1+M_0)-1}\left[\frac{5t_0(1-M_0)}{16}-\frac{5+3M_0}{8(1+M_0)}\right]\right\}-\int_{\frac{2}{1+M_0}-t_0}^{1-M_0t_0}(x_0+M_0t_0)\left(\frac{\Delta p}{q_0}\right)_5 dx_0 \tag{A9b}$$

Pitching wing

$0 \leq t_0 \leq \frac{1}{1+M_0}$

$$c_{l_q}'=\frac{2}{M_0}\left[t_0^2\left(M_0-\frac{M_0^2}{2}\right)+t_0(M_0-1)+1\right] \tag{A10a}$$

$$c_{m_q}'=-\frac{4}{3M_0}\left\{t_0^3\left[\frac{1}{8}(1-M_0)^3+\frac{1}{2}M_0\right]+\frac{3}{8}t_0^2(1-M_0)^2-\frac{3}{2}t_0(1-M_0)+1\right\} \tag{A11a}$$

$\frac{1}{1+M_0} \leq t_0 \leq \frac{1}{1-M_0}$

$$c_{l_q}'=\frac{8}{\pi M_0}\left\{\sqrt{t_0+t_0M_0-1}\left[\frac{t_0(-5M_0^2+2M_0-3)}{12(1+M_0)}+\frac{5M_0^2+7M_0+3}{3(1+M_0)^2}\right]-\sqrt{t_0^2-(1-M_0t_0)^2}\left(\frac{3}{8}-\frac{M_0t_0}{8}\right)+\left[t_0^2\frac{(-M_0^2+2M_0+1)}{4}-t_0\frac{(1-M_0)}{2}+1\right]\arctan\sqrt{\frac{1}{t_0+t_0M_0-1}}-\left(\frac{t_0^2}{4}+\frac{1}{2}\right)\left[\arctan\sqrt{\frac{t_0+1-t_0M_0}{t_0+t_0M_0-1}}\right]-\frac{1}{2}\frac{M_0}{\sqrt{1-M_0^2}}\tanh^{-1}\sqrt{\left(\frac{1-M_0}{1+M_0}\right)\left(\frac{t_0+t_0M_0-1}{t_0+1-t_0M_0}\right)}\right\}+\int_{-t_0+\frac{2}{1+M_0}}^{1-M_0t_0}\left(\frac{G_2}{c}\right)dx_0 \tag{A10b}$$

where G_2 is defined under equation (A7e).

$$c_{m_q}'=-\frac{8}{\pi M_0}\left\{-\frac{1}{3}\frac{M_0}{\sqrt{1-M_0^2}}\tanh^{-1}\sqrt{\left(\frac{1-M_0}{1+M_0}\right)\left[\frac{t_0(1+M_0)-1}{t_0(1-M_0)+1}\right]}-\left[-\frac{t_0^3}{24}(M_0+1)(-M_0^2+4M_0+1)-\frac{t_0^2}{8}(1-M_0)^2+\frac{t_0}{2}(1-M_0)-\frac{2}{3}\right]\arctan\sqrt{\frac{1}{t_0(1+M_0)-1}}-\left(\frac{M_0t_0^3}{6}+\frac{1}{3}\right)\arctan\sqrt{\frac{t_0(1-M_0)+1}{t_0(1+M_0)-1}}+\sqrt{t_0(1+M_0)-1}\left\{\frac{-t_0^2[(1-M_0)^3+8M_0]}{24(1+M_0)}+\frac{t_0(9M_0^2-6M_0-11)}{72(1+M_0)}+\frac{39M_0^2+54M_0+19}{36(1+M_0)^2}\right\}+\sqrt{t_0^2-(1-M_0t_0)^2}\left[\frac{t_0^2(2+M_0^2)+t_0M_0-8}{36}\right]\right\}+\int_{-t_0+\frac{2}{1+M_0}}^{1-M_0t_0}(x_0+M_0t_0)\left(\frac{G_2}{c}\right)dx_0 \tag{A11b}$$

APPENDIX B

DETERMINATION OF SUPERSONIC, INDICIAL, SECTION LIFT AND PITCHING-MOMENT CURVES

THE LOAD DISTRIBUTION

In the case of the unsteady supersonic wing the expression for the velocity potential may be readily obtained by placing the values of w_u given by equations (2) and (3) of the text in the equation

$$\varphi=-\frac{1}{\pi}\int\int_{\tau}\frac{w_u dx_1}{\sqrt{(t-t_1)^2-(x-x_1)^2}} \tag{B1}$$

where τ is the area on the plan form included in the Mach forecone. The loading may then be calculated from the relationship given in equation (12).

SINKING WING

The load distribution over the regions A, B, and C shown in figure 34 are given by the following expressions:

$$\frac{1}{\alpha}\left(\frac{\Delta p}{q_0}\right)_A=\frac{4}{M_0} \tag{B2a}$$

$$\frac{1}{\alpha}\left(\frac{\Delta p}{q_0}\right)_B=\frac{4}{\sqrt{M_0^2-1}}\left[\frac{1}{\pi}\text{ arc cos }\frac{M_0x_0+t_0}{x_0+M_0t_0}+\frac{\sqrt{M_0^2-1}}{\pi M_0}\text{ arc cos }\left(-\frac{x_0}{t_0}\right)\right] \tag{B2b}$$

$$\frac{1}{\alpha}\left(\frac{\Delta p}{q_0}\right)_C=\frac{4}{\sqrt{M_0^2-1}} \tag{B2c}$$

PITCHING WING

For the case of the pitching wing the values of $\frac{1}{q}\left(\frac{\Delta p}{q_0}\right)$ in regions A, B, and C are, respectively,

$$\frac{1}{q}\left(\frac{\Delta p}{q_0}\right)_A=\frac{4}{M_0}(x_0+M_0t_0) \tag{B3a}$$

$$\frac{1}{q}\left(\frac{\Delta p}{q_0}\right)_B=\frac{4}{\pi}\left[\frac{x_0+M_0t_0}{\sqrt{M_0^2-1}}\text{ arc cos }\frac{M_0x_0+t_0}{x_0+M_0t_0}+\frac{x_0+M_0t_0}{M_0}\text{ arc cos }\left(-\frac{x_0}{t_0}\right)+\frac{1}{M_0}\sqrt{t_0^2-x_0^2}\right] \tag{B3b}$$

$$\frac{1}{q}\left(\frac{\Delta p}{q_0}\right)_C=\frac{4}{\sqrt{M_0^2-1}}(x_0+M_0t_0) \tag{B3c}$$

LIFT AND PITCHING-MOMENT COEFFICIENTS

The lift and pitching-moment coefficients may be obtained by suitable integrations of equations (B2) and (B3) and are given in the time intervals indicated in figure 34 by the following expressions:

SINKING WING

$0\leq t_0\leq\frac{1}{1+M_0}$

$$c_{l_\alpha}=\frac{4}{M_0} \tag{B4a}$$

$$c_{m_\alpha}'=-\frac{1}{M_0}(2-t_0^2) \tag{B5a}$$

$\frac{1}{1+M_0}\leq t_0\leq\frac{1}{M_0-1}$

$$c_{l_\alpha}=\frac{4}{\pi}\left[\frac{1}{M_0}\text{ arc cos }\frac{M_0t_0-1}{t_0}+\frac{1}{\sqrt{M_0^2-1}}\text{ arc cos }(t_0+M_0-t_0M_0^2)+\frac{1}{M_0}\sqrt{t_0^2-(1-M_0t_0)^2}\right] \tag{B4b}$$

$$c_{m_\alpha}'=-\frac{2}{\pi}\left[\frac{1}{M_0}\left(1-\frac{t_0^2}{2}\right)\text{ arc cos }\frac{M_0t_0-1}{t_0}+\frac{1}{\sqrt{M_0^2-1}}\text{ arc cos}(t_0+M_0-t_0M_0^2)+\frac{1}{M_0}\left(\frac{1+M_0t_0}{2}\right)\sqrt{t_0^2-(1-M_0t_0)^2}\right] \tag{B5b}$$

$\frac{1}{M_0-1}\leq t_0\leq\infty$

$$c_{l_\alpha}=\frac{4}{\sqrt{M_0^2-1}} \tag{B4c}$$

$$c_{m_\alpha}'=-\frac{2}{\sqrt{M_0^2-1}} \tag{B5c}$$

PITCHING WING

$0\leq t_0\leq\frac{1}{1+M_0}$

$$c_{l_q}'=\frac{2}{M_0}\left(1+\frac{t_0^2}{2}\right) \tag{B6a}$$

$$c_{m_q}'=-\frac{4}{3M_0}\left(1+\frac{M_0t_0^3}{2}\right) \tag{B7a}$$

$\frac{1}{1+M_0}\leq t_0\leq\frac{1}{M_0-1}$

$$c_{l_q}'=\frac{2}{\pi}\left[\frac{1}{M_0}\left(1+\frac{t_0^2}{2}\right)\text{ arc cos }\frac{M_0t_0-1}{t_0}+\frac{1}{\sqrt{M_0^2-1}}\text{ arc cos }(t_0+M_0-t_0M_0^2)+\frac{(3-M_0t_0)}{2M_0}\sqrt{t_0^2-(1-M_0t_0)^2}\right] \tag{B6b}$$

$$c_{m_q}'=-\frac{4}{3\pi}\left[\frac{1}{M_0}\left(1+\frac{M_0t_0^3}{2}\right)\text{ arc cos }\frac{M_0t_0-1}{t_0}+\frac{1}{\sqrt{M_0^2-1}}\text{ arc cos }(t_0+M_0-t_0M_0^2)+\frac{(8-M_0t_0-2t_0^2-M_0^2t_0^2)}{6M_0}\sqrt{t_0^2-(1-M_0t_0)^2}\right] \tag{B7b}$$

$\frac{1}{M_0-1}\leq t_0\leq\infty$

$$c_{l_q}'=\frac{2}{\sqrt{M_0^2-1}} \tag{B6c}$$

$$c_{m_q}'=-\frac{4}{3\sqrt{M_0^2-1}} \tag{B7c}$$

REFERENCES

1. Baker, Bevan B., and Copson, E. T.: The Mathematical Theory of Huygens' Principle. The Clarendon Press, Oxford, England, 1939.
2. Miles, John W.: Transient Loading of Supersonic Rectangular Airfoils. Jour. Aero. Sci., vol. 17, no. 10, Oct. 1950, pp. 647–652.
3. Strang, W. J.: Transient Lift of Three-Dimensional Purely Supersonic Wing. Proc. Royal Soc., Series A, June 22, 1950, pp. 54–80.
4. Miles, John W.: Transient Loading of Wide Delta Airfoils at Supersonic Speeds. NAVORD. Rep. 1235, 1950.
5. Garrick, I. E., and Rubinow, S. I.: Flutter and Oscillating Air-Force Calculations for an Airfoil in a Two-Dimensional Supersonic Flow. NACA Rep. 846, 1946. (Formerly TN 1158)
6. Watkins, Charles E.: Effect of Aspect Ratio on the Air Forces and Moments of Harmonically Oscillating Thin Rectangular Wings in Supersonic Potential Flow. NACA TN 2064, 1950.
7. Miles, John W.: On Harmonic Motion of Wide Delta Airfoils at Supersonic Speeds. NOTS, Inyokern, Tech. Memo. RRB–36, Feb. 1950.
8. Watkins, Charles E.: Air Forces and Moments on Triangular and Related Wings with Subsonic Leading Edges Oscillating in Supersonic Potential Flow. NACA TN 2457, 1951.
9. Miles, John W.: The Oscillating Rectangular Airfoil at Supersonic Speeds. Quart. Appl. Math., vol. IX, no. 1, 1951, pp. 47–65.
10. Runyan, Harry L.: Single-Degree-of-Freedom-Flutter Calculations for a Wing in Subsonic Potential Flow and Comparison With an Experiment. NACA TN 2396, 1951.
11. Busemann, A.: Infinitesimal Conical Supersonic Flow. NACA TM 1100, 1947.
12. Lagerstrom, P. A., and Van Dyke, M. D.: General Considerations about Planar and Non-Planar Lifting Systems. Douglas Aircraft Company, Inc., Rept. SM 13432, June 1949.
13. Lomax, Harvard, and Heaslet, Max. A.: Linearized Lifting-Surface Theory for Swept-Back Wings with Slender Plan Forms. NACA TN 1992, 1949.
14. Wagner, Herbert: Uber die Entstehung des dynamischen Auftriebes von Tragflugeln. Zeits. für angewandte Math. und Mechanik, Bd. 5, Heft 1, Feb. 1925, S. 17–35.
15. Jones, Robert T.: Properties of Low-Aspect-Ratio Pointed Wings at Speeds Below and Above the Speed of Sound. NACA Rep. 835, 1946. (Formerly NACA TN 1032)
16. Garrick, I. E.: On Some Reciprocal Relations in the Theory of Nonstationary Flows. NACA Rep. 629, 1938.
17. Cohen, Doris: Theoretical Loading at Supersonic Speeds of Flat Swept-Back Wings with Interacting Trailing and Leading Edges. NACA TN 1991, 1949.
18. Wieghardt, K.: Chordwise Load Distribution of a Simple Rectangular Wing. NACA TM 963, 1940.
19. Lomax, Harvard, Heaslet, Max. A., and Fuller, Franklyn B.: Integrals and integral equations in linearized wing theory. NACA Rep. 1054, 1951. (Formerly NACA TN 2252, 1950)
20. Ribner, Herbert S.: Some Conical and Quasi-Conical Flows in Linearized Supersonic-Wing Theory. NACA TN 2147, 1950.
21. Heaslet, Max. A., and Lomax, Harvard: Two-Dimensional Unsteady Lift Problems in Supersonic Flight. NACA Rep. 945, 1949. (Formerly NACA TN 1621)
22. Jones, Arthur L., and Alksne, Alberta: The Load Distribution Due to Sideslip on Triangular, Trapezoidal, and Related Plan Forms in Supersonic Flow. NACA TN 2007, 1950.
23. Heaslet, Max, A., Lomax, Harvard, and Spreiter, John R.: Linearized Compressible-Flow Theory for Sonic Flight Speeds. NACA Rep. 956, 1950. (Formerly NACA TN 1824)
24. Lagerstrom, P. A., and Graham, Martha E.: Low Aspect Ratio Rectangular Wings in Supersonic Flow. Douglas Aircraft Co., Inc. Rept. SM 13110, Dec. 1947.
25. Lomax, Harvard, and Sluder, Loma: Chordwise and Compressibility Corrections to Slender-Wing Theory. NACA TN 2295, 1951.
26. Stewartson, K.: Supersonic Flow Over an Inclined Wing of Zero Aspect Ratio. Proc. Cambridge Phil. Soc., vol. 46, pt. 2, April 1950, pp. 307–315.
27. Ribner, Herbert S.: The Stability Derivatives of Low-Aspect-Ratio Triangular Wings at Subsonic and Supersonic Speeds NACA TN 1423, 1947.
28. Mirels, Harold: A Lift-Cancellation Technique in Linearized Supersonic-Wing Theory. NACA Rep. 1004, 1951. (Formerly NACA TN 2145)
29. Goodman, Theodore R.: The Lift Distribution on Conical and Non-Conical Flow Regions of Thin Finite Wings in a Supersonic Stream. Jour. Aero. Sci., vol. 16, no. 6, June 1949, pp. 365–374
30. Evvard, John C.: Use of Source Distributions for Evaluating Theoretical Aerodynamics of Thin Finite Wings at Supersonic Speeds. NACA Rep. 951, 1950.